Alterations of nuclear Ca^{2+} regulation in ventricular myocytes during development and progression of hypertensive heart disease

Dissertation

zur

Erlangung des Doktorgrades

der Naturwissenschaften

(Dr. rer. nat.)

dem

Fachbereich Pharmazie der

Philipps-Universität Marburg

vorgelegt von

Jelena Plačkić

aus Novi Sad, Serbien

Marburg/Lahn **2017**

Erstgutachter: **Prof. Dr. Jens Kockskämper**

Zweitgutachter: **Prof. Dr. Moritz Bünemann**

Eingereicht am **10.02.2017**

Tag der mündlichen Prüfung am **28.03.2017**

Hochschulkennziffer: 118

To my beloved husband

Dragan Nenad

Table of contents

1. Summary **1**

2. Zusammenfassung **3**

3. Introduction **6**

3.1. Hypertension and hypertensive heart disease – prevalence, etiology and morbidity **7**

3.2. Left ventricular hypertrophy – prevalence, etiology and morbidity **9**

3.3. Heart failure **11**

3.3.1. Definition, etiology, classification and symptoms 11

3.3.2. Prevalence, morbidity and mortality 13

3.3.3. Management of heart failure 13

3.3.4. Pathophysiology of heart failure 14

3.4. Essential role of Ca^{2+} for the heart function **16**

3.4.1. Ca^{2+} regulation under normal physiological conditions 16

3.4.2. Molecular basis for cardiac remodeling during compensatory hypertrophy and heart failure 20

3.4.3. Remodeling of Ca^{2+} handling in left ventricular hypertrophy 22

3.4.4. Ca^{2+} mishandling in heart failure 24

3.4.5. Ca^{2+}-dependent hypertrophic signaling pathways 25

3.5. Role and regulation of nuclear Ca^{2+} signaling **29**

3.6. Spontaneously hypertensive rats (SHR) as a model for hypertensive heart disease **32**

3.7. Aims of the study **35**

4. Materials and methods **37**

4.1. Animals **38**

4.2. Isolation of left ventricular myocytes **38**

4.2.1. Chemicals and reagents 38

4.2.2. Solutions for ventricular myocytes isolation 38

4.2.3. Principles of retrograde heart perfusion: the Langendorff method 41
4.2.4. Myocyte isolation procedure 43
4.2.5. Plating of isolated ventricular myocytes 43
4.3. Confocal Ca^{2+} imaging 44
4.3.1. Measuring free intracellular [Ca^{2+}] 44
4.3.2. Loading of the ventricular cells with Fluo-4/AM 47
4.3.3. Confocal Ca^{2+} imaging of subcellular CaTs 48
4.3.3.1. Principles of laser scanning confocal microscopy (LSCM) 48
4.3.3.2. Recordings of subcellular CaTs in left ventricular myocytes 51
4.3.3.3. Analyses of subcellular CaTs 52
4.3.3.4. In situ calibration of Fluo-4 fluorescence in ventricular myocytes 53
4.3.3.5. Recording of Ca^{2+} in perinuclear Ca^{2+} stores 56
4.3.3.5.1. Imaging of perinuclear Ca^{2+} stores 57
4.3.3.5.2. Measurements of NE Ca^{2+} load using Mag-Fluo-4 58
4.4. Protein expression analyses 58
4.4.1. Left ventricular tissue isolation 58
4.4.2. Purification of cardiomyocyte nuclei from left ventricular tissue from 12-14 weeks old WKY/SHR using magnetic assisted cell sorting 59
4.4.3. Homogenization of left ventricular tissue from 15-24 months old WKY/SHR 60
4.4.4. Protein assay 62
4.4.5. Western blot protocol 62
4.4.5.1. Sample preparation 63
4.4.5.2. Gel preparation 64
4.4.5.3. SDS-PAGE electrophoresis 65
4.4.5.4. Wet Blotting 66
4.4.5.5. Blocking, immunostaining and detection 67
4.5. Statistics 71
5. Results 72
5.1. EARLY STAGE OF HYPERTENSIVE HEART DISEASE –Enhanced nucleoplasmic Ca^{2+} signaling in ventricular myocytes from young hypertensive rats 73

5.1.1. Elevated cytoplasmic and nucleoplasmic CaTs in SHR in early hypertension....74
5.1.2. Increased SR and NE Ca^{2+} load in SHR....80
5.1.3. Number and density of nuclear tubules in SHR is not altered....83
5.1.4. Accelerated intranuclear Ca^{2+} propagation in SHR....85
5.1.5. Altered expression of Ca^{2+} handling proteins in SHR nuclei....90
5.1.6. Altered Ca^{2+}-dependent regulation of transcription in SHR....93
5.2. ADVANCED STAGE OF HYPERTENSIVE HEART DISEASE – Remodeling of nuclear calcium handling and structure in ventricular myocytes of spontaneously hypertensive rats with heart failure....96
5.2.1. Cardiovascular characteristics and incidence of HF in SHR with advanced HHD....96
5.2.2. Augmented cytoplasmic and nucleoplasmic CaTs in old SHR....98
5.2.3. Increased SR and NE Ca^{2+} load and fractional Ca^{2+} release in old SHR....104
5.2.4. Increased number and density of nuclear tubules in SHR-HF....106
5.2.5. Faster intranuclear Ca^{2+} propagation in SHR-HF....110
5.2.6. Altered expression of Ca^{2+} handling proteins in left ventricular tissue of SHR-HF....112
6. Discussion....120
6.1. Early hypertension....121
6.1.1. Structural remodeling of LV myocytes and nuclei in early hypertension 121
6.1.2. Remodeling of nuclear Ca^{2+} handling in early hypertension....122
6.1.3. Activation of CaMKIIδ–HDAC5 signaling and elevated histone acetylation in early hypertension....125
6.2. Advanced hypertension....128
6.2.1. Structural remodeling of LV myocytes and nuclei from SHR in advanced HHD....128
6.2.2. Functional remodeling – Alterations of subcellular Ca^{2+} handling in SHR with advanced HHD....130
6.2.2.1. Altered cytoplasmic Ca^{2+} handling in SHR with advanced HHD....131
6.2.2.2. Altered nucleoplasmic Ca^{2+} handling in SHR with advanced HHD 134

6.3. Conclusions 137

7. References 138

8. List of abbreviations 151

9. List of figures 157

10. List of tables 160

11. Publications 161

11.1. Original manuscripts 161

11.2. Abstracts and poster presentations 161

Curriculum vitae 165

Acknowledgements 168

1. Summary

Hypertension is the leading risk factor for developing hypertrophy and heart failure. Pathological changes in myocardial structure and function caused by hypertension are termed ''hypertensive heart disease''. In response to elevated mechanical stress in hypertension and a special neurohormonal environment (catecholamines, angiotensin II, endothelin-1), the heart grows as a means of increasing pump function and decreasing wall tension thus inducing a state of ''compensated hypertrophy''. Initially, hypertrophy is beneficial, but chronic activation of neurohormonal mediators and altered Ca^{2+} signaling ultimately lead to maladaptive alterations in gene expression and progressive cardiac remodeling, which eventually becomes detrimental and impairs cardiac function. Impairment of Ca^{2+} handling is critically implicated in the pathophysiology of hypertrophy and heart failure. Two important Ca^{2+}-dependent signaling pathways involved in cardiac remodeling are the Ca^{2+}/calmodulin-dependent protein phosphatase calcineurin (CaN)–NFAT–GATA4/6 and the Ca^{2+}/calmodulin-dependent protein kinase II (CaMKII)–HDAC–MEF2 pathway. The mechanisms by which the cardiomyocytes distinguish between Ca^{2+} involved in excitation-contraction coupling in the cytoplasm and transcriptional regulation in the nucleus are poorly understood.

While alterations in cytoplasmic Ca^{2+} regulation have been clearly implicated in the pathophysiology of hypertrophy and heart failure, nucleoplasmic Ca^{2+} signaling has been studied much less. Increases in nucleoplasmic [Ca^{2+}] may activate Ca^{2+}-dependent enzymes and transcription factors modulating gene expression and may be critical for the pathogenesis of hypertrophy and heart failure. However, there is lack of studies dealing with the regulation and alterations of nucleoplasmic Ca^{2+} handling under pathophysiological conditions.

We used spontaneously hypertensive rats (SHR) to investigate potential alterations in nuclear Ca^{2+} handling in response to hypertension. During the course of hypertensive heart disease, very little is known about the onset and progression of hypertrophy and heart failure. We hypothesized that maladaptive remodeling of nuclear structure and nuclear Ca^{2+} signaling might occur early in hypertension triggering initiation and progression of hypertrophy, and in advanced hypertension contributing to the transition from compensated hypertrophy to heart failure.

Therefore, in the first part of the thesis, we studied early hypertension-induced structural and functional (Ca^{2+} handling) remodeling of left ventricular (LV) myocytes and nuclei. We found that LV myocytes and nuclei from early hypertensive SHR (≈3 months of age) were already in the stage of compensatory hypertrophy. Cytoplasmic and nucleoplasmic $[Ca^{2+}]_i$ transients (CaTs) were enlarged in SHR. The increase in nucleoplasmic Ca^{2+} exceeded the increase in cytoplasmic Ca^{2+}, suggesting enhanced nuclear Ca^{2+} signaling in SHR. Ca^{2+} load of SR and perinuclear Ca^{2+} stores was also enlarged in SHR, while fractional release from both stores was unaltered. Intranuclear Ca^{2+} propagation was faster in SHR, associated with preserved density of nuclear envelope invaginations and elevated nuclear expression of nucleoporins and SR-Ca^{2+}-ATPase. Increased nucleoplasmic Ca^{2+} signaling was associated with activation of the CaMKIIδ–HDAC5 pathway and increased histone acetylation, suggesting increased gene transcription. The observed remodeling of nuclear Ca^{2+} handling might represent an early event in hypertension that contributes to initiation and progression of pathological hypertrophy in hypertensive heart disease.

In the second part of the thesis, we studied structural and functional nuclear remodeling in advanced hypertension. LV myocytes and nuclei from old SHR (15-25 months of age) were larger compared to young hypertrophic SHR, suggesting further growth of the ventricle with progression of cardiac disease. Cytoplasmic and nucleoplasmic CaTs were augmented (as in young hypertrophic SHR). SR and perinuclear Ca^{2+} load was increased (as in young hypertrophic SHR). There were profound alterations in the kinetics of both cytoplasmic and nucleoplasmic CaTs. Development of heart failure in old SHR was associated with increased density of nuclear envelope invaginations, faster intranuclear Ca^{2+} propagation, acceleration of both rise time and tau of decay of nuclear CaTs and alterations in the cytoplasmic protein levels of major Ca^{2+}-regulating proteins. Thus, we identified distinct alterations in nuclear structure and Ca^{2+} handling during development of heart failure in SHR, providing new insights into mechanisms of nuclear Ca^{2+} regulation under pathophysiological conditions.

Normalization of nucleoplasmic Ca^{2+} handling may represent a novel target for the treatment of hypertrophy and heart failure in hypertensive heart disease.

2. Zusammenfassung

Hypertonie ist einer der bedeutsamsten Risikofaktoren bei der Entwicklung von Hypertrophie und Herzinsuffizienz. Die zugrundeliegenden pathologischen Veränderungen der myokardialen Struktur und Funktion unter Einfluss der Hypertonie werden als „hypertensive Herzkrankheit“ bezeichnet. Als Reaktion auf die mechanische Überbeanspruchung und vermehrte neurohumorale Stimulation (Katecholamine, Angiotensin II, Endothelin-1) wächst das Herz zur Steigerung der Pumpleistung und Verringerung der Wandspannung an, und gelangt so in den Zustand einer „kompensierten Hypertrophie“. Zu Beginn ist diese Form der Hypertrophie der Herzfunktion zuträglich, bei chronischer Aktivierung durch neurohumorale Botenstoffe und veränderte Ca^{2+}-Signalübertragung führt dies jedoch zu maladaptiven Änderungen in der Genexpression und fortschreitenden kardialen Umbauvorgängen, bis diese schließlich die Herzfunktion einschränken und nachhaltig verschlechtern. Eine gestörte Ca^{2+}- Homöostase ist dabei maßgeblicher Bestandteil der zugrundeliegenden Pathophysiologie der Hypertrophie und Herzinsuffizienz. Zwei wichtige Ca^{2+} abhängige Signalwege die am kardialen Umbau beteiligt sind, werden als der Ca^{2+}/Calmodulin-abhängige Proteinphosphatase Calcineurin (CaN)–NFAT–GATA4/6– und der Ca^{2+}/Calmodulin-abhängige Proteinkinase II (CaMKII)–HDAC–MEF2– Signalweg bezeichnet. Die Mechanismen nach welchen ein Kardiomyozyt Ca^{2+} im Zytoplasma für die elektromechanische Kopplung von Ca^{2+} im Zellkern zur transkriptionellen Regulation unterscheidet, sind nur unzureichend verstanden.

Während Änderungen in der cytoplasmatischen Ca^{2+} Regulation klar mit der Pathophysiologie der Hypertrophie und Herzinsuffizienz in Verbindung gebracht werden können, so ist die nukleoplasmatische Ca^{2+}-Signalübertragung in dieser Hinsicht weit weniger gut erforscht. Erhöhte nukleoplasmatische [Ca^{2+}] können Ca^{2+}-abhängige Enzyme und Transkriptionsfaktoren aktivieren, die eine kritische Rolle bei der Pathogenese der Hypertrophie und Herzinsuffizienz spielen können. Allerdings fehlen bisher Studien, die sich mit der Regulation und den Änderungen des nukleoplasmatischen Ca^{2+}-Handlings unter pathophysiologischen Bedingungen beschäftigen.

Wir haben spontan-hypertensive Ratten (SHR) verwendet, um potenzielle Änderungen im nukleären Ca^{2+}-Handling als Reaktion auf eine Hypertonie zu untersuchen. Bisher ist nur wenig bekannt über den Beginn und den zeitlichen Fortschritt der Hypertrophie und Herzinsuffizienz während des Verlaufs einer hypertensiven Herzkrankheit. Wir haben die Hypothese aufgestellt, dass maladaptive Umbauvorgänge der nukleären Struktur und Ca^{2+}-Signalübertragung bereits in einem frühen Stadium der Hypertonie die Initiierung und Progression der Hypertrophie anstößt und im fortgeschrittenen Verlauf der Hypertonie den Übergang von kompensierter Hypertrophie zur Herzinsuffizienz begünstigt.

Im ersten Teil der vorliegenden Arbeit haben wir daher die durch Hypertonie-induzierten strukturellen und funktionellen (Ca^{2+}-Handling) Umbauvorgänge in linksventrikulären (LV) Myozyten und Zellkernen untersucht. Wir haben hierbei herausgefunden, dass sich LV Myozyten und Zellkerne von früh-hypertensiven SHR (im Alter von etwa 3 Monaten) bereits in einem Stadium der kompensatorischen Hypertrophie befinden. Sowohl zyto- als auch nukleoplasmatische $[Ca^{2+}]_I$-Transienten (CaTs) waren vergrößert in den SHR. Hierbei überstieg die Erhöhung im nukleoplasmatischen Ca^{2+} die des zytoplasmatischen Ca^{2+}, was auf eine erhöhte nukleäre Ca^{2+}-Signalübertragung in den SHR schließen lässt. Die Ca^{2+}-Beladung des sarkoplasmatischen Retikulums (SR) und der perinukleären Ca^{2+}-Speicher war erhöht, während die fraktionelle Freisetzung aus beiden Speichern unverändert war. Die intranukleäre Ca^{2+}-Propagation war in den SHR schneller, unter Erhalt der Dichte von Invaginationen der Kernhülle und erhöhter Expression von Nukleoporinen und der SR-Ca^{2+}-ATPase. Die verstärkte nukleoplasmatische Ca^{2+}-Signalübertragung ging einher mit einer Aktivierung des CaMKIIδ–HDAC5 Signalwegs und vermehrter Histonazetylierung, was auf eine erhöhte Transkriptionsrate schließen lässt. Die beobachtete Umorganisation des nukleären Ca^{2+}-Handlings kann als ein frühes Ereignis im Verlauf der Hypertonie verstanden werden, welches der Initiierung und Progression der pathologischen Hypertrophie in der hypertensiven Herkrankheit zugrunde liegt.

Im zweiten Teil der Arbeit haben wir die strukturellen und funktionellen Umbauvorgänge im Zellkern bei fortgeschrittener Hypertonie untersucht. Die linksventrikulären Myozyten und Zellkerne von alten SHR (im Alter von 15-25 Monaten) waren größer als die der jungen hypertrophen SHR, was auf eine Wachstumszunahme der Ventrikel mit Fortschreiten der kardialen Erkrankung schließen lässt. Die zyto- und

nukleoplasmatischen CaTs waren vergrößert bei einer erhöhten Beladung des SR und der perinukleären Ca^{2+}-Speicher (wie schon zuvor in den jungen hypertrophen Tieren). Es wurden profunde Änderungen in der Kinetik von sowohl zytoplasmatischen als auch nukleoplasmatischen CaTs gefunden. Die Entwicklung der Herzinsuffizienz in den alten SHR war verbunden mit einer erhöhten Dichte an Invaginationen der Kernhülle, schnellerer intranukleärer Ca^{2+}-Propagation, einem beschleunigten Anstieg und Abfall der nukleären CaTs und Änderungen in den zytoplasmatischen Proteinkonzentrationen der wichtigsten Ca^{2+}-Regulationsproteine.

Wir konnten somit deutlich ausgeprägte Änderungen in der nukleären Struktur und dem nukleären Ca^{2+}-Handling während der Entwicklung der Herzinsuffizienz in SHR nachweisen, welche uns neue Einblicke in die Mechanismen der nukleären Ca^{2+}-Regulation unter pathophysiologischen Bedingungen erlauben.

Die Normalisierung des nukleoplasmatischen Ca^{2+}-Handlings stellt ein mögliches neues Target für eine gerichtete Behandlung der Hypertrophie und Herzinsuffizienz bei der hypertensiven Herzkrankheit dar.

3. Introduction

3.1. Hypertension and hypertensive heart disease – prevalence, etiology and morbidity

Hypertension is defined as values ≥140 mmHg of systolic blood pressure and/or ≥90 mmHg of diastolic blood pressure. The prevalence of hypertension amounts to 30–45% of the general population, with a steep increase with ageing (ESH/ESC Guidelines, 2013).

Hypertension is a common multifactorial vascular disorder that results from combinations of genetic and environmental factors (obesity, insulin resistance, high alcohol intake, high salt intake, aging and sedentary lifestyle, stress, low potassium intake, and low calcium intake). It is defined as essential (primary or idiopathic) hypertension if the cause is unknown (in 95% of the hypertensive population). The remaining 5% of adults with hypertension have the secondary form of hypertension, where the cause could be identified and, in many cases, the hypertension can be controlled with surgery or medications. Secondary causes of hypertension include renal parenchymal disease, renovascular diseases, coarctation of the aorta, Cushing's syndrome, primary hyperaldosteronism, pheochromocytoma, hyperthyroidism and hyperparathyroidism (Akpunonu et al, 1996).

There is a strong positive correlation of hypertension with the risk of cardiovascular disease (stroke, myocardial infarction, heart failure), renal disease and mortality. This correlation is more robust with systolic than with diastolic hypertension (Carretero et al, 2000).

Several mechanisms contribute to the increased risk for a cardiac event in the hypertensive patients (Figure 3-1). First, the development of left ventricular (LV) hypertrophy and myocardial fibrosis leads to LV dysfunction, an important factor in the evolution of congestive heart failure. Second, hypertension promotes the development of coronary artery atherosclerosis, which increases the risk for an acute myocardial infarction, with subsequent systolic dysfunction and congestive heart

failure. Prolonged action potential duration is a consistent finding in myocardial hypertrophy, independent of cause. This may lead to early afterdepolarizations (EADs) and triggered activity, and in the intact heart increased dispersion of repolarization may sustain the arrhythmia. In the hypertrophic myocardium myofibrillar disarray, heterogeneous gap junction distribution, and fibrosis are additional potentially arrhythmogenic components (Kahan et al, 2005).

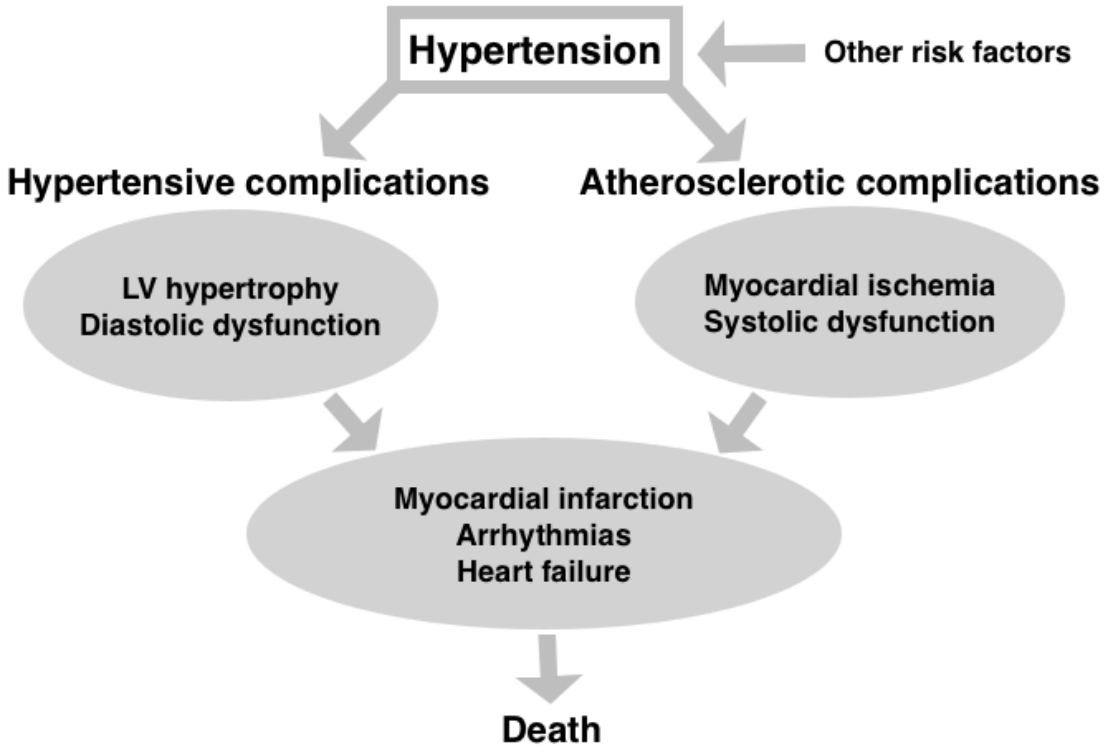

Figure 3-1. The risk for cardiac events in hypertension.

(modified from Kahan et al, 2005)

Pathological changes in myocardial structure and function, coronary vessels and the cardiac conduction system as a result of prolonged hypertension are termed ''hypertensive heart disease (HHD)''. The resulting abnormalities include LV hypertrophy, systolic and diastolic dysfunction, and their clinical manifestations including arrhythmias and symptomatic heart failure (Drazner et al, 2011, Diamond et al, 2005).

3.2. Left ventricular hypertrophy – prevalence, etiology and morbidity

LV hypertrophy occurs in 30–70% of hypertensive patients and represents a strong and independent risk factor for cardiovascular morbidity (including congestive heart failure, coronary heart disease, atrial fibrillation, supraventricular and ventricular arrhythmias and stroke) and mortality (Kahan et al, 2005).

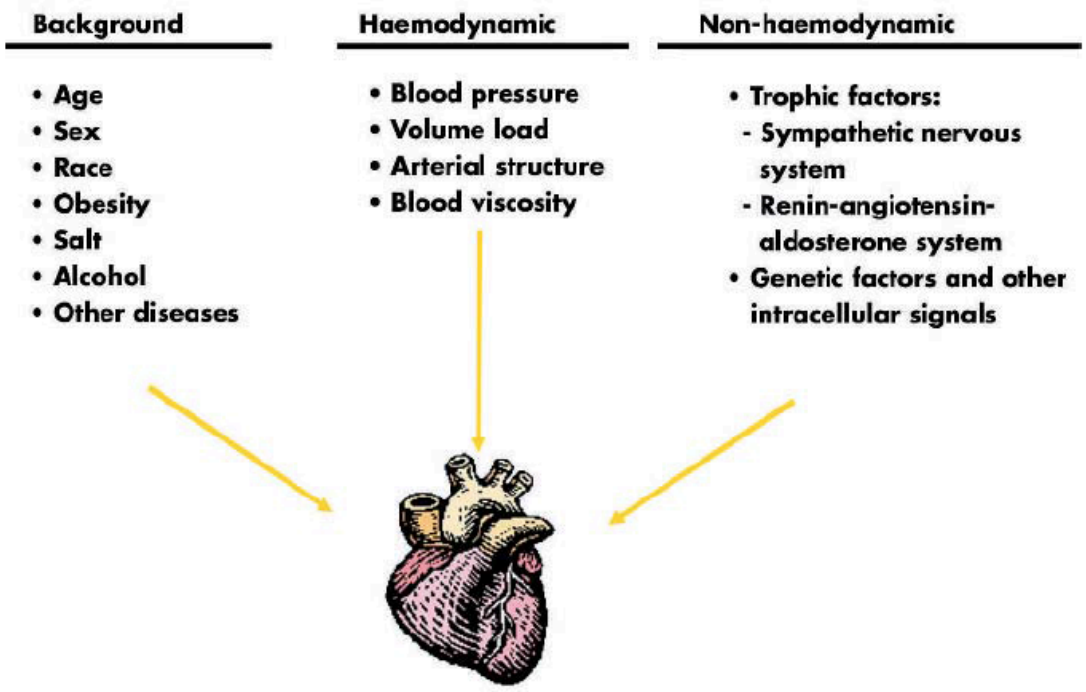

Figure 3-2. Multiple determinants for left ventricular hypertrophy.

(from Kahan et al, 2005)

A combination of hemodynamic and non-hemodynamic factors (genetic and non-genetic) is involved in the development of LV hypertrophy (Figure 3-2). The classic paradigm of HHD is that the LV wall thickens in response to elevated blood pressure (increased mechanical stress) as a compensatory mechanism to minimize wall stress. The mechanisms responsible for the development of hypertrophy include also the trophic influence mediated by the sympathetic nervous system (SNS), the renin–angiotensin–aldosterone (RAAS) system, insulin, growth factors, cytokines and

putative genetic risk factors that modulate LV mass. An increasing number of genes (Diamond et al, 2005) is being identified that contribute to the development of hypertrophy. These include genes related to the RAAS, natriuretic peptide receptors, adrenergic receptors or sarcomeric proteins.

When the relative wall thickness is increased, LV hypertrophy is classified as concentric (the early compensatory response), and when the relative wall thickness is not increased, LV hypertrophy is classified as eccentric. Hypertensive patients can have any of these patterns of LV geometry. Various factors influence the hypertrophic response and LV geometric pattern: severity and duration of pressure overload, demographic factors (gender, age, race), medical conditions (diabetes mellitus, obesity, coronary artery disease, valvular heart disease), variations in neurohormonal activation (renin, angiotensin II (ATII), aldosterone levels), alterations in the extracellular matrix and genetic background (Drazner et al, 2011).

The pathway from hypertension to concentric LV hypertrophy is reversible. With pharmacological control of blood pressure, LV mass decreases and is associated with reduced risk of clinical events including cardiovascular death, myocardial infarction and stroke. The current antihypertensive drugs routinely used are angiotensin-converting enzyme (ACE) inhibitors (e.g. enalapril), angiotensin II type-1 receptor blockers (e.g. valsartan), beta-blockers (e.g. bisoprolol), calcium antagonists (dihydropyridines, verapamil, diltiazem) and diuretics (e.g. thiazides) (ESH/ESC Guidelines, 2013).

3.3. Heart failure

3.3.1. Definition, etiology, classification and symptoms

Heart failure (HF) describes the complex clinical syndrome, in which a structural and/or functional disorder of the heart impairs the capacity of the ventricle to eject and/or fill with blood and is incapable of maintaining a cardiac output that is adequate to meet the metabolic requirements of the body. Therefore, HF limits the ability of the patient to exercise or carry out activities of daily living without symptoms of dyspnea or fatigue (Felker et al, 2003, Kemp and Conte, 2012, Liew et al, 2004, ESC Guidelines, 2005).

Heart failure is caused by a loss of a critical amount of functional cardiomyocytes after injury to the heart from a number of causes. The most common etiologies are ischemic heart disease, long-standing hypertension and diabetes. Three quarters of all HF patients have preexisting hypertension, which makes hypertension the leading risk factor for developing HF. Less common, but important, causes of HF are inherited monogenic conditions such as cardiomyopathies (hypertrophic cardiomyopathies, dilated cardiomyopathies), infections (e.g. viral myocarditis, Chagas' disease), toxins (e.g. alcohol, cytotoxic drugs), valvular disease and prolonged arrhythmias (Brugada syndrome, long QT syndrome) (Kemp and Conte, 2012, Liew et al, 2004, McMurray and Pfeffer, 2005, ESH/ESC Guidelines, 2013).

Heart failure is termed acute HF, when symptoms of HF occur suddenly (anxiety, tachycardia, dyspnea, cardiogenic shock). This syndrome is usually associated with acute MI, sustained cardiac arrhythmias (atrial fibrillation or ventricular tachycardia) or mechanical complications such as papillary muscle rupture or fulminant myocarditis (Felker et al, 2003, Millane et al, 2000). More commonly, HF occurs in patients with an established diagnosis of cardiovascular disease, who develop increasing symptoms of HF after a period of relative stability. In this case it is termed chronic HF. Chronic HF can be “compensated” or “decompensated”. In compensated

HF, symptoms are stable, and many overt features like fluid retention and pulmonary edema are absent. Decompensated HF refers to a deterioration, which may occur either as an acute episode of pulmonary edema or as lethargy and malaise, a reduction in exercise tolerance or increasing breathlessness on exertion (Felker et al, 2003, Millane et al, 2000).

Heart failure could result from both left and/or right ventricular failure and is classified as systolic HF (impaired ventricular contraction with reduced LV ejection fraction (EF), termed as HF with reduced EF (HFrEF)) and diastolic HF (impaired ventricular relaxation and filling with preserved LV ejection fraction (EF), termed as HF with preserved EF (HFpEF)). Systolic HF represents HF in which the primary symptoms relate to a decrease in cardiac output and end-organ perfusion: fatigue, decreased mental functioning, prerenal azotemia and abnormal hepatic enzymes. Dyspnea, cough and wheezing result from the increased pressure in the pulmonary capillary bed due to ineffective forward flow of blood from the left ventricle. Patients with preserved systolic function (diastolic HF) commonly develop acute onset of severe dyspnea and signs of pulmonary congestion because of their reduced ventricular distensibility, in which small changes in ventricular volume status lead to large changes in filling pressures. Seventy percent of patients with HF have systolic dysfunction compared to 30% with diastolic dysfunction (Kemp and Conte, 2012, Liew et al, 2004, Felker et al, 2003).

A common cause of right ventricular (RV) failure is LV failure. In RV failure, an increase in the amount of blood in the RV leads to elevated right ventricular and right atrial pressure and increased pressure in the vena caval system, which impairs venous drainage from the body. This leads to increased pressure in the liver, the gastrointestinal tract, and the lower extremities and to the clinical signs and symptoms of systemic volume-overload characterized by abdominal pain, hepatomegaly and peripheral edema and ascites. Patients with systemic volume-overload HF represent the majority of patients with decompensated HF (Kemp and Conte, 2012, Felker et al, 2003).

3.3.2. Prevalence, morbidity and mortality

Heart failure affects about 1–2% of the population in Europe and the United States, but 6-10% of people older than 65 years (Liew et al, 2004, McMurray and Pfeffer, 2005). The quality of life is reduced much more by HF than by other chronic illnesses. HF is deadly and disabling. Despite the large number of effective treatments available, patients with HF continue to experience progressively worsening symptoms, frequent admissions to the hospital and premature death. Comorbidity seems to be an increasing problem, which in many cases limits the use of proven treatments. Community-based surveys show that 10-17% of patients die within a year of diagnosis, most from worsening HF or suddenly (mostly because of ventricular arrhythmias) (McMurray and Pfeffer, 2005, ESC Guidelines, 2016). Annual mortality from HF remains in the range of 6-12% (Rivera and Lowes, 2005).

3.3.3. Management of heart failure

Management of HF is complex, since HF usually does not occur in isolation. HF occurs generally in elderly individuals, many of whom are being treated for other medical problems. Many patients with HF have comorbidities related to the underlying cardiac problem and its treatment (e.g. gout from diuretics), its cause (e.g. angina, hypertension, diabetes, smoking-related lung disease) or related to the age (e.g. osteoarthritis). Some common comorbidities may have various causes (e.g. renal dysfunction), whereas others are not fully explained (e.g. anaemia, depression, disorders of breathing and cachexia) (McMurray and Pfeffer, 2005). HF patients take, on average, six HF-related medications, and 78% have at least two hospital admissions per year, leading to annual costs of $10–38 billion (Kemp and Conte, 2012). HF medications include ACE inhibitors, beta-blockers, mineralocorticoid/aldosterone receptor antagonists (e.g. spironolacton), angiotensin II type 1 receptor blockers, diuretics, pacemaker (I_f)-channel inhibitors (e.g. ivabradine), vasodilators (e.g. hydralazine and isosorbide dinitrate) and Na^+/K^+ ATPase inhibitors (e.g. cardiac glycoside digoxin) (ESC Guidelines, 2016).

3.3.4. Pathophysiology of heart failure

Mean arterial pressure (MAP) is defined as the product of cardiac output and total peripheral resistance. A patient with HF has decreased cardiac output which in turn leads to a decrease in MAP and therefore decreased tissue perfusion. The body thus tries to maintain adequate tissue perfusion using several compensatory mechanisms (Figure 3-3). In early HF, increased diastolic filling causing stretch of the myocardium leads to stronger contraction and an increase in cardiac output, which is known as the Frank – Starling mechanism (Westerhof and O'Rourke,1995). However, as HF advances cardiac output only increases slightly for the increase in diastolic filling and an excessive increase in diastolic pressure ultimately leads to pulmonary congestion. Another important compensatory mechanism during early stages of HF is activation of neurohormonal pathways (Lee et al, 2008, Kemp and Conte, 2012). The decrease in MAP seen in HF leads to a stimulation of the sympathetic nervous system and release of catecholamines (norepinephrine and epinephrine). This stimulation has direct effects on the heart (increased heart rate and contractility) and on the peripheral vasculature (vasoconstriction). In the peripheral vasculature, activation of the α1 adrenergic receptors causes vasoconstriction. The kidneys secrete renin in response to this sympathetic activation (via β1 adrenergic receptors) and reduced renal blood flow (from a decrease in MAP). Renin then acts on angiotensinogen to make angiotensin I. Angiotensin I is converted by ACE to angiotensin II which directly causes vasoconstriction and promotes the release of aldosterone from adrenal glands and vasopressin from the posterior pituitary gland. They both also contribute to the augmentation of MAP in HF. In addition to the components of the RAAS, as a compensatory mechanism, vascular endothelium in the heart produces locally the potent vasoconstrictor endothelin-1 (Kemp and Conte, 2012, Liew et al, 2004). Besides effects on total peripheral resistance, neurohormonal activation leads to alterations in the structure and function of the ventricle in a process known as remodeling. Neurohormones, in the short-term, have beneficial compensatory effect on the heart, but in the long-term their persistent presence stimulates maladaptive alterations in gene expression, encourages further enlargement of the myocardium and a progressive increase in myocardial fibrosis and apoptosis, which eventually

becomes detrimental and impairs cardiac contractility. Natriuretic peptides (atrial natriuretic peptide (ANP) and brain natriuretic peptide (BNP)) are found in the atria and ventricles, respectively, and are released following atrial or ventricular stretch to counteract the vasoconstricting effects of the other neurohormonal systems previously discussed. Elevated BNP is thought to be one of the first signs of HF and is used as HF marker to follow the progression of the disease. Increased oxidative stress and levels of proinflammatory cytokines in damaged failing myocardium (including tumor necrosis factor α, interleukin 1α, interleukin 6, and interferon α), which act as negative inotropes and profibrotic factors, also contribute to the decompensation of the heart (Kemp and Conte, 2012, Liew et al, 2004).

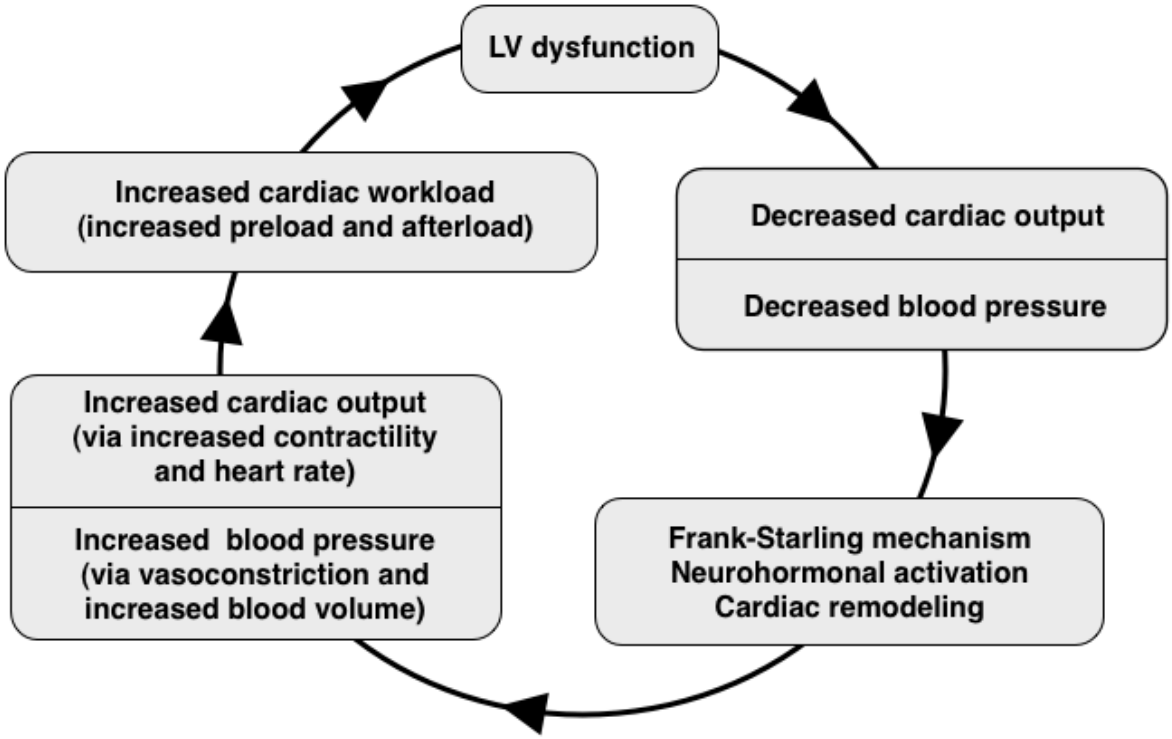

Figure 3-3. The vicious cycle of HF.

(reproduced from Kemp and Conte, 2012)

3.4. Essential role of Ca^{2+} for the heart function

3.4.1. Ca^{2+} regulation under normal physiological conditions

Ca^{2+} is the ubiquitous second messenger important for cardiac myocytes electrophysiology, excitation-contraction (E-C) coupling, contraction itself, energy consumption (by contraction and Ca^{2+} transport) and production, cell death and transcriptional regulation (Bers, 2008). E-C coupling (Figure 3-4) is the process that enables the heart to contract and relax.

A propagating action potential (AP) originating at the sino-atrial node depolarizes the myocytes' plasma membrane leading to opening of the voltage-dependent L-type calcium channels (LTCCs) generating an inward current ($I_{Ca,L}$) that is responsible for the plateau phase of the ventricular AP. LTCCs are located primarily at sarcolemmal (T tubule and surface) membrane – sarcoplasmic reticulum (SR) junctions where the SR Ca^{2+} release channels (or ryanodine receptors (RyRs)) are clustered, constituting a local Ca^{2+} signaling complex termed couplon. Ca^{2+} entry through LTCCs locally increases [Ca^{2+}] in the junctional cleft near RyRs and triggers Ca^{2+} release from the SR (via a process named Ca^{2+}-induced Ca^{2+} release, CICR). Ca^{2+} influx and SR Ca^{2+} release raises the free intracellular [Ca^{2+}] from about 100 nM to 1 µM. Turnoff of $I_{Ca,L}$ is mediated by voltage- and Ca^{2+}-dependent inactivation, that may function as a negative feedback system to limit Ca^{2+} influx and protect against cellular Ca^{2+} overload. SR Ca^{2+} release is turned off before the SR is fully depleted (fractional SR Ca^{2+} release is only approximately 50–60%) due to (a) RyR inactivation or adaptation that depends on cytoplasmic [Ca^{2+}] and (b) RyR inactivation by a decrease in luminal SR [Ca^{2+}].
The rise of intracellular [Ca^{2+}] activates contraction. Ca^{2+} binds to troponin C (TnC), a part of the thin-filament regulatory complex, leading to stronger binding of TnC to troponin I (TnI) and pulling TnI off its actin-binding site, in such way that the conformational change of the troponin/tropomyosin complex allows myosin heads to interact with actin (Bers, 2008). The actin and myosin filaments slide past each other

causing shortening of the sarcomere and myocyte contraction. For synchronous contractile activation, all ≈20000 couplons in the ventricular cell must be simultaneously activated, which is normally accomplished by the AP and LTCC activation (Bers, 2008).

For relaxation to occur intracellular [Ca^{2+}] must decline, allowing Ca^{2+} to dissociate from the myofilaments. Ca^{2+} removal from the cytosol during relaxation is mainly mediated by the SR Ca^{2+} ATPase (SERCA) and the sarcolemmal Na^{+}/Ca^{2+} exchanger (NCX), with a very minor contribution of sarcolemmal (SL) Ca^{2+}-ATPase and the mitochondrial Ca^{2+} uniporter. Quantitative importance of these four Ca^{2+} extrusion pathways varies between species (Bers and Despa, 2006). In mouse and rat ventricles, 90–95% of the activator Ca^{2+} cycles through the SR, with only 5–8% cycling through the SL. In contrast, in rabbit, dog, cat, guinea pig, ferret, and human ventricles, this balance is closer to 70% SR and 25–28% SL. During a normal Ca^{2+} transient decline only 1% of the cytosolic Ca^{2+} is taken up by mitochondria. The beat-to-beat changes in mitochondrial [Ca^{2+}] are small but cumulative changes over several seconds cause regulatory changes in ATP production providing an important feedback between energy supply and demand. Slow cumulative changes in intra-mitochondrial [Ca^{2+}] stimulate key dehydrogenases of the Krebs cycle that increase the production of NADH (nicotinamide adenine dinucleotide) and ATP to match increased energetic demands. However, Ca^{2+} uptake by mitochondria can be dramatically increased when intracellular [Ca^{2+}] is chronically elevated to greater than 1 μM. Mitochondrial Ca^{2+} overload stimulates the opening of the mitochondrial permeability transition pore (MPTP), which causes swelling of the internal mitochondrial matrix, leading to rupture of the outer mitochondrial membrane and release of cytochrome c, causing caspase activation and apoptosis (Denton and McCormack, 1990).

Rat and mouse ventricular myocytes also have an unusually short AP duration, without a prominent plateau, with a different set of K^{+} currents and relatively higher intracellular [Na^{+}]. Species differences in E-C coupling are important to keep in mind, as mouse and rat are often used as animal models for cardiovascular studies (Bers, 2008).

To maintain cellular steady-state the amount of Ca^2 that enters the myocyte via LTCC and NCX must equal the amount of Ca^2 extruded from the cell via NCX, and at the level of the SR, the amount of Ca^{2+} released through RyRs must equal the amount taken up back into the SR by SERCA.

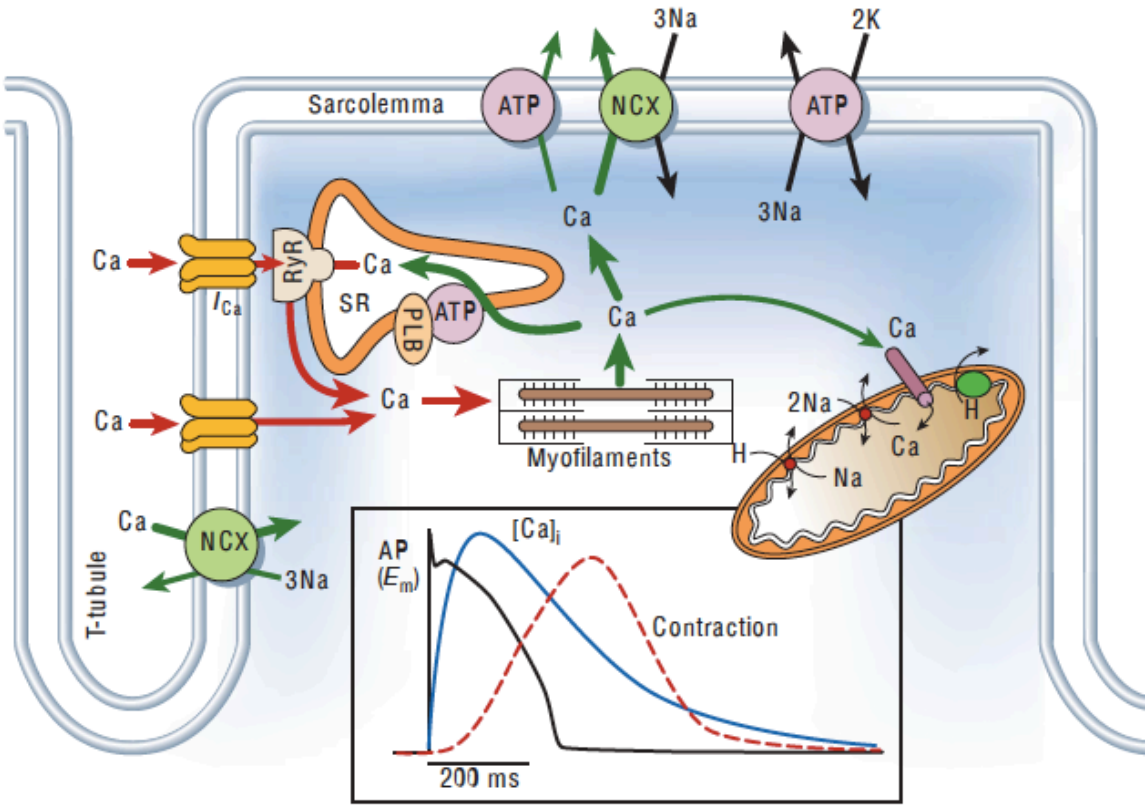

Figure 3-4. Excitation-contraction coupling.

(taken from Bers, 2002)

The dynamic regulation of E-C coupling is essential for the varying metabolic demands. Under normal physiological condition, Ca^{2+}-handling proteins are primarily regulated by adrenergic stimulation upon the activation of sympathetic nerves. Adrenergic stimulation ultimately activates cAMP-dependent protein kinase A (PKA) and/or Ca^{2+}/calmodulin-dependent protein kinase II (CaMKII). Both PKA and CaMKII can phosphorylate and regulate LTCCs and RyRs. These kinases phosphorylate distinct sites on these proteins but, in general, stimulate the activity of each Ca^{2+} channel. Also, both PKA and CaMKII can regulate SR Ca^{2+} uptake via phospholamban (PLB) phosphorylation, the most important endogenous regulator of

SERCA function. In dephosphorylated form, PLB is binding and inhibiting SERCA activity, while phosphorylation of PLB causes dissociation from SERCA and prevents the inhibitory effect. Therefore, adrenergic stimulation increases the intracellular [Ca^{2+}], the force and shortening velocity of contraction (positive inotropy) and the rate of relaxation (positive lusitropy) (Bers, 2002).

NCX is the electrogenic Ca^{2+} transporter (the extrusion of 1 Ca^{2+} is coupled to inward flux of 3 Na^{+}) that is largely responsible for extruding the Ca^{2+} that enters via LTCCs. However, NCX can operate in both Ca^{2+} efflux and Ca^{2+} influx (or reverse) mode, depending on the internal and external concentrations of Na^{+} and Ca^{2+} and the membrane potential (E_m). In simpler terms, high intracellular [Ca^{2+}] favours Ca^{2+} efflux (inward $I_{Na/Ca}$), while positive membrane potential (E_m) and high intracellular [Na^{+}] favours Ca^{2+} influx (outward $I_{Na/Ca}$). Under normal physiological conditions outward $I_{Na/Ca}$ exists for only a few ms during the rise in submembrane [Na^{+}] at the beginning of the AP, and the late plateau phase of most atrial and rodent ventricular APs can be almost entirely due to inward I_{NCX}. However, in HF, when SR Ca^{2+} release is low, intracellular [Na^{+}] elevated and AP duration long, the amount of Ca^{2+} influx through NCX can increase greatly. This will raise the cellular and SR Ca^{2+} content, resulting in larger Ca^{2+} transients and therefore enhanced contractility (Bers and Despa, 2006).

The ability of NCX to carry depolarizing inward I_{NCX} current raises its role in pacemaker action and arrhythmias (Bers, 2008). For instance, delayed afterdepolarizations (DADs), which take off from the resting E_m after AP repolarization, are caused by spontaneous SR Ca^{2+} release events (mediated via RyR2 or IP3R) causing a transient inward current (I_{ti}), for which I_{NCX} is responsible, that depolarizes E_m reaching threshold for an AP genesis. On the other hand, early afterdepolarizations (EADs) take off during the AP plateau or phase 3 repolarization by the reactivation of LTCCs that have recovered from Ca^{2+}-dependent inactivation once intracellular [Ca^{2+}] has significantly declined.

Impairment of Ca^{2+} handling is critically implicated in the pathophysiology of hypertrophy and HF (Bers, 2002, Bers and Despa, 2006).

3.4.2. Molecular basis for cardiac remodeling during compensatory hypertrophy and heart failure

As mentioned before, activation of neurohormonal mediators (catecholamines, ATII, ET-1) initially aims to maintain cardiac output by either increasing arterial pressure by vasoconstriction to maintain perfusion of vital organs or by increasing myocardial contractility and heart rate. Most of these stimuli first induce a phase of cardiac hypertrophy in which individual myocytes grow as a means of increasing cardiac pump function and decreasing ventricular wall tension (inducing a state of ''compensatory hypertrophy''). However, chronic stimulation of these factors is detrimental, causing eventually maladaptive remodeling of the heart (Berrige et al, 2003, Heineke et al, 2006).

ATII, ET-1 and α-adrenergic agonists (catecholamines epinephrine and norepinephrine) bind to specific seven-transmembrane-spanning receptors that are coupled to heterotrimeric G proteins of the $G_{\alpha q}$ subclass. These G proteins are coupled to phospholipase Cβ (PLCβ). Activation of PLCβ induces the generation of diacyl glycerol (DAG), which activates protein kinase C (PKC), and production of inositol-1,4,5-trisphosphate (IP3). Accumulation of IP3 leads to the mobilization of internal Ca^{2+} by binding to the IP3Rs located in the SR or the nuclear envelope (NE) (Heineke, 2006). IP3Rs are Ca^{2+} release channels and, unlike the short bursts and removals of Ca^{2+} induced by CICR, IP3-mediated Ca^{2+} signaling results in a lower amplitude, but sustained Ca^{2+} release (Salazar et al, 2007, Heineke et al, 2006). Increases in $[Ca^{2+}]$ are involved in regulation of cardiac gene transcription, which will be discussed in the next chapter.

Stimulation of β-adrenergic receptors activates a GTP-binding protein ($G_{\alpha S}$), which stimulates adenylyl cyclase (AC) to produce cAMP, which in turn activates PKA. This kinase phosphorylates several proteins related to E-C coupling (PLB, LTCC, RyR, TnI and myosin binding protein C). PKA increases contractions (positive inotropy) and accelerates relaxation (positive lusitropy). The positive lusitropic effect of PKA is mediated by phosphorylation of PLB and TnI, which speed up SR Ca^{2+} re-uptake

and dissociation of Ca^{2+} from the myofilaments, respectively. The faster SR Ca^{2+} uptake also contributes to an increase in SR Ca^{2+} content. The positive inotropic effect of PKA activation is mediated by the combination of increased $I_{Ca,L}$ and greater availability of SR Ca^{2+} (Bers, 2002).

During compensatory hypertrophy, an increased release of neurohormones enhances Ca^{2+} signaling and contributes to the hypertrophic response and the increase in cardiac output. These pathways are involved in the regulation of cardiac gene expression, thus contributing to molecular cardiac remodeling. The maladaptive remodeling during hypertrophy includes reactivation of a “fetal gene program” (Cappola et al, 2008). Although many changes occur, the most well-characterized include a shift in the expression of sarcomeric proteins (α-MHC switches to the fetal β-MHC), increased expression of natriuretic peptides (ANP and BNP), alterations in expression of calcium cycling genes (SERCA2a downregulation, NCX upregulation), prolongation of the AP due to reductions in outward K^+ currents, upregulation of genes involved in cell death (c-myc and c-fos), upregulation of components of the extracellular matrix (ECM) (collagen I, III, fibronectin, matrix metalloproteinases (MMPs)), upregulation of immune-response genes and changes in the energetic and metabolic state of the myocyte (Rivera and Lowes, 2005, Liew et al, 2004, Kehat et al, 2010). The enhancement of Ca^{2+} signaling early in compensated hypertrophy is seriously compromised when downregulation of β adrenergic receptors coincides with a Ca^{2+}-handling remodelling process of key components such as the SERCA.

3.4.3. Remodeling of Ca^{2+} handling in LV hypertrophy

Human data on ventricular Ca^{2+} remodeling during compensatory hypertrophy are scarce, because obtaining tissues is a major obstacle. Evidence from animal models suggests that early during compensatory hypertrophy stronger myocardial contractility is due to the augmented CaTs of isolated myocytes (Brooksby et al, 1993, Shorofsky et al, 1999, Tomaselli, 1999, Sipido et al, 2000, Fowler et al, 2004, Chen-Izu et al, 2007, Harzheim et al, 2009, Kapur et al, 2010).

One possible explanation for increased CaTs is electrical remodeling of the LV, manifested as AP prolongation (Brooksby et al, 1993, Coulombe et al, 1994, Tomita et al, 1994, Cerbai et al, 1994, Tomaselli, 1999, Wang et al, 2001, Chen-Izu et al, 2007). Longer period of AP depolarization in hypertrophic myocytes leads to more Ca^{2+} influx via $I_{Ca,L}$ and reduced calcium extrusion (or greater calcium entry) via the NCX1 in these cells. This results in an increased amount of calcium remaining in the cytoplasm, a substantial proportion of which is taken up by the SR due to its active SERCA2a pump. This leads to an increase of the SR Ca^{2+} content, often observed in hypertrophy (Brooksby et al, 1993, Fowler et al, 2004, Sipido et al, 2000). SERCA2a activity was reported to be unaltered (Shorofsky et al, 1999, Fowler et al, 2006) or increased (Boknik et al, 2001, Zvadlo et al, 2004, Carvahlo et al, 2006) in hypertrophy. AP prolongation is a compensatory mechanism that is potentially arrhythmogenic and may predispose the heart to EADs and DADs and underlies the increased propensity to arrhythmia (Wickenden et al, 1998). In mild hypertrophy, an increase in $I_{Ca,L}$ density (accompanied by the accelerated recovery from $I_{Ca,L}$ inactivation) and a decrease in inward I_{NCX} appear to be important for prolongation of the AP (Wang et al, 2001, Zwadlo et al, 2004). In severe hypertrophy, however, prolongation of AP duration may be attributable to the reduction in the repolarizing K^+ currents, mainly I_{to} (Benitah et al., 1993, Coulombe et al, 1994, Tomita et al, 1994, Cerbai et al, 1994).

Another explanation for increased CaTs would be increased E-C coupling gain, caused by modulation of RyR2 activity. With unchanged trigger $I_{Ca,L}$ the CICR from

the SR was significantly increased (Shorofsky et al, 1999, Chen-Izu et al, 2007). Increased IP3R2 expression in the junctional SR, where they are in close proximity to RyRs, is suggested to modulate RyR activity. IP3R2–mediated Ca^{2+} release is shown to sensitize RyRs, thereby increasing diastolic Ca^{2+} leak, the incidence of extra-systolic CaTs and E-C coupling mediated CaTs (Harzheim et al, 2009). Decreased coupling efficiency between LTCC and RyRs due to an increase in the width of the dyadic cleft has been observed (Xu et al, 2007). Sensitization of RyR opening due to increased Ca^{2+} release through IP3R2s could compensate for the lack of coupling efficiency (Harzheim et al, 2009). IP3R2 expression was also increased in hypertrophic hearts from patients with ischemic dilated cardiomyopathy, demonstrating that increased IP3R2 expression may be a general phenomenon that underlies Ca^{2+} changes during hypertrophy (Go et al, 1995). Coupled to increased systemic levels of IP3-generating agonists, such as ET-1, ATII and NE, increased IP3R2 expression during hypertrophy provides a possible explanation for why hypertrophic hearts are more likely to develop lethal ventricular arrhythmias. Prolonged AP and increased E-C coupling gain act synergistically to increase the CaT during excitation and cause enhanced myocardial contraction.

Alterations in SR Ca^{2+} release may be among the primary cellular mechanisms that underlie the enhanced contractility and increased CaTs associated with cardiac hypertrophy. Several studies reported that hypertrophic myocytes exhibit pogressive increase in susceptibility to cellular Ca^{2+} alternans, the high incidence of spontaneous and triggered Ca^{2+} waves and increased mean amplitude of Ca^{2+} sparks, all contributing to spontaneous beats and triggered arrhythmias (Shorofsky et al, 1999, Kapur et al, 2010, Harzheim et al, 2009). As cells develop defects that lead to increased spontaneous Ca^{2+} release, they are removed from providing any contribution to mechanical performance, since Ca^{2+} overload may activate mitohondrial-dependent apoptosis. These cells are replaced by fibrosis. With the progression of the disease, increasing myocyte loss and fibrosis eventually impairs cardiac contractility.

3.4.4. Ca^{2+} mishandling in HF

Profound remodeling of Ca^{2+} handling proteins in human HF and in animal HF models is the basis for contractile dysfunction.

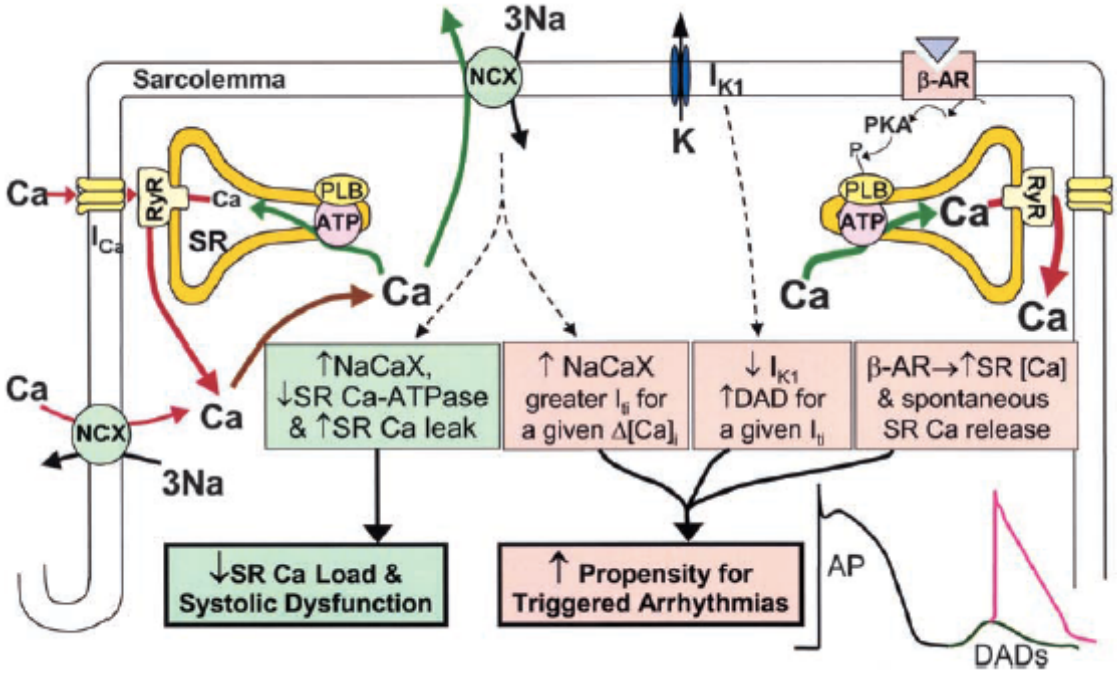

Figure 3-5. Ca^{2+} mishandling in HF.

(taken from Pogwizd and Bers, 2004, for details see text)

With progression of cardiac disease during HF decompensation depressed contractile force is shown to be a result of reduced CaTs due to reductions in SR Ca^{2+} content. The decreased SERCA activity in HF coupled with an increased NCX activity allows NCX to compete better with SERCA in extruding Ca^{2+} from the cytosol during relaxation, bringing the overall Ca^{2+} transported by the SR and sarcolemma closer to equal in HF, thus contributing to lower SR Ca^{2+} load frequently observed in HF models (Hasenfuss and Pieske, 2002, Bers and Despa, 2006). Another factor that may contribute to lower SR Ca^{2+} content in HF is an increased diastolic SR Ca^{2+} leak via hyperphosphorylated RyRs (Eisner and Trafford, 2002, Scoote and Williams, 2002, Dobrev and Wehrens, 2014, Bers et al, 2003). ‘’Leaky RyRs’’, increased NCX activity and prolongation of AP (due to reductions in outward K^+ currents) may contribute to instability of resting E_m and increased propensity for arrhythmias

(Figure 3-5). DADs would initially seem unlikely in HF (since SR Ca^{2+} load is decreased), but hyperadrenergic state in HF can easily drive SR Ca^{2+} content to the point where spontaneous Ca^{2+} release is occuring. Any given SR Ca^{2+} release causes greater inward depolarizing current (due to upregulated NCX and increased membrane resistance caused by reduction of I_{k1}) and causes greater DADs, enough to trigger an extra AP and arrhythmic contractions (Pogwizd and Bers, 2004).

All these changes contribute to structural and functional remodeling in HF ultimately causing contractile dysfunction, arrhythmias and decompensation of HF (McMurray and Pfeffer, 2005, Berrige et al, 2003).

3.4.5. Ca^{2+}-dependent hypertrophic signaling pathways

Two important Ca^{2+}-dependent signaling pathways (Figure 3-7) critically involved in cardiac remodeling are the Ca^{2+}/calmodulin-dependent protein phosphatase calcineurin (CaN)–NFAT–GATA4/6 and the Ca^{2+}/calmodulin-dependent protein kinase II (CaMKII)–HDAC–MEF2 pathway (Wilkins et al, 2004, Backs et al, 2009, Passier et al, 2000, Molkentin, 2000, Zhang and Brown, 2004, Backs and Olson, 2006, Liew et al, 2004).

Calmodulin (CaM) is a critical second messenger that transduces Ca^{2+} signals in virtually all cell types. As a consequence of Ca^{2+} binding, CaM undergoes a conformational change that enables its binding to target proteins (Maier and Bers, 2002). CaM is known to stimulate CaMKII, a serine/threonine protein kinase that is involved in the regulation of various transcription factors, e.g. activation protein-1, activating transcription factor-1, serum response factor, cAMP-response element binding protein, and myocyte enhancer factor 2 (MEF2) (Bers, 2008). CaMKII-dependent MEF2 activation is strongly implicated in the development and progression of hypertrophy. There are four distinct CaMKII isoforms (α, β, γ, δ), with α and β restricted to neuronal tissue, while γ and δ are more ubiquitous, with δ as the predominant isoform in the heart. They all contain a N-terminal catalytic, a

central regulatory (with autophosphorylation site T286) and a C-terminal association domain. During CaMKII activation, Ca^{2+}-CaM displaces the autoinhibitory domain thereby activating the enzyme. The kinase can then lock itself into the activated state by auto-phosphorylation at T286 (Maier and Bers, 2002). To date, 13 splice variants of the CaMKIIδ have been identified, with δB and δC shown to be present at the protein level in the adult mammalian myocardium (Zhang and Brown, 2004). CaMKIIδB contains a nuclear localization sequence (NLS) and therefore compartmentalizes to the nucleus, while CaMKIIδC without NLS accumulates in the cytoplasm, but neither localization is exclusive. CaMKIIδC is mostly involved in tuning E-C coupling by modulation of Ca^{2+} handling proteins such as PLB, RyR, and LTCC, whereas CaMKIIδB targets proteins involved in the regulation of transcription, e.g. class II HDACs. Acetylation of conserved lysine residues in histone tails by histone acetyltransferases (HATs) stimulates gene expression by neutralizing positive charge, resulting in destabilization of histone–histone and histone–DNA interactions, while histone deacetylases (HDACs) promote chromatin condensation and thereby repress transcription (Figure 3-6). The association of HATs and HDACs with sequence-specific DNA-binding factors enables target gene-specificity to their actions (Backs and Olson, 2006, Heineke and Molkentin, 2006). Most class II HDACs (HDAC4, -5, -7, and -9) are expressed in the heart and have a unique MEF2-binding domain and two conserved serines in the N-terminal extension. When these serines are phosphorylated, HDACs bind to the chaperone 14-3-3 (masking a nuclear localization signal), and the complex is exported from the nucleus via CRM1

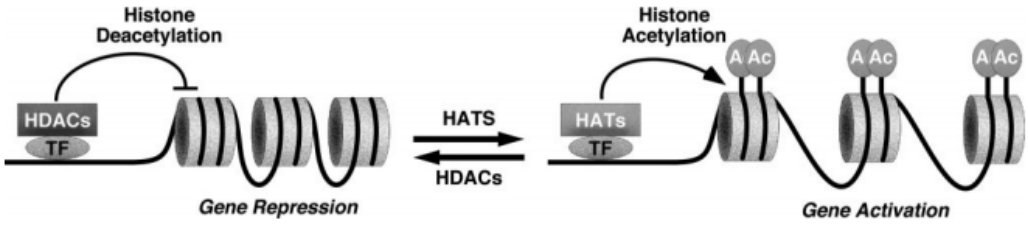

(chromosomal region maintenance protein 1) (thereby relieving MEF2 repression).

Figure 3-6. Role of histone acetylation and deacetylation.

(taken from Backs and Olson, 2006)

Another target for CaM is a Ca^{2+}/CaM-dependent serine/threonine protein phosphatase 2B or calcineurin (CaN). Calcineurin (phosphatase 2B) is a heterodimer that consists of two subunits: the catalytic unit CnA and the regulatory unit CnB (Heineke and Ritter, 2012). Calcineurin binds Ca^{2+}-CaM with much higher affinity than CaMKII. Therefore, whereas CaMKII may be activated preferentially by high-amplitude CaTs (at systole) and requires autophosphorylation for full activation, calcineurin may be better at sensing smaller sustained Ca^{2+} elevations (Molkentin, 2004). Upon activation by Ca^{2+}-CaM, calcineurin dephosphorylates four cardiac NFAT isoforms (c1-c4), leading to their import into the nucleus, where NFAT can work cooperatively with the cardiac-restricted zinc finger transcription factor GATA4/6 to activate hypertrophic gene transcription (Molkentin, 2004, Lunde et al, 2011).

These Ca^{2+}-CaM-dependent excitation-transcription coupling pathways are involved in altering the transcription of key Ca^{2+} regulatory proteins such as SERCA, PLB, NCX, RyR2, CaM, and CaMKII and may be part of a long-term feedback loop that either normalizes cardiac myocyte function or contributes to the exacerbation of hypertrophy or HF phenotypes. It is not completely understood, however, how the key signaling molecules (including Ca^{2+}) interact functionally and are targeted to the appropriate Ca^{2+} microdomains and how cells distinguish between Ca^{2+} involved in E-C coupling and transcriptional regulation.

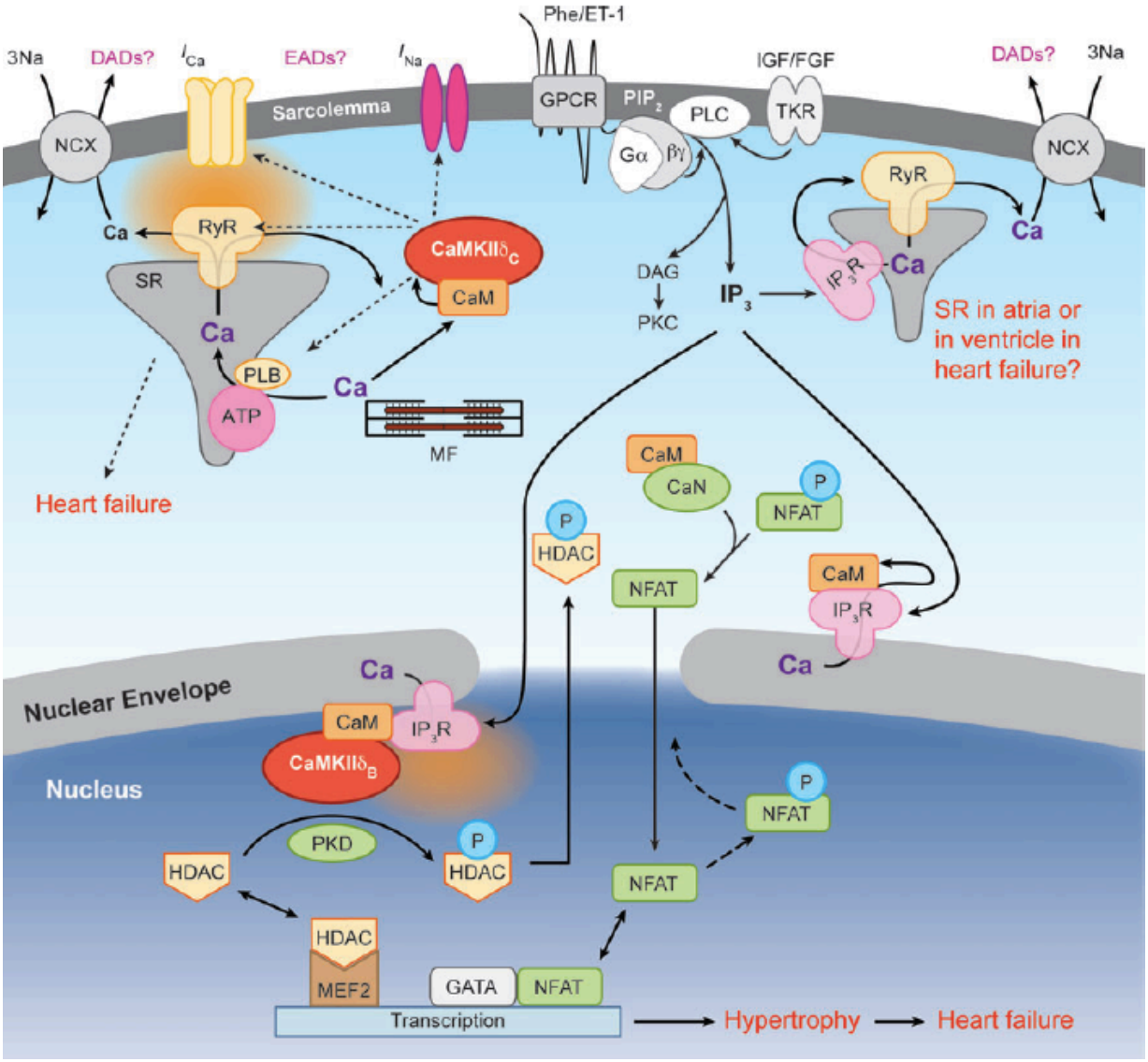

Figure 3-7. Ca^{2+}-dependent transcriptional activation in cardiac myocytes.

Gq protein–coupled receptor (GPCR) agonists (ET-1, ATII or α-adrenergic agonists) and tyrosine kinase receptor (TKR) agonists (insulin-like growth factor (IGF) and fibroblast growth factor (FGF)) can activate PLC to produce DAG and IP3. IP3Rs in the nuclear envelope associate with calcium-calmodulin-dependent kinase $II\delta_B$ ($CaMKII\delta_B$), and upon activatation by local IP3 mediate Ca^{2+} release, resulting in HDAC phosphorylation (which also occurs by PKD) and nuclear export. This relieves HDAC-dependent suppression of MEF2-driven transcription. CaN is activated by Ca^{2+}-CaM and can dephosphorylate NFAT, causing its translocation to the nucleus, where, along with the transcription factor GATA, it can stimulate hypertrophic gene transcription. The orange clouds indicate where local [Ca^{2+}] elevation is critical for signaling near RyR and IP3R. P indicates phosphorylation, MF denotes myofilaments, and Gα and Gβγ are subunits of the G protein Gq. (image taken from Bers, 2008)

3.5. Role and regulation of nuclear Ca^{2+} signaling

Ca^{2+} is probably the most versatile second messenger used by all cell types, but no other cell type uses Ca^{2+} in such different ways as cardiac myocytes. Ca^{2+} is essential for normal cardiac physiology and at the same time represents a major contributor to heart disease. The mechanisms by which the heart distinguishes between different Ca^{2+} signals are only beginning to be elucidated.

A major problem in understanding how Ca^{2+} controls cardiac hypertrophy is the fact that the heart is continuously subjected to large periodic Ca^{2+} signals that flood through the cytoplasm during each heart beat. The question is how excitation-transcription (E-T) coupling functions in cardiomyocytes, where intracellular [Ca^{2+}] is constantly oscillating. During each heart beat the cytoplasmic Ca^{2+} CaT also elicits a nucleoplasmic CaT with some delay (Ljubojevic et al, 2011). It is speculated that Ca^{2+}-dependent hypertrophic gene transcription might result from subtle alterations in the spatio-temporal properties of cytoplasmic CaTs, prolongation of CaTs or increases in the amplitude of CaTs integrated over time (Berridge et al, 2003).

While alterations in cytoplasmic Ca^{2+} regulation have been clearly implicated in the pathophysiology of cardiac disease, nucleoplasmic Ca^{2+} signaling has been studied much less, but may be critical for the development of cardiac hypertrophy and the progression of HF. Increases in nucleoplasmic [Ca^{2+}] may activate the broad array of transcription factors, thereby modulating gene expression (Dolmetsch et al, 1998), and it has been reported to be involved in the development of cardiac hypertrophy and HF (Zhang et al, 2004, Dominguez-Rodrigez et al, 2012).

As mentioned above, nuclear Ca^{2+} is involved in the regulation of transcription (referred to as E-T coupling), but the mechanisms regulating nuclear Ca^{2+} levels are not well understood. Whether or not nuclear Ca^{2+} signaling is independently regulated from cytosolic Ca^{2+} is not completely clear. The reason for the slower kinetics of nucleoplasmic CaTs lies in the fact that the nucleus is insulated from the surrounding cytoplasm by the nuclear envelope (NE). The NE controls bidirectional

transport of ions (including Ca^{2+}) and macromolecular cargo and acts as a Ca^{2+} reservoir contiguous with the SR that regulates nucleoplasmic Ca^{2+} concentration (Wu and Bers, 2006). The NE is perforated by macromolecular nuclear pore complexes (NPCs) connecting the nucleoplasm and the cytoplasm and enabling the passive diffusion of small molecules and ions between these two compartments (Capelson et al, 2011). The NE surface has deep folds (invaginations) that reach deep into the centre of the nucleus, forming so-called ‘’nucleoplasmic reticulum’’ or ‘’ nuclear tubules’’. Such a network of NE invaginations has been identified in many cell types and cardiomyocytes (Echevarria et al, 2003, Bootman et al, 2009, Escobar et al, 2011, Malhas et al, 2011, Alonso and Sancho, 2011, Ljubojevic et al, 2014). The lumen in the centre of the nuclear tubules is contiguous with the cytosol, allowing cytosolic messengers to gain increased access to the deeper regions of the nucleus that would otherwise be remote from the nuclear periphery (Escobar et al, 2011). Thus, during each heart beat, cytoplasmic Ca^{2+} can passively diffuse into the nucleus through nuclear pore complexes, causing a delayed nuclear CaT. The question whether and how nuclear [Ca^{2+}] can be regulated actively remains controversial. In favor of the possibility of the existence of independent nuclear Ca^{2+} signals are many reports of Ca^{2+} signaling systems in the nucleus. Several proteins involved in calcium signaling directly or indirectly have been observed within the NE including: Ca^{2+} release channels (RyRs, IP3Rs), Ca^{2+} reuptake proteins (SERCA on the outer membrane, NCX on the inner membrane, PLB), and Na^{+},K^{+}-ATPase (Gerasimenko et al, 2004, Marius et al, 2006, Ledeen and Wu, 2007, Wu et al., 2006, Bootman et al, 2009, Galva et al, 2012, Wu et al, 2016). Furthermore, the entire phosphoinositide network is present in the NE: GPCRs for ET-1 and ATII, phosphoinositide-specific phospholipase C (PLC) and phosphatidylinositol 4,5-bisphosphate (PIP2) (Tadevosyan et al, 2012). Moreover, it has been shown that the prohypertrophic agonist ET-1 – via IP3R-induced Ca^{2+} release (IICR) from the nuclear envelope – may preferentially elevate nuclear [Ca^{2+}] (Kockskämper et al, 2008, Wu et al, 2006).

Taken together, nucleoplasmic [Ca^{2+}] elevations result from Ca^{2+} that passively diffuses from the cytoplasm through NPCs and Ca^{2+} that is actively released from the NE (Figure 3-8). The increase in nucleoplasmic [Ca^{2+}] is an important determinant for regulation of transcription and might play a role in the pathogenesis of HF. However, there is lack of studies dealing with the regulation and alterations of nucleoplasmic Ca^{2+} handling under pathophysiological conditions.

As mentioned before, hypertension is the most common stimulus implicated in inducing pathological cardiac hypertrophy and HF. Better understanding of the fundamental processes that initiate and novel strategies to prevent or regress cardiac hypertrophy are needed. Nuclear Ca^{2+} represents a novel interesting target.

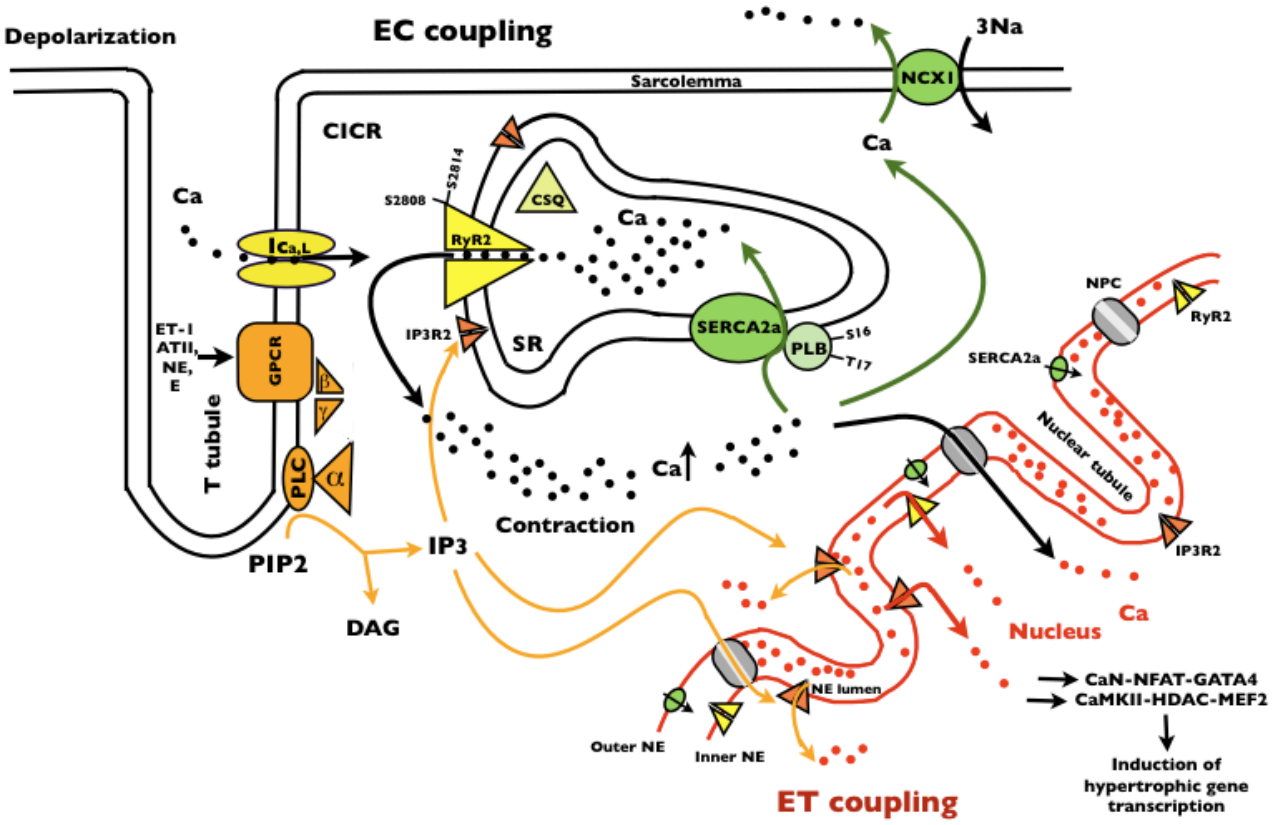

Figure 3-8. Mechanisms of nucleoplasmic [Ca^{2+}] regulation.

(for details see text)

3.6. Spontaneously hypertensive rats (SHR) as a model for hypertensive heart disease

Spontaneously hypertensive rats (SHR) represent a useful and well-characterized model of genetic hypertension and naturally evolving HHD (Doggrell and Brown, 1998, Kokubo et al, 2005). The SHR strain was obtained by Okamoto and colleagues during the 1960s by selective inbreeding of Wistar-Kyoto rats (WKY) with the highest blood pressure (Okamoto & Aoki, 1963). Therefore, the normotensive WKY are employed as controls for SHR (Doggrell & Brown, 1998).

The effects of hypertension in SHR resemble many aspects of hypertension in humans (Brooksby et al, 1993, Tomanek and Hovanec, 1981), making these rats a suitable animal model for studying of hypertension-induced ventricular remodeling during hypertrophy and HF. As in the case of human hypertension, first comes the pre-hypertensive period, followed by a sustained elevation of blood pressure lasting for months, mimicking long lasting development of HHD in humans (Doggrell and Brown 1998). As in the case of human essential hypertension, specific genes involved in the development of hypertension have not been identified in SHR. Although some studies revealed several changes in genes that might be responsible for hypertension development in these rats (Doggrell & Brown 1998), the link between these alterations and hypertension remains unclear.

There are several studies suggesting possible factors that might contribute to the development of hypertension in SHR. Again, as in humans, the kidney is the first suspect in the pathophysiology of hypertension. An impairment of kidney function was reported in SHR. Transplantation of kidneys from SHR to normotensive rats increased the blood pressure of the recipients, while transferring a WKY kidney to SHR normalized blood pressure in the hypertensive recipients (Bianchi et al. 1974, Vaneckov et al, 2002). SHR were also shown to exhibit increased activity of the RAAS (Kodavanti et al, 2000, Shanks and Herring, 2013). Neonatal sympathectomy with anti-nerve growth factor reduced hyperplasia of the arterial smooth muscle and

prevented the development of hypertension in SHR, suggesting a role of increased sympathetic innervation in elevating blood pressure in SHR (Brock et al, 1997).

Cardiovascular changes during progression of HHD throughout the lifespan of SHR are well characterized (Figure 3-9). SHR are normotensive the first 6 weeks of age, rapidly develop hypertension at 8–12 weeks of age, and remain hypertensive thereafter. After the onset of hypertension, LV hypertrophy gradually develops in SHR from 3–15 months of age, and HF typically occurs at 15-24 months of age (Figure 3-9). Hypertrophy is associated with extensive fibrosis and HF is characterized as diastolic and systolic with dilatation of the left ventricle (Chan et al. 2011).

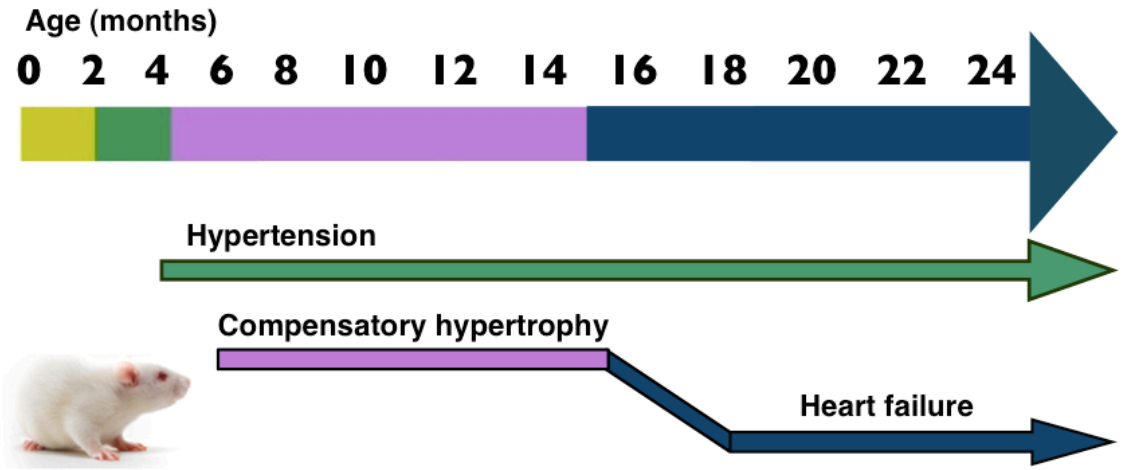

Figure 3-9. Development of hypertension and HHD throughout the lifespan of SHR.

SHR have been used intensively to study hypertension-induced ventricular remodeling during hypertrophy and HF. SHR is a suitable model to study the transition from compensated LV hypertrophy to HF, since this progression is associated with aging, the same as in humans (Bing et al. 2002). Very little is known, however, about the onset of hypertrophy and the onset of HF and what is the trigger for initiation of hypertrophy and transition to HF.

Earlier studies have shown a link between hypertension and remodeling of E-C coupling and cytoplasmic Ca^{2+} signaling in SHR (Brooksby et al, 1993, Chen-Izu et al, 2007, Harzheim et al, 2009, Fowler et al, 2005, Shorofsky et al, 1999). It is not known, however, whether there are also specific alterations in nuclear Ca^{2+} handling in response to hypertension. This might be particularly important since nuclear Ca^{2+} alterations could be linked directly to altered transcription and, thus, the development and progression of hypertrophy and HF in HHD.

3.7. Aims of the study

During the course of HHD, there is evidence for alterations of cytoplasmic Ca^{2+} handling associated with hypertrophy and HF. However, very little is known about the onset of hypertrophy and HF, about the trigger for initiation of hypertrophy and HF and about the time course of the critical changes. Cytoplasmic Ca^{2+} is important in the activation of specific hypertrophic signaling cascades. However, nuclear Ca^{2+} handling may directly impact gene expression and may play a crucial role in the initiation and progression of hypertrophy. There is, however, almost no data available regarding cytoplasmic vs. nucleoplasmic Ca^{2+} handling, the mechanisms involved in regulating nuclear Ca^{2+} levels and the potential alterations of these mechanisms in the pathogenesis of hypertrophy and heart failure.

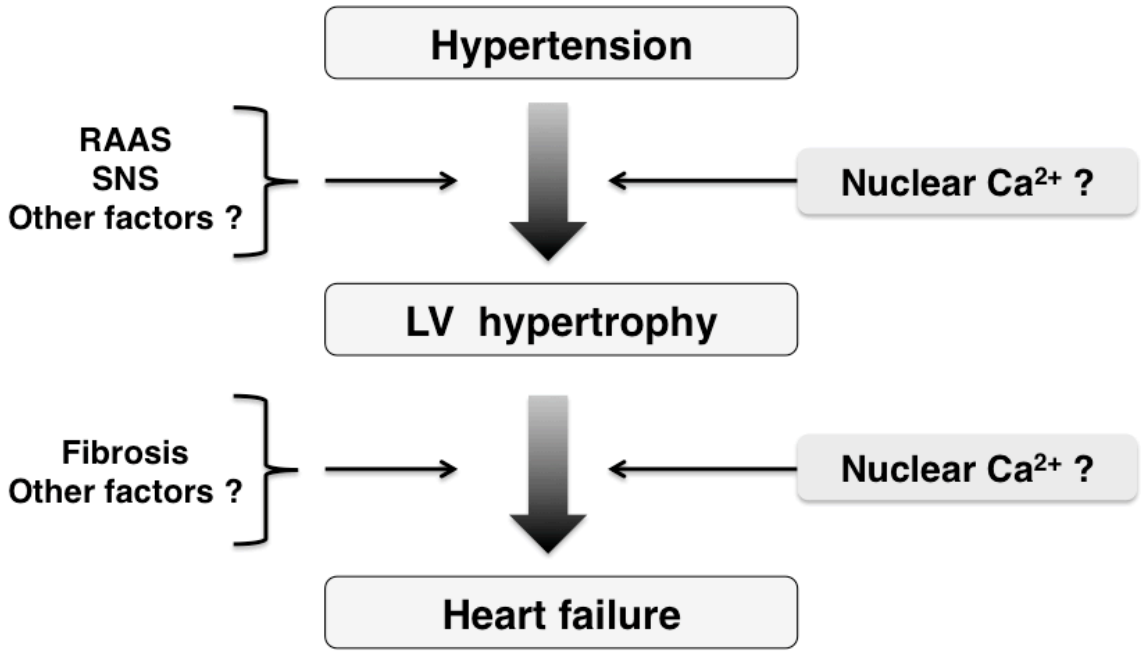

Figure 3-10. Nuclear [Ca^{2+}] regulation during the onset of hypertrophy and HF.

We hypothesized that maladaptive remodeling of nuclear structure and nuclear Ca^{2+} signaling might occur early in hypertension (Figure 3-10), contributing to initiation and progression of hypertrophy, and at later stages of HHD, therefore also contributing to the transition from compensated hypertrophy to HF.

To test our hypothesis we studied hypertension-induced structural and functional (Ca^{2+} signaling) remodeling of LV myocytes and nuclei from SHR at different ages and disease stages:

1. in 6 weeks old SHR, i.e. prehypertensive rats,
2. in 12-14 weeks old SHR, i.e. shortly after the development of hypertension and
3. in 15-25 months old SHR, in the period when they gradually develop HF.

Age-matched WKY were used as normotensive controls for SHR.

The major goals of this study were:

1. To compare subcellular CaTs in the cytoplasm and nucleoplasm between WKY and SHR at three age points using Fluo-4 as Ca^{2+} indicator.
2. To compare Fluo-4 properties in the cytoplasm and nucleoplasm between WKY and SHR and perform proper quantification of nucleoplasmic and cytoplasmic CaTs by means of transforming raw fluorescence signals into calibrated [Ca^{2+}].
3. To elucidate possible mechanisms and factors that contribute to changes in cytoplasmic vs. nuclear Ca^{2+} handling
    - by measuring SR and perinuclear (PN) Ca^{2+} content and fractional Ca^{2+} release
    - by analysing intranuclear Ca^{2+} propagation
    - by assessing potential underlying structural alterations of the nucleus
    - by analysing protein expression of major Ca^{2+}-regulating proteins
4. To unravel the consequences of altered Ca^{2+} signaling on Ca^{2+}-dependent regulation of transcription.

4. Materials and methods

4.1. Animals

Male spontaneously hypertensive rats (SHR) at the age of 6 weeks to 25 months and age-matched normotensive Wistar-Kyoto control rats (WKY) were obtained from Charles River (Köln, Germany) or Janvier (Saint Berthevin, France). Animals were anesthetized with isoflurane and sacrificed by decapitation. The study was performed in accordance with European Union Council Directive 2010/63/EU and the German Animal Welfare Act (Tierschutzgesetz) and approved by local animal welfare authorities (Regierungspräsidium Gießen, experimental project V 54 - 19 c 20 15 (1) MR 20/29 Nr. A 21/2010 and AK-9-2014-Kockskämper, approved by animal welfare officer, University of Marburg).

4.2. Isolation of left ventricular myocytes

4.2.1. Chemicals and reagents

Preparation of all solutions and buffers were performed using demineralised, ultrapure water (ddH_2O), processed with the Milli-Q Reference A+ system (Merck Millipore, Darmstadt, Germany). Most chemicals were purchased from Roth (Karsruhe, Germany) or Sigma-Aldrich (München, Germany). All companies will be listed in the following tables or mentioned in the text.

4.2.2. Solutions for ventricular myocytes isolation

All solutions (listed in Table 4-2) were made freshly on the day of cell isolation from the basic isolation Tyrode's solution (Table 4-1). Basic isolation Tyrode's solution was prepared one day in advance, kept in the fridge and used in the following 1-2 weeks.

Table 4-1. Basic isolation Tyrode's solution (1 l, pH 7.4)

Substance	Quantity	Company	Final concentration
NaCl	7.597 g	Roth	130 mM
KCl	0.403 g	Roth	5.4 mM
1 M $MgCl_2$	0.5 ml	Sigma	0.5 mM
0.33 M NaH_2PO_4 x $2H_2O$	1 ml	Roth	0.33 mM
HEPES	5.958 g	Roth	25 mM
Glucose x H_2O	4.356 g	Roth	22 mM
100 U/ml Insulin human	100 µl	Sigma	0.01 U/ml
1 M NaOH was used for adjusting pH			

Table 4-2. Solutions made from basic isolation Tyrode's solution

Solution name	Basic Tyrode's solution (ml)	Substance	Quantity	Company	Final concentration
1. Cannulation solution	250	1 M $CaCl_2$	37.5 µl	Sigma	0.15 mM
		5 kU/ml Heparine-Na^+	100 µl	Roth	2 U/ml
2. Ca^{2+}-free solution	50	100 mM EGTA	200 µl	Roth	0.4 mM
		BDM	50 mg	Roth	1 mg/ml
		5 kU/ml Heparine-Na^+	20 µl	Roth	2 U/ml
3. Enzyme solution	50	Collagenase Type-2 (255-330 U/mg)	40 mg	Worthington, USA	0.8 mg/ml
		Protease Type XIV	2.5 mg	Sigma	0.05 mg/ml
		1 M $CaCl_2$	10 µl	Sigma	0.2 mM
		BDM	50 mg	Roth	1 mg/ml
4. Stop solution	15	1 M $CaCl_2$	7.5 µl	Sigma	0.5 mM
		BDM	15 mg	Roth	1 mg/ml
		Albumin fraktion V	30 mg	Roth	2 mg/ml
5. Ca^{2+} solution 1	15	1 M $CaCl_2$	15 µl	Sigma	1 mM
		Albumin fraktion V	30 mg	Roth	2 mg/ml
6. Ca^{2+} solution 2	100	1 M $CaCl_2$	150 µl	Sigma	1.5 mM

4.2.3. Principles of retrograde heart perfusion: the Langendorff method

The retrograde heart perfusion method was developed by Oscar Langendorff in 1895. With this technique the heart is perfused by cannulating the aorta. Due to the fact that the perfusion buffer flows opposite to normal physiologic flow (retrogradely) down the aorta, the aortic valve stays closed under pressure. The perfusion buffer fills the coronary arterial vasculature via the two coronary ostia (left and right) in the aortic root, passes through the vascular bed to the coronary veins and reaches the coronary sinus in the right atria, located superior to the septal leaflet of the tricuspid valve on the posterior atrial wall (Bell et al, 2011).

The Langendorff perfusion technique represents the basis for isolating viable cardiac myocytes from intact hearts. For this purpose, the Langendorff apparatus is running in the constant flow mode, where the heart perfusion is achieved by a peristaltic pump filling a compliance chamber, to which the aortic cannula is attached. This is an important setting, because digestion with collagenases is impairing normal vascular function. Quick and efficient cannulation and transfer of the heart to the Langendorff system is crucial for the quality of myocyte preparations. While transferring, special care should be taken in preventing the air to enter the coronary vasculature leading to emboli and microvascular obstruction, which has detrimental influence on experimental outcomes and myocyte yield. Additionally, during the isolating procedure the cannula should not be inserted too deeply into the aorta, as this can lead to mechanical rupture of the aortic valve leaflets. The time taken from the moment of the opening of the thorax till the heart is mounted and perfused on the Langendorff system should be under 5 min to avoid either the potential effect of ischaemic preconditioning due to delayed perfusion or damaging the heart due to prolonged hypoxia. Maintenance of the heart temperature at 37°C throughout the Langendorff perfusion is also critical. This is accomplished by using waterbath-jacketed tubes for keeping the circulating perfusion buffer at 37°C and by immersion of the perfused heart in a waterbath-jacketed organ bath fillled with perfusion buffer. In this way the heart is digested more efficiently from inside and outside. To maintain sufficient O_2 supply of the heart, all solutions used for perfusion must be oxygenated through bubbling with 100% O_2 through sintered glass oxygenators.

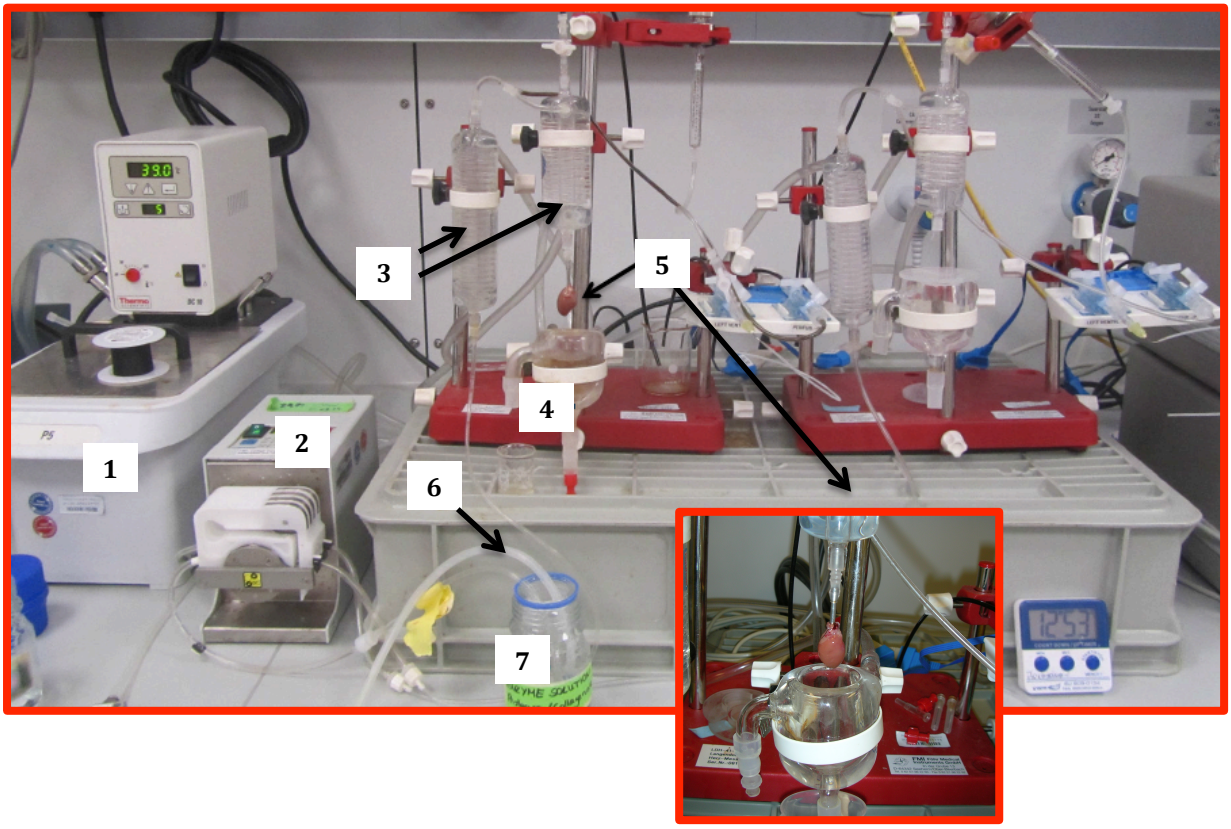

Figure 4-1. Langendorff system.

1-circulating waterbath, 2-peristaltic pump, 3-waterbath-jacketed tubes, 4-waterbath-jacketed organ bath, 5-heart cannulated through the aorta, 6-O_2-bubbling system, 7-perfusate reservoir

4.2.4. Myocyte isolation procedure

Rats were anesthetized with isoflurane and killed by decapitation. After opening the thorax, heparin solution (1000 U/ml) was injected directly into the hearts. Hearts were removed in oxygenated ice-cold cardioplegic solution (cannulation solution with 20 mM KCl in addition), rapidly cannulated through the ascending aorta, transferred to the Langendorff system and perfused with oxygenated cannulation solution (37°C) to remove the rest of the blood. Subsequently, hearts were washed with Ca^{2+}-free solution (37°C) for another 4 min before being perfused with enzyme solution (37°C). When digested, the heart becomes very soft and pale. When pressed with the forceps, the heart loses shape and hangs like a bag. In a drop of the solution taken from the surface of the heart, lots of cells can be found. At that point, the LV wall with septum was separated from the heart, put into the stop solution (37°C), gently cut and filtered through sieve cloths with 300 µm pores (Kobe, Germany). The extracellular [Ca^{2+}] was increased gradually by allowing the cells to reach normal intracellular [Ca^{2+}] without becoming Ca^{2+} overloaded and depolarized, in such a way preventing cell damage (Louch et al, 2011). The cells were precipitated for 10 min and the stop solution was gently exchanged for Ca^{2+} solution 1 (RT). Cells were adapted to the Ca^{2+} solution 1 for 10 min before solution exchange to Ca^{2+} solution 2 (without BDM, RT). Isolated myocytes were stored at RT and used within 10 hours after isolation.

4.2.5. Plating of isolated ventricular myocytes

Glass coverslips or glass-bottomed culture dishes (WillCo, Netherlands) were coated with 50 µg/ml laminin (Sigma-Aldrich, München, Germany) diluted with Ca^{2+} solution 2 for about 1 h at RT. After that, the remaining laminin was removed and the myocytes were seeded onto the coverslips and allowed to attach for about 20 min before being loaded with fluorescent dyes.

4.3. Confocal Ca^{2+} imaging

4.3.1. Measuring free intracellular [Ca^{2+}]

There are various Ca^{2+} indicators in current use, but the most popular are BAPTA-based fluorescent compounds that undergo large fluorescence enhancements or spectral shifts upon binding Ca^{2+}. Quantification of Ca^{2+} using fluorescent ion indicators can be performed using ratiometric or non-ratiometric methods. Principally, those compounds that only show an ion-dependent fluorescence intensity increase (intensity shift) are used for non-ratiometric recordings (most popular Fluo-3 and Fluo-4). Compounds which present a shift in their spectra (emmision or excitation spectral shift) upon binding ions are commonly referred to as ratiometric indicators (commonly used Fura-2 and Indo-1) (Figure 4-2).
Therefore, changes in [Ca^{2+}] are related (http://www.embl-heidelberg.de/eamnet/html/calcium/dyes/fluorescentdyes1.htm) either to changes in fluorescence intensity (non-ratiometric indicators) or fluorescence intensity ratio (ratiometric indicators) of a chosen dye.

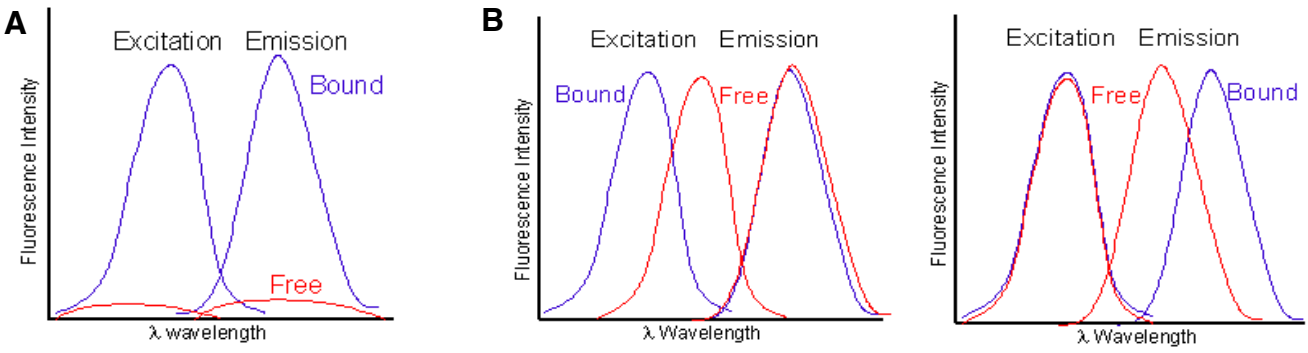

Figure 4-2. Principles of Ca^{2+} measuring using non-ratiometric and ratiometric methods.

(A) Non-ratiometric fluorescent ion indicators (undergoing *intensity shift* upon binding Ca^{2+}), **(B)** Ratiometric fluorescent ion indicators (undergoing *spectral shift* upon binding Ca^{2+}) (taken from http://www.embl-heidelberg.de/eamnet/html/calcium/dyes/fluorescentdyes1.htm)

Usefulness of fluorescent Ca^{2+} indicators is determined by their key characteristics, which include excitation and emission wavelengths (λ_{ex}, λ_{em}), fluorescence enhancements induced by Ca^{2+} binding, Ca^{2+} dissociation constants ($K_{d(Ca2+)}$) and ease of use.

Ratiometric indicators are the most useful for quantitative measurements of [Ca^{2+}]. Compared to non-ratiometric indicators, their dynamic range (difference in intensities between Ca^{2+}-free and Ca^{2+}-bound indicator) is often smaller, which is a disadvantage, making it harder to detect modest Ca^{2+} changes. As the most popular ratiometric Ca^{2+} indicators, Fura-2 and Indo-1 are excited by UV light, which has potential drawbacks such as known biological effects and its generally poorly transmission by most objectives and other optical components such as light guides (Paris et al, 2014).

Fluo-4 is a commonly used non-ratiometric Ca^{2+} dye, stable and easy to handle, and it can be loaded into cells in membrane-permeable (AM (acetoxymethyl) ester form) or in salt form. It displays high Ca^{2+}-dependent fluorescence enhancement and a $K_{d(Ca2+)}$ of 345 nM (in vitro), making it well suited for recording physiologically relevant Ca^{2+} changes in a variety of cell types. Fluo-4 and related dyes possess a BAPTA-like Ca^{2+} chelator component covalently bound to a fluorogenic, fluorescein-like component (Figure 4-3 taken from Molecular Probes, Handbook of fluorescent probes and research products (9th edition), www.probes.com). Fluo-4 absorbs 488 nm excitation light (from argon laser) more efficiently than Fluo-3, generating more intense fluorescence, so lower dye concentrations can be used to produce the same fluorescence signal intensity, reducing Ca^{2+} buffering effects and minimizing the levels of toxic by-products (formaldehyde and acetic acid) from acetoxymethyl ester hydrolysis and photobleaching of the dye (Gee et al, 2000).

A

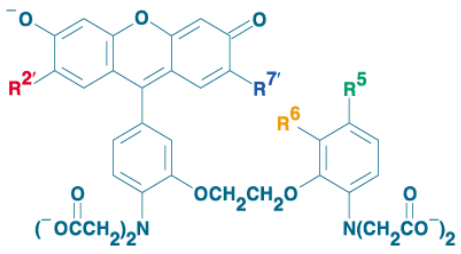

Indicator	$K_d(Ca^{2+})$	$R^{2'}$	$R^{7'}$	R^5	R^6
Fluo-3	0.39 µM	Cl	Cl	CH_3	H
Fluo-4	0.35 µM	F	F	CH_3	H
Fluo-5F	2.3 µM	F	F	F	H
Fluo-5N	90 µM	F	F	NO_2	H
Fluo-4FF	9.7 µM	F	F	F	F

B

Property	Fluo-4
$K_{d\ (Ca2+)}$ in vitro	345 nM
Absorption maximum (Ca^{2+}-bound)	494 nm
Emission maximum (Ca^{2+}-bound)	516 nm

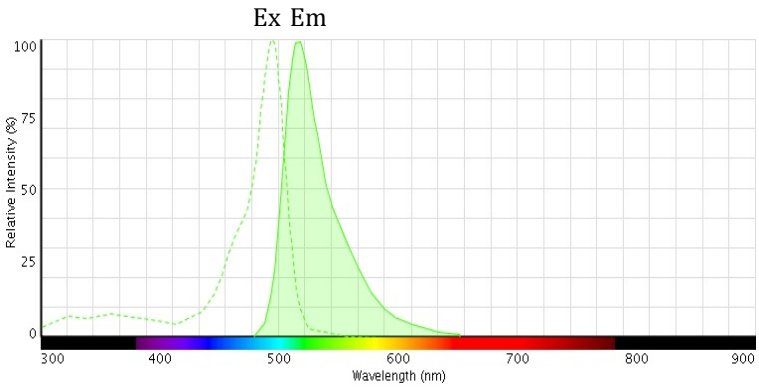

Figure 4-3. Structure of Fluo-X-dyes (A) and major properties of Fluo-4 (B).

(taken from Molecular Probes, Handbook of fluorescent probes and research products (9th edition), www.probes.com)

The K_d of fluorescent ion indicators is influenced by a number of environmental factors, including pH, temperature, ionic strength, viscosity, the presence of competing ions, and protein binding. Usually, the K_d values measured inside living cells are significantly higher than those measured in vitro and there are variations of indicator properties between various organelles. Indeed, it has been reported that Fluo-4 fluorescence emission can be twofold greater in nucleoplasm than in cytoplasm under normalized Ca^{2+} indicator and [Ca^{2+}] levels. The differences in K_d likely result from indicator-protein interactions or possible variation in viscosity (Hagen et al, 2012). So, since Fluo-4 fluorescence changes do not present accurate Ca^{2+} changes, for quantitative [Ca^{2+}] values calibration of the dye is usually recommended. For relative values of calcium concentration (semi-quantitative values) fluorescence intensity values for each cell during an experiment should be divided by their resting intensities, to account for the differences in loading of the dye between the cells.

4.3.2. Loading of the ventricular cells with Fluo-4/AM

Fluo-4 cannot easily cross cellular membranes in anionic polycarboxylate free form. The carboxylates can be masked as AM esters, making the Fluo-4 molecule hydrophobic and membrane-permeant (Figure 4-4 taken and modified from Dojindo Molecular Technologies http://www.dojindo.com/store/p/541-Fluo-3-AM.html). Once inside the cell, cellular esterases cleave the labile AM esters to release the polycarboxylate Ca^{2+}-sensitive form. As a polar structure, it is membrane-impermeant, trapped and accumulated inside the cell (Hagen et al, 2012).

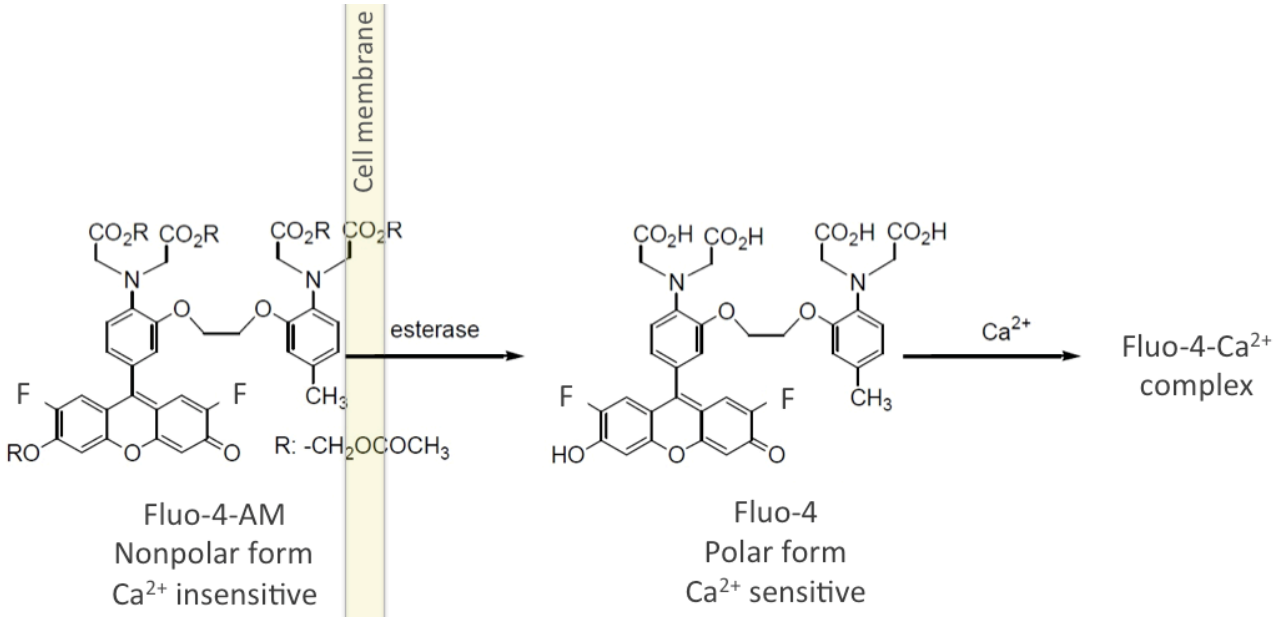

Figure 4-4. Fluo-4-AM loading into the cells.

(taken and modified from Dojindo Molecular Technologies
http://www.dojindo.com/store/p/541-Fluo-3-AM.html)

For my experiments, concentrated 1 mM stock solutions of Fluo-4/AM (Invitrogen) were prepared in 20% (w/v) Pluronic® F-127/DMSO (Invitrogen). Pluronic acid as a nonionic, surfactant polyol, has been shown to facilitate the solubilization of water-insoluble dyes in physiological media (Johnson and Spence, 2010). Before Ca^{2+} recordings, 8 µM Fluo-4/AM was prepared by diluting concentrated 1 mM Fluo-4/AM stock with recording Tyrode's solution (Table 4-3) and myocytes were loaded for 30 min and >20 min were allowed for de-esterification.

Table 4-3. Tyrode's solution used for loading and recording (1 l, pH=7.4)

Substance	Quantity	Company	Final concentration
NaCl	8.182 g	Roth	140 mM
KCl	0.373 g	Roth	5 mM
1 M $MgCl_2$	0.5 ml	Sigma	0.5 mM
1 M $CaCl_2$	1.5 ml	Sigma	1.5 mM
HEPES	2.383 g	Roth	10 mM
Glucose x H_2O	1.982 g	Roth	10 mM
1 M NaOH was used for adjusting pH			

4.3.3. Confocal Ca^{2+} imaging of subcellular CaTs

4.3.3.1. Principles of laser scanning confocal microscopy (LSCM)

The laser scanning confocal microscope is an essential tool for many biomedical imaging applications using fixed or living cells labeled with one or more fluorescent probes. When imaged using a conventional widefield optical microscope, fluorescence in the specimen in focal planes away from the region of interest influences resolution of structures in focus. Confocal microscopy has the ability to eliminate the "out-of-focus" light from thick fluorescently labeled specimens. The resolution achieved by the LSCM is a little better than that achieved in a conventional widefield light microscope (0.2 µm), but much less than that in the transmission electron microscope (0.1 nm), making LSCM a bridge between these two common techniques (Paddock et al, 2000).

Modern confocal imaging systems are based on the principle of confocal imaging patented by Marvin Minsky (illustrated in Figure 4-5 taken from Claxton et al., www.aptechnologies.co.uk) in 1955. The term ''confocal'' is derived from the fact that the point source of light, produced by a pinhole placed in front of a laser system

(excitation source), is in a conjugate plane (confocal) with a scanning point on the specimen and a second pinhole positioned in front of the detector (a photomultiplier tube). As the laser light gets reflected by a dichromatic mirror onto the specimen in a defined focal plane, secondary fluorescence emitted from the points on the specimen (in the same focal plane) pass back through the dichromatic mirror and get focused at the detector pinhole aperture, which has the same focus as the first pinhole (it is confocal with it). This second pinhole is the key for the elimination of out-of-focus light by spatial filtering. The fluorescence emitted from the points above and below the objective focal plane is not confocal with the pinhole and is not detected by the photomultiplier and, therefore, does not contribute to the resulting image. Confocal microscopy thus allows “optical sectioning” of a sample.

In traditional widefield optical microscopy, the entire specimen is illuminated from an incoherent mercury or xenon lamp, and the resulting secondary fluorescence emission can be viewed directly by eyes or projected to the electronic array detector or film plane. Image formation in a confocal microscope is fundamentally different and the sample is scanned with a finely focused spot of illumination (point scanning) that is centered in the focal plane. Fluorescence emission that is passed through the pinhole is converted into an analog electrical signal by the photomultiplier. The analog signal is sampled and converted into pixels by an analog-to-digital (A/D) converter and the final image is then displayed on a high-resolution video monitor. So the confocal image is reconstructed, point-by-point, from the emission photon signals by photomultiplier and accompanying electronics, but never exists as a real image that could be observed via microscope eyepieces (Paddock et al, 2000 and www.aptechnologies.co.uk).

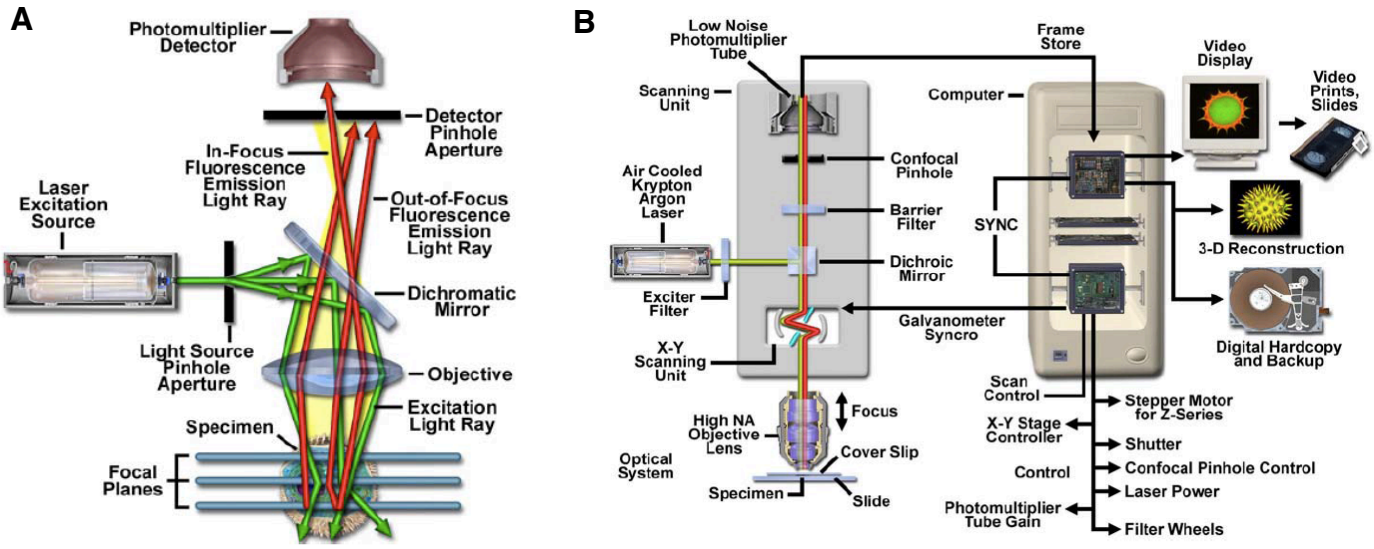

Figure 4-5. Principles of LSCM.

(A) Schematic diagram of the optical pathway and principal components in a LSCM,

(B) LSCM configuration and mechanism of image formation

(taken from Claxton et al, www.aptechnologies.co.uk)

So, major parts of the confocal microscope are (Figure 4-5): multiple laser excitation sources, a scan head with optical and electronic components (consisting of fluorescence filter sets (for excitation and emission), dichromatic mirrors, a galvanometer-based raster scanning mirror system and variable pinhole apertures), electronic detectors (usually photomultipliers) and a computer for acquisition, processing, display of images and analyses.

Confocal microscopes are classified by the method of the sample scanning. Minsky's original design was a stage-scanning system where the stage is moving in the x, y and z directions, while the laser illumination spot is held fixed. In modern LSCM a focused beam of light is raster scanned across the still sample. There are two different methods of beam scanning. The single-beam scanning technique is using either a pair of computer-controlled galvanometric mirrors to scan the sample at a rate of 1 frame per second (slow scanning) or acousto-optic devices or oscillating mirrors to obtain faster scanning (near video rates). The alternative is to scan the specimen with multiple beams (almost real time) usually using a spinning Nipkow disk containing an array of pinholes and microlenses.

4.3.3.2. Recordings of subcellular CaTs in left ventricular myocytes

Recordings of subcellular CaTs were performed using the linescan mode of a confocal microscope (LSM510, Carl Zeiss, Germany) possessing an argon ion laser (488 nm) and a x63 1.3 NA oil immersion objective (Figure 4-6).

Cells were electrically stimulated at 1 Hz at RT and constantly perfused with recording Tyrode's solution. Linescan images were acquired at a sampling rate of 3 ms per line (512 pixels per line; thickness of confocal plane was set to ≈1 μm). Fluo-4 was excited with the 488 nm line of the argon laser and fluorescence emission was collected at >505 nm.

Simultaneous recording of cyto- and nucleoplasmic CaTs was achieved by setting the confocal plane to the central depth (z axis) of the nucleus and positioning the line transversely through the cell crossing the nucleus.

In some cells, 10 mM caffeine was applied rapidly in order to estimate SR and NE Ca^{2+} load and fractional Ca^{2+} release.

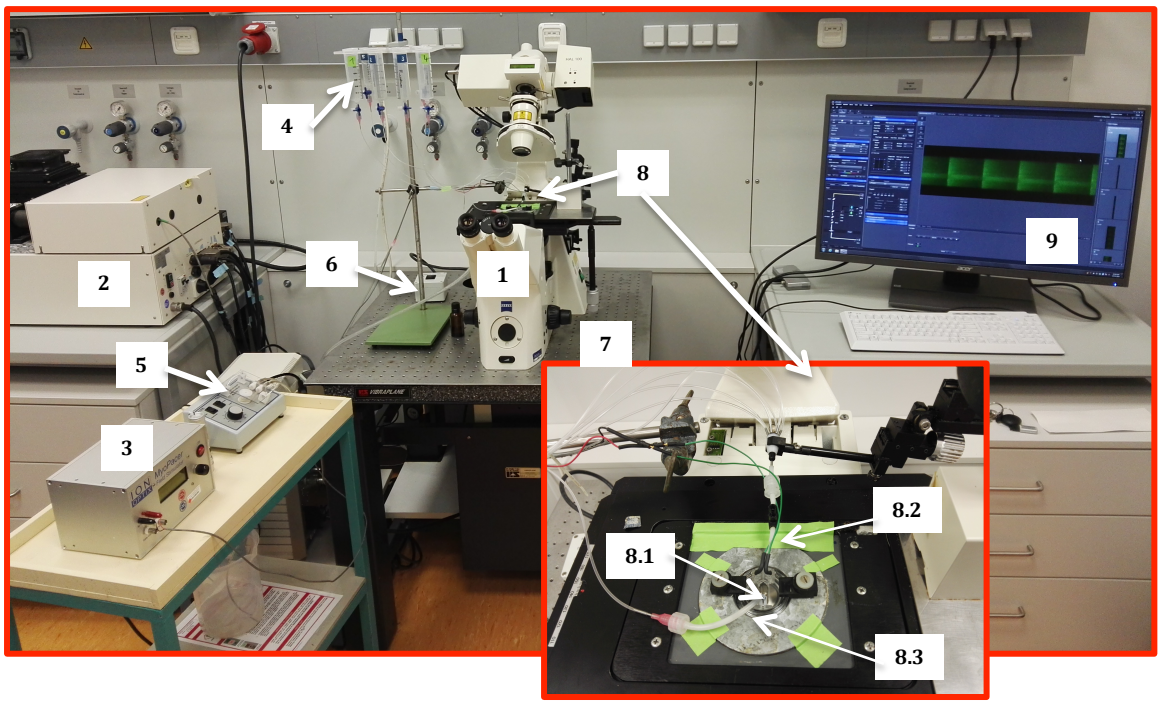

Figure 4-6. Laser scanning confocal microscope setup.

1-Axiovert 100 M microscope with the LSM 510 scanning module, 2-Laser module, 3-MyoPacer Cell Stimulator, 4-Gravity controlled perfusion system, 5-Peristaltic pump, 6-Remote control power switch, 7-Pneumatic vibration optical table, 8-Sample chamber (8.1-Platinum stimulation wires, 8.2-inflow, 8.3-outflow), 9-Acquisition computer

4.3.3.3. Analyses of subcellular CaTs

Confocal linescan images (Fluo-4 fluorescence) were analysed using ImageJ (NIH, Bethesda, USA). After background subtractions, 4-5 consecutive CaTs were averaged and the following parameters were analyzed: diastolic Ca^{2+} (F_o), peak systolic Ca^{2+} (F), amplitude of CaTs (dF), rise time (time from 10-90% of the peak) and the time constant τ of CaT decay (Figure 4-7). For relative calcium values, the diastolic (F_o) and systolic (F) fluorescence levels were normalized to the resting fluorescence measured 1 min after stopping stimulation (F_{rest}).

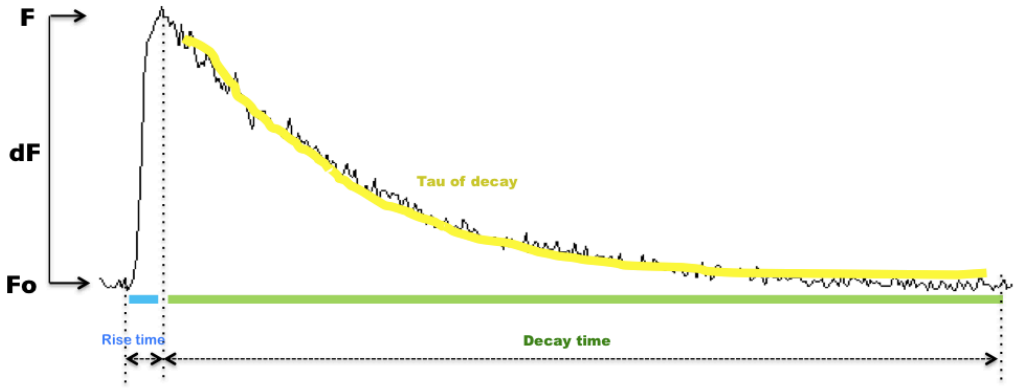

Figure 4-7. Analyses of CaTs.

For quantification of SR and NE Ca^{2+} load, the amplitude of the caffeine-evoked CaT (dF_{caff}) was normalized to the F_{rest}, and fractional release from SR and NE was calculated as the amplitude of the CaT just before caffeine application (dF_{ctrl}) divided by dF_{caff}.

Analysis of intranuclear Ca^{2+} propagation was performed according to a previously described method (Ljubojevic et al, 2014). Four to five consecutive CaTs of a very small (<1 μm) cytoplasmic region (C) close to the NE, a neighboring subnucleolemmal region (SN) and a central nuclear (CN) region were averaged. The velocities of Ca^{2+} propagation between these regions were calculated using the distance between the regions divided by the difference in the time to peak of the CaTs.

To confirm that nuclear borders defined by this method were accurately selected, nuclei of ventricular myocytes loaded with Fluo-4 were stained using the fluorescent

nucleic acid dye Syto-16 (Kockskämper et al, 2008). For this experiment, 1 mM Syto-16 stock solution was diluted 10 times with recording Tyrode's solution to get 100 µM Syto-16 working solution. 10 µl of 100 µM Syto-16 solution was then added directly onto the cells to the sample chamber with roughly 200 µl of circulating recording Tyrode's solution in it, giving a final Syto-16 concentration of 5 µM. The 2D image of the Fluo-4 loaded ventricular cell with confocal plane set to the middle of the nuclei and the linescan image acquired in the same way as described above were recorded before and 4 min after addition of Syto-16. Since Syto-16 produced very bright fluorescence, laser power had to be slightly reduced.

4.3.3.4. In situ calibration of Fluo-4 fluorescence in ventricular myocytes

The calibration experiments and the preparation of calibration solutions were done according to protocols described previously (Ljubojevic et al, 2011 and Allen and Hebert, Chapter 12, Methods in molecular biology: Nuclear G-protein coupled receptors, Methods and protocols, 2015).

The MaxChelator program http://maxchelator.stanford.edu/webmaxc/webmaxcS.htm was used to calculate total [Ca^{2+}] required to obtain the desired free [Ca^{2+}] in the presence of 1 mM EGTA and 0.5 mM $MgCl_2$, background ionic strength of 0.15 M, at 23°C and pH=7.4.

Initially, one main background solution was prepared containing (in mM): 138 NaCl, 5 KCl and 10 HEPES, pH=7.4. This solution was treated with Chelex 100 resin (200-400 mesh sodium, Bio Rad, CA, USA) for a week to make it Ca^{2+}-free and used for preparing two solutions: (a) EGTA solution and (b) CaEGTA solution containing 3 mM $CaCl_2$ in addition (Table 4-4). After adding $CaCl_2$ to the EGTA solution, pH was readjusted to pH=7.4. To assure an accurate EGTA concentration, we prebaked EGTA at 150°C for 3 h before dissolving.

Table 4-4. Two main solutions for preparing calibration solutions (pH 7.4)

EGTA solution	Substance	Quantity (For 2 l ddH_20)	Final C (mM)
	NaCl	16.146 g	138
	KCl	0.7456 g	5
	$MgCl_2$	1 ml (1 M $MgCl_2$)	0.5
	HEPES	4.766 g	10
	EGTA	20 ml (100 mM EGTA in 200 mM NaOH)	1
CaEGTA solution	**Substance**	**Quantity (For 1 l EGTA solution)**	**Final C (mM)**
	$CaCl_2$	3 ml (1 M $CaCl_2$)	3

On the day of experiments, calibration solutions of 0 nM, 250 nM, 1500 nM, 5000 nM and 2 mM free [Ca^{2+}] were prepared freshly by mixing appropriate amounts of EGTA and CaEGTA solution (Table 4-5). After confirming the appropriate temperature (23°C) and pH (7.4) of the solutions, to each solution I added the following inhibitors (Table 4-6) in final concentration (in mM): 15 BDM (2,3 butanedione monoxime, Roth), 1.8 2-deoxy-D-glucose (Merck Millipore), 0.01 rotenone (Merck Milipore), 0.005 CPA (cyclopiazonic acid, Merck Milipore) and 0.005 ionomycin (Enzo). BDM was used to inhibit contractures of the myocytes, 2-deoxy-D-glucose and rotenone to prevent energy production, ionomycin as Ca^{2+} ionophore to help equilibrate Ca^{2+} concentration across the membranes and CPA as SERCA inhibitor to block active Ca^{2+} transport.

Table 4-5. Preparation of calibration solutions

Free Ca^{2+} (µM)	Total Ca^{2+} (µM) Using MaxChelator Program	EGTA solution (ml)	CaEGTA solution (ml)
0	0	50	/
0.25	783	36.95	13.05
1.5	957	34.05	15.95
5	991	33.483	16.517
2000	3000	/	50

Table 4-6. Adding inhibitors to calibration solutions

Inhibitor	Stock	Quantity (For 50 ml)	Final C (mM)
BDM	-	75 mg	15
2-deoxy-D-glucose	-	15 mg	1.8
Cyclopiazonic acid (CPA)	50 mM in DMSO	5 µl	0.005
Rotenone (*light sensitive)	100 mM in DMSO	5 µl	0.01
Ionomycin (*light sensitive)	10 mM in DMSO	25 µl	0.005

Before starting with the calibration, Fluo-4-loaded cells were stimulated at 1 Hz for at least 2 min and cyto- and nucleoplasmic CaTs and resting fluorescence was recorded in the presence of the usual recording Tyrode's solution. Afterwards, cells were allowed to equilibrate in each calibration solution for 10-20 min. During this time, 2D fluorescence images (≈1 s scanning time) were recorded every minute. Minimum Fluo-4 fluorescence (F_{min}) was recorded in the presence of 0 nM [Ca^{2+}] and maximum Fluo-4 fluorescence (F_{max}) during exposure to a saturating free [Ca^{2+}] of 2 mM.

Concentration-response curves were constructed by plotting cyto- and nucleoplasmic Fluo-4 fluorescence versus [Ca^{2+}] and fitting the curves using the Hill equation:

$$F = ((F_{max} - F_{min}) / (1 + (K_d / [Ca^{2+}])^n)) + F_{min}. \quad (1)$$

From these curves we obtained the apparent Ca^{2+} dissociation constants (K_d) and the dynamic range ($R_f = F_{max}/F_{min}$) of Fluo-4 and the Hill coefficients (n) in both cyto- and nucleoplasm. Resting Ca^{2+} concentration, $[Ca^{2+}]_{rest}$, in cyto- and nucleoplasm was obtained from myocytes used for in situ calibration of Fluo-4 fluorescence by transforming resting Fluo-4 fluorescence using the equation for non-ratiometric dyes:

$$[Ca^{2+}] = K_d (F - F_{min}) / (F_{max} - F), \quad (2)$$

where F stands for F_{rest}.

Using $[Ca^{2+}]_{rest}$, K_d and R_f values, we applied the following equation for transforming the Fluo-4 fluorescence signals into absolute $[Ca^{2+}]$ in cells not subjected to the in situ calibration protocol (Ljubojevic et al, 2011):

$$[Ca^{2+}] = K_d (R (K_d + R_f [Ca^{2+}]_{rest}) - (K_d + [Ca^{2+}]_{rest})) / (R_f (K_d + [Ca^{2+}]_{rest}) - R (K_d + R_f [Ca^{2+}]_{rest})), \quad (3)$$

where R stands for the normalized Fluo-4 fluorescence signal, F/F_{rest}.

Peak systolic $[Ca^{2+}]$ calculated by equation (3) was in the range between ≈500 and 3000 nM for the majority of cells studied (>90%) from both WKY and SHR at all ages. A few cells, however, displayed very high systolic Fluo-4 fluorescence ratios (F/F_{rest}), which fell into the shallow non-linear part of the calibration curves. These cells were excluded from analysis when calculated peak systolic $[Ca^{2+}]$ exceeded a value of 10 µM.

4.3.3.5. Recording of Ca^{2+} in perinuclear Ca^{2+} stores

High affinity Ca^{2+} indicators can be used to quantify Ca^{2+} levels in the cytosol while low affinity Ca^{2+} indicators can be used for measuring Ca^{2+} in subcellular compartments with higher $[Ca^{2+}]$. The cell-permeant Mag-fluo-4/AM is an analog of Fluo-4 with a K_d for Ca^{2+} of 22 μM, making it useful as a low-affinity Ca^{2+} indicator. Mag-fluo-4/AM is a single wavelength (non-ratiometric) Ca^{2+} indicator with the excitation peak at 490 nm and the emission peak at 517 nm (Figure 4-8 taken from www.probes.com). To visualize this indicator, most investigators use a 488 nm excitation source (argon ion laser) and a 505-550 emission filter, the same settings as for Fluo-4/AM (Paredes et al, 2009).

Concentrated 1 mM stock solutions of Mag-Fluo-4/AM were prepared in 20% (w/v) Pluronic® F-127/DMSO (Invitrogen) and working concentrations were obtained by dilution in Tyrode's recording solution.

A

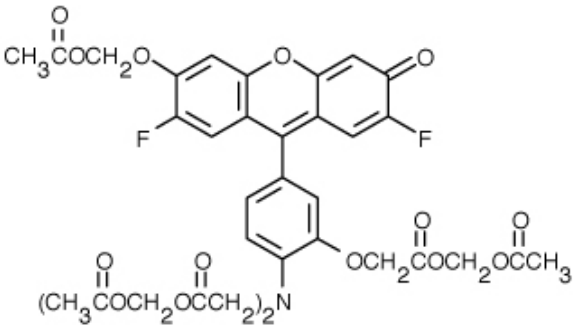

B

Property	Mag-Fluo-4
$K_{d\ (Ca2+)}$ in vitro	22 µM
Absorption maximum (Ca^{2+}-bound)	490 nm
Emission maximum (Ca^{2+}-bound)	517 nm

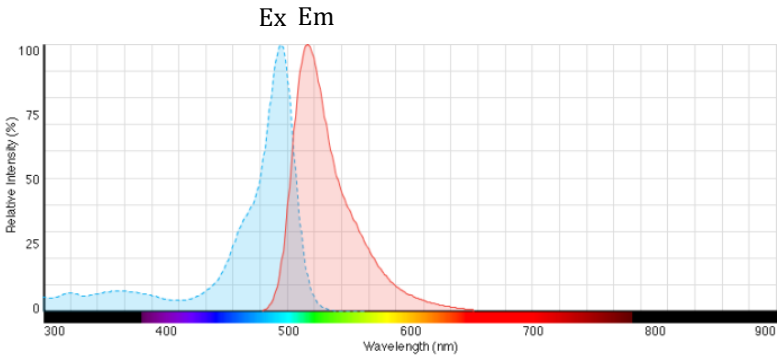

Figure 4-8. Mag-Fluo-4/AM structure (A) and spectral properties (B).

(taken from www.probes.com)

4.3.3.5.1. Imaging of perinuclear Ca^{2+} stores

An LSM700 (Carl Zeiss, Germany) confocal microscope was used to visualize perinuclear Ca^{2+} stores, i.e. the NE and its invaginations, further referred to as nuclear tubules (NTs). Myocytes were loaded for 2 h with 10 µM Mag-Fluo-4/AM (Invitrogen) and 1 h was allowed for de-esterification of the dye before two-dimensional (2D) images were recorded. Two 2D images were acquired for every cell, one image of the entire myocyte obtained at a central depth of the cell (for cellular measurements) and one image of the nucleus obtained at a central depth of the nucleus (for nuclear measurements). The optical slice thickness was ≈0.5-0.8 µm. Images were analyzed using ImageJ. Length (L) and width (W) of the cells and nuclei were defined as the longest lines parallel to the longitudinal or transversal axes of the cells and nuclei. Cell and nucleus area was then calculated assuming a rectangular shape of the cell (cell area = LxW) and an ellipsoidal shape of the nucleus (nucleus area = LxWxπ/4). For characterization of NTs additional z-stack images of the nuclei were collected. NTs were counted along the longitudinal half of the NE, which contained more invaginations, as previously described (Ljubojevic et al, 2014).

4.3.3.5.2. Measurements of NE Ca^{2+} load using Mag-Fluo-4

NE Ca^{2+} load was determined in myocytes using a low-affinity Ca^{2+} dye. Myocytes were loaded with 10 µM Mag-Fluo-4/AM for 1 h and allowed to de-esterify the dye for 1 h before linescan images were acquired on the LSM510 confocal microscope (Carl Zeiss, Germany). Prior to the recordings, myocytes were incubated with 50 µM cytochalasin D (Merck Milipore) for 10-20 min to avoid movement artifacts (Calaghan et al, 2000). Cells were then field-stimulated at 1 Hz and Mag-Fluo-4 fluorescence from the NE was recorded by positioning the line transversely through the cell crossing the nucleus (3 ms per line, thickness of confocal plane was set to ≈1 µm). After cessation of stimulation, 10 mM caffeine was applied, causing reduction of NE fluorescence, which recovered partially after restarting the stimulation.
NE Ca^{2+} load was quantified by normalizing the amplitude of the caffeine-evoked fluorescence decrease (dF_{caff}) to the resting fluorescence of the NE obtained before caffeine application (F_{rest}).

4.4. Protein expression analyses

4.4.1. Left ventricular tissue isolation

Following sacrifice of the animals, hearts were removed quickly and placed in ice-cold cardioplegic solution. LV walls (with septum) were cut, weighed, rapidly frozen in liquid nitrogen and stored at -80°C.

4.4.2. Purification of cardiomyocyte nuclei from left ventricular tissue from 12-14 weeks old WKY/SHR using magnetic assisted cell sorting

Isolation of cardiac myocyte nuclei from LV tissue was performed in Freiburg by Sebastian Preissl as previously described (Gilsbach et al, 2014 and Preissl et al, 2015). This method is based on the detection of a protein named pericentriolar material 1 (PCM1), which in the heart is found specifically only in cardiac myocyte nuclei and not in endothelial or smooth muscle cell nuclei. Briefly, LV tissue was first homogenized and nuclei released (lysis buffer composition: 5 mM $CaCl_2$, 3 mM MgAc, 2 mM EDTA, 0.5 mM EGTA, 10 mM Tris-HCL, pH 8) using a gentle MACS dissociator (Miltenyi) with gentle MACS M tubes (Miltenyi) using the protocol ''protein_01''. Next, lysis buffer containing 0.4 % triton-X was added and the combined cell suspension was filtered through 40 µm gaze (BD Biosciences). The filter was washed with lysis buffer containing 0.2 % triton-X (1:1 mixture of the two buffers above). The flow-through was centrifuged (1000 x g, 5min). The pellet was resuspended and overlayed on 1 M sucrose (3 mM MgAc, 10 mM Tris-HCl, pH 8). After centrifugation (1000 x g, 5 min) the pellet was resuspended in 500 µl staining buffer (PBS containing 5 % BSA and 0.2 % NP-40). Isolated nuclei were subsequently used for magnetic-assisted purification with an antibody targeting PCM1 attached to magnetic beads. For magnetic-assisted cell sorting (MACS) nuclei suspensions were incubated with a PCM1 antibody (1:1000, HPA023370, Sigma) for 30 min and subsequently incubated with anti-rabbit IgG MicroBeads (Miltenyi) for 15 min at 4°C. After addition of MACS buffer (PBS containing 2 mM EDTA, 1% BSA and 2% skimmed milk powder), the nuclei suspension was applied to M columns (Miltenyi), washed with MACS buffer and nuclei were eluted with MACS buffer from the column after removal of the magnet. The eluate was applied to another M column, washed again and cardiomyocyte nuclei were eluted in elution buffer (1 mM EDTA in PBS). Sorting purity of cardiomyocyte nuclei was confirmed using flow cytometric analysis (Cy Flow Space, Partec) by staining aliquots before and after nuclei sorting with an Alexa647-labeled anti-rabbit antibody (1:1000, Life Technologies). Nuclei were identified and DNA content was measured by DAPI (4',6-diamidino-2-phenylindole, 1:1000, Life Technologies) fluorescence. After

centrifugation, nuclei were lysed in lysis buffer containing 50 mM Tris (pH=6.7), 2% SDS, phosphatase and protease inhibitors (ArNr: 116974980014, Roche). Protein concentration was measured using the BCA protein assay kit (Pierce).

4.4.3. Homogenization of left ventricular tissue from 15-25 months old WKY/SHR

The homogenization procedure was performed manually on ice using micro tissue grinders (Wheaton UK Limited, Rochdale, United Kingdom). Small pieces of frozen LV tissue were placed in the homogenizers with 100 µl of the ice-cold homogenization buffer (Table 4-7). The tissue was manually homogenized with pestle for around 20 min and the homogenizers were centrifuged for 3 minutes at 3000 revolutions per minute (rpm) and the first supernatant fractions were then transferred into the collecting Eppendorf tubes. Another 100 µl of the homogenization buffer was added on the top of the resting pellets, homogenized, centrifuged (3 minutes at 3000 rpm) and the second supernatant fractions were collected in the same collecting Eppendorf tubes. These steps of homogenization were repeated till the supernatants became light yellowish and the tissue flaccid and pale. In the end, the total extract was centrifuged for 3 minutes at 13000 rpm and the supernatant was transferred into another final Eppendorf tube, quickly frozen in liquid nitrogen and stored at -80°C.

Table 4-7. Homogenization (lysis) buffer

Component	Final concentration	Stock	Inhibitor's target (Component's role)
NP-40	1%	100%	Mild non-denaturating detergent
Glycerol	10%	100%	Protein's stability/solubility
NaCl	137 mM	-	Ionic strength control
Tris-HCl (pH 7.4)	20 mM	1 M	pH control
Beta-Glycerol phosphate	50 mM	-	Ser/Thr phosphatases
EDTA (pH 8)	10 mM	100 mM	Metalloproteases (Mg^{2+} chelation)
EGTA (pH 7.4)	1 mM	100 mM in 200 mM NaOH	Metalloproteases (Ca^{2+} chelation)
NaF*	20 mM	1 M	Ser/Thr and acidic phosphatases
PMSF*	1 mM	0.1 M in isopropanol	Serine/thiol proteases
Sodium pyrophosphate*	1 mM	0.1 M	Ser/Thr phosphatases
Na_3VO_4*	1 mM	0.1 M, pH=10	Tyr and alkaline phosphatases, P-type ATPases
Aprotinin*	4 µg/ml	4 mg/ml	Serine proteases
Leupeptin*	4 µg/ml	4 mg/ml	Cysteine/serine/threonine proteases
Pepstatin A*	4 µg/ml	1 mM in MeOH:Acetic Acid (9:1)	Aspartyl proteases

As endogenous proteases may be liberated upon cell disruption and may degrade the target molecules, the sample should be protected during homogenization by the use of a cocktail of protease and phosphatase inhibitors to avoid uncontrolled protein loss and dephosphorylation of proteins. Homogenization buffer aliquots (pH=7.4) without major inhibitors (marked with * in the table) and concentrated stock solutions of inhibitors were prepared in advance and stored at -20°C. On the day of homogenization, inhibitors were then added freshly.

4.4.4. Protein assay

Protein concentration of ventricular tissue homogenates was measured using the Pierce BCA (bicinchoninic acid) Protein assay kit (Thermo Fisher Scientific, Schwerte, Germany). This assay is based on two reactions. First Cu^{2+} ions are reduced to Cu^{+} by peptide bonds in proteins at alkaline pH. In the second step, two BCA molecules bind to the cuprous ion, resulting in a chelating complex of intense purple color. This water-soluble complex is showing strong linear absorbance at 562 nm with increasing protein concentrations (Walker, 1994).

Practically, homogenates were 50 or 100 times diluted in lysis buffer. Following manufacturer's instructions, working reagent (containing BCA) was prepared by mixing reagent A and reagent B in the ratio 1:50. Samples were then prepared for the BCA assay by mixing 5 µl of diluted homogenates, 20 µl of ddH_2O and 200 µl of working reagent (in duplicates). Quickly thereafter, the reaction was developed by incubating that mixture at 37°C for 30 minutes. Afterwards, samples were put on ice to stop the reaction and absorbance was measured at 562 nm by a spectrophotometer (GENESYS™ 10S UV-Vis, Thermo Fisher Scientific, Schwerte, Germany). The protein concentration of the samples was calculated using a standard curve, which was freshly obtained each time by performing the BCA assay with 0-1 mg/ml standard bovine serum albumin (Thermo Fisher Scientific, Schwerte, Germany).

4.4.5. Western blot protocol

Western blotting, also known as immunoblotting, is a well-established and widely used technique for the detection and analysis of proteins. Ca^{2+}-handling proteins were separated using SDS polyacrylamide gel (PAGE) electrophoresis in the presence of the reducing agents dithiothreitol (DTT) and β-mercaptoethanol. In this way, proteins are separated solely on the basis of their size and not the net charge or 3D structure. For the majority of proteins we used gradient polyacrylamide gels

(convenient for separation of proteins with a wide range of molecular weights) and a Tris-glycine based buffering system. For the resolution of proteins smaller than 30 kDa, like PLB, we used tricine gels and a Tris-tricine buffering system (Schägger, 2006).

4.4.5.1. Sample preparation

LV tissue and nuclei lysate volume corresponding to 3, 15 or 20 µg of total protein, 4x Lämmli buffer (Table 4-8) containing 5% β-mercaptoethanol (added in the loading buffer on the day of the experiment) and lysis buffer were mixed on ice prior to loading on the gel. As an internal control 3, 15 or 20 µg of ventricular pool was prepared in the same way and loaded next to the samples. To identify the molecular weight of the investigated proteins 5 µl of PageRuler™ Plus Prestained Protein Ladder (Thermo Fisher Scientific, Schwerte, Germany) was also loaded in parallel to the samples.

Table 4-8. 4x Lämmli buffer (sample loading buffer), pH 6.8

Component	Final concentration	Stock
EGTA	16 mM	100 mM (in 200 mM NaOH), pH 7.4
SDS	4%	20%
Tris HCL (pH 6.8)	40 mM	1 M
Dithiothreitol (DTT)	16 mM	1 M
glycerol	47%	100%
Br-Ph Blue	0.05%	1%

Table 4-9. Preparation of 1 M Tris-HCl, pH 6.8

Component	Amount
ddH_20	100 ml
Tris Base	12.1 g
5 M HCl	pH adjustment

4.4.5.2. Gel preparation

Four to twenty percent gradient gels were from Bio-Rad (Bio-Rad, München, Germany). Tris-tricine-SDS-PAGE gel was prepared using the Bio-Rad gel casting system (Bio-Rad, München, Germany). They were composed of a 16% running gel (Table 4-10) and a 6% stacking gel (Table 4-11).

Table 4-10. Composition of 16% Tris-tricine running gel

Component	≈ 9 ml (1 gel)
ddH_20	1.15 ml
PAA/BIS 30%	4.8 ml
3 M Tris HCl/SDS (3x), pH 8.45	3 ml
10% APS	50 µl
TEMED	10 µl

Table 4-11. Composition of 6% stacking gel for Tris-tricine-SDS-PAGE

Component	≈ 3 ml (1 gel)
ddH_20	1.4 ml
PAA/BIS 30%	0.6 ml
3 M Tris HCl/SDS (3x), pH 8.45	1 ml
10% APS	25 µl
TEMED	10 µl

Table 4-12. Preparation of 3 M Tris HCl/SDS (3x), pH 8.45

Adding order	Amount
1. Tris Base	182 g
2. ddH_20	300 ml
3. 5 M HCl	pH adjustment
4. ddH_20	Add to 500 ml
5. SDS	1.5 g

4.4.5.3. SDS-PAGE electrophoresis

Loaded gels were placed in the Mini Trans-Blot Electrophoretic Transfer Cell (Bio-Rad, München, Germany) and the tank was filled with corresponding buffers (Tables 4-13 and 4-14). Tris-glycine-SDS-PAGE was performed first at 90 V for 1 hour and then at 120 V, while Tris-tricine-SDS-PAGE was performed first at 90 V for 30 min and then at 70 V, until optimal separation was obtained.

Table 4-13. Running buffer for 4-20% gradient gels (Tris-glycine-SDS-PAGE), pH 8.3

Component	Final concentration (1x)	Amount for 1 l (10x)
Tris Base	25 mM	30.2 g
Glycine	192 mM	144 g
SDS	0.1%	50 ml 20% (or 10 g)

Table 4-14. Running buffers for Tris-tricine-SDS-PAGE

Cathode buffer (upper chamber), pH 8.25	**Final concentration**	**Amount for 1 l**
Tris Base	100 mM	12.1 g
Tricine	100 mM	17.9 g
SDS	0.1%	5 ml 20%
Anode buffer (lower chamber), pH 8.9	**Final concentration**	**Amount for 1 l**
Tris Base	200 mM	24.2 g
5 M HCl	pH adjustments	

4.4.5.4. Wet Blotting

Separated proteins were electro-transferred from the gel to a nitrocellulose membrane (0.45 µm, BioRad, Germany) using the wet blotting procedure. Transfer buffer (1x) without methanol was prepared the night before and kept in the fridge. During electrophoresis methanol was added to the transfer buffer to reach 20% and cooled down in the fridge (Table 4-15). The addition of methanol is necessary to achieve efficient protein binding to the membrane. The nitrocellulose membranes (cut on the gel size) were incubated in ddH_2O for 10 minutes and then, at the same time as the gel, filter papers and sponges, in the cold transfer buffer for at least 15 min. The "blotting sandwich" was assembled as following:

- **Black electrode (cathode (-))**
- Sponge
- Thick filter paper
- **Gel**
- **Nitrocellulose membrane**
- Thin filter paper
- Thick filter paper
- Sponge
- **White electrode (anode (+))**

Wet blotting was performed in a Mini Trans-Blot Electrophoretic Transfer Cell (Bio-Rad, München, Germany) filled with transfer buffer, in the presence of ice blocks and constant magnetic stirring for 2-3 hours at 100 mA per gel and then at 15 mA per gel overnight at 4°C (for the majority of Ca^{2+}-handling proteins) or only 15 mA per gel overnight at 4°C (for proteins with molecular weight < 30 kDa, like PLB).

Table 4-15. Transfer buffer containing 20% methanol

Component	Final concentration (1x)	Amount for 1 l (10x)
Tris Base	33 mM	39.4 g
Glycine	192 mM	144 g
Freshly before blotting: 100 ml 10x Transfer buffer + 700 ml ddH_20 + 200 ml MeOH = 20% MeOH		

4.4.5.5. Blocking, immunostaining and detection

The next day, membranes were washed with ddH_20 for 5 min and stained with Ponceau S (1 min) for evaluation of transfer efficacy. After additional washing with ddH_20, membranes were washed 3 times for 10 min with Tris-buffered saline Tween (TBST) buffer (Table 4-16) and afterwards blocked for 1 hour at RT with 5% skimmed milk (Sigma) in TBST.

After that, membranes were washed 3 times for 10 min with TBST and immunoblotted with primary antibodies dissolved in 0.5% skimmed milk in TBST. Dilutions of primary antibodies and the conditions we used are presented in Table 4-17.

After the incubation with primary antibodies, membranes were washed 3 times for 10 minutes with TBST buffer and incubated with horseradish peroxidase (HRP)-conjugated secondary antibodies (dissolved in 0.5% skimmed milk in TBST) for 1 hour at RT (Table 4-18).

Afterwards, membranes were washed again 3 times for 10 minutes with TBST buffer and chemiluminescence was detected with the Chemidoc-XRS Imaging system (BioRad, München, Germany) using HRP-Juice (PJK GmbH, Germany) or the more sensitive chemiluminescent Super Signal West Femto Maximum Sensitivity Substrate (Thermo Fisher Scientific, Germany) reagent. The chemiluminescence method is based on secondary antibodies conjugated with horseradish peroxidase enzyme, which in the presence of the peroxide-based reagent catalyse the oxidation of luminol resulting in the emission of light (Handbook from GE Healthcare Bio-Sciences, Western Blot, Principles and methods, 2011).

Some membranes (in the phosphorylation studies, in the case of tRyR, tPLB and tCamKII) were stripped for 7 min with stripping buffer (containing 200 mM Glycine, 0.1% SDS, 1% Tween 20, pH 2.2 adjusted with 6 M HCl) to remove bound primary and secondary antibodies, then washed twice for 10 min with TBST buffer, reblocked in blocking buffer again and reprobed with different antibodies.

GAPDH or actin were used as loading controls for tissue lysates and H3 for isolated nuclei samples.

Blots were analyzed using ImageJ (NIH, Bethesda, Maryland, USA).

Table 4-16. Tris-buffered saline (TBS) buffer, pH 7.5

Component	Final concentration (1x)	Amount for 1l (20x)
NaCl	170 mM	198.2 g
Tris Base	10 mM	24.2 g
5 M HCl	pH adjustment	
TBST washing buffer (1x): 50 ml TBS (20x) + 950 ml ddH_20 + 1 ml Tween 20 = 0.1% Tween 20		

Table 4-17. Primary antibodies

Protein (MW kD)	Primary antibody	Company, catalogue number	Host Species	Dilution	Incubation	Gel type
RyR (565)	Anti-RyR mAb (C3-33)	Thermo Scientific, MA3-916	mouse	1:5000	2.5 h, RT	4-20% gradient gel
RyR2 pSer2808	Anti-phospho-RyR2 (Ser-2808) pAb	Badrilla, A010-30	rabbit	1:5000	2 h, RT	4-20% gradient gel
RyR2 pSer2814	Anti-phospho-RyR2 (Ser-2814) pAb	Badrilla, A010-31	rabbit	1:5000	2 h, RT	4-20% gradient gel
NCX1 (120)	Anti NCX1 mAb	Thermo Scientific, MA1-4672	mouse	1:1000	2 h, RT	4-20% gradient gel
CSQ (55)	Anti-Calsequestrin pAb	Thermo Scientific, PA1-913	rabbit	1:2500	2 h, RT	4-20% gradient gel
LTCC (250)	Anti-Cav1.2a (Cardiac Type α1C)	Alomone Labs, ACC-013	rabbit	1:1000	2.5 h, RT	4-20% gradient gel

PLB (25)	Anti-Phospholamban (PLN, PLB) A1 mAB	Badrilla, A010-14	mouse	1:5000	2.5 h, RT	16% tricine gel
PLB pS16	Anti-Phospholamban Phospho-Ser16 pAb	Badrilla, A010-12	rabbit	1:5000	2 h, RT	16% tricine gel
PLB pT17	Anti-Phospholamban Phospho-Thr17 pAb	Badrilla, A010-13	rabbit	1:5000	2 h, RT	16% tricine gel
SERCA2a (100)	Anti-Serca2a pAb	Badrilla, A010-20	rabbit	1:5000	2 h, RT	4-20% gradient gel
Actin (44)	Mouse Anti-Actin, mAB (Clone:C4)	MP Biomedicals LLC, #69100	mouse	1:100000	2 h, RT	16% tricine gel
GAPDH (34)	Anti-GAPDH Mouse mAB (6c5)	Calbiochem, CB1001	mouse	1:50000	2 h, RT	4-20% gradient gel
HDAC5 (124)	Anti-HDAC5 (Ab-498) Antibody	Signalway Antibody, USA, SAB-21142	rabbit	1:500	ON, 4°C	4-20% gradient gel
H3 (15)	Anti-Histone H3 Antibody-Chip grade	Abcam, ab1791	rabbit	1:1000	2 h, RT	4-20% gradient gel, 16% tricine gel
Acetyl-H3	Anti-acetyl-Histone H3 pAb	Merck Millipore, 06-599	rabbit	1:10000	ON, 4°C	4-20% gradient gel
Nup106 (106)	Anti-Nuclear Pore Complex Proteins Antibody	Abcam, ab50008	mouse	1:3000	ON, 4°C	4-20% gradient gel

Nup 62 (62)	Anti-Nucleoporin p62	BD Transduction Laboratories™, UK, 610497	mouse	1:1000	ON, 4°C	4-20% gradient gel
CaMKII (45-50)	anti-CaMKIIδ	Badrilla, UK, A010-55AP	rabbit	1:5000	ON, 4°C	4-20% gradient gel
	CamKII (M-176)	Santa Cruz Biotechnology, sc-9036	rabbit	1:500	ON, 4°C	4-20% gradient gel
pCaMKII pT286	Anti-CamKII (phospho T286) Antibody	Abcam, ab32679	rabbit	1:1000	ON, 4°C	4-20% gradient gel
IP3R2 (313)	Anti-ITPR2 Antibody	Abcam, ab77838	rabbit	1:1000	2.5 h, RT	4-20% gradient gel

Table 4-18. Secondary antibodies

Secondary antibodies	Company, catalogue number	Dilution
Immunopure Goat Anti-Mouse IgG, (H+L), Peroxidase Conjugated	Thermo Scientific, Germany, 31430	1:5000
Immunopure Goat Anti-Rabbit IgG, (H+L), Peroxidase Conjugated	Thermo Scientific, Germany, 31460	1:5000

4.5. Statistics

Statistical analysis was performed using GraphPad Prism (GraphPad Software, Inc., San Diego, USA). The data are presented as mean±SEM for n myocytes and N rats. Differences between data sets were evaluated by unpaired, two-tailed Student's t-test. When multiple groups were compared, analysis of variance (ANOVA) and Bonferroni's post hoc test were applied. Groups were considered significantly different when $p<0.05$ (levels of significance are indicated by asterisks (* $p<0.05$; ** $p<0.01$)).

5. Results

5.1. EARLY STAGE OF HYPERTENSIVE HEART DISEASE – Enhanced nucleoplasmic Ca^{2+} signaling in ventricular myocytes from young hypertensive rats

Cardiovascular changes during development and progression of HHD throughout the lifespan of SHR are well defined offering the possibility to investigate specific age points and disease stages. SHR are normotensive the first 6 weeks of age, rapidly develop hypertension at 8–12 weeks of age, and remain hypertensive thereafter. After the onset of hypertension, cardiac hypertrophy gradually develops in SHR from 3–18 months of age.

Aiming to see whether there are some alterations in nuclear Ca^{2+} handling in response to hypertension, we investigated normotensive 6 weeks old and young hypertensive 12-14 weeks old SHR. We studied subcellular CaTs in the cytoplasm and nucleoplasm, measured SR and perinuclear (PN) calcium load and fractional calcium release and analysed intranuclear calcium propagation velocities in LV myocytes of WKY and SHR. Additionally, we performed structural characterization of ventricular cells and nuclei and Western blot analysis of Ca^{2+}-regulating proteins and Ca^{2+}-dependent regulation of transcription in LV tissue and nuclei of WKY and SHR.

5.1.1. Elevated cytoplasmic and nucleoplasmic CaTs in SHR in early hypertension

Early after the development of hypertension in isolated LV myocytes from 12-14 weeks old SHR subcellular CaTs were recorded using linescan confocal microscopy (Figure 5-1A). Cyto- and nucleoplasmic CaTs were electrically evoked (1 Hz) and simultaneously imaged as Fluo-4 fluorescence (Figure 5-1B). As linescan images show, the nuclear region (N, Nuc, gray) always lagged behind the cytoplasmic region (C, Cyto, black). Slower kinetics of nucleoplasmic CaTs was also evident from the normalized fluorescence traces (F/F_{rest}) below. Figure 5-1C presents the mean results of the Fluo-4 fluorescence traces. There was no difference in cyto- and nucleoplasmic diastolic Ca^{2+} between SHR and WKY. SHR myocytes, however, had significantly larger cyto- and nucleoplasmic CaT amplitudes compared to WKY myocytes. More interestingly, the nucleoplasmic-to-cytoplasmic ratio of the CaT amplitude was bigger in SHR than in WKY. We also found CaT kinetics alterations between SHR and WKY. CaT decay was faster in SHR than in WKY both in the cyto- and nucleoplasm. Rise time of cytoplasmic CaTs was prolonged in SHR, with no change in the nucleoplasm, resulting in significantly decreased nucleoplasmic-to-cytoplasmic (nuc-to-cyto) rise time ratio in SHR.

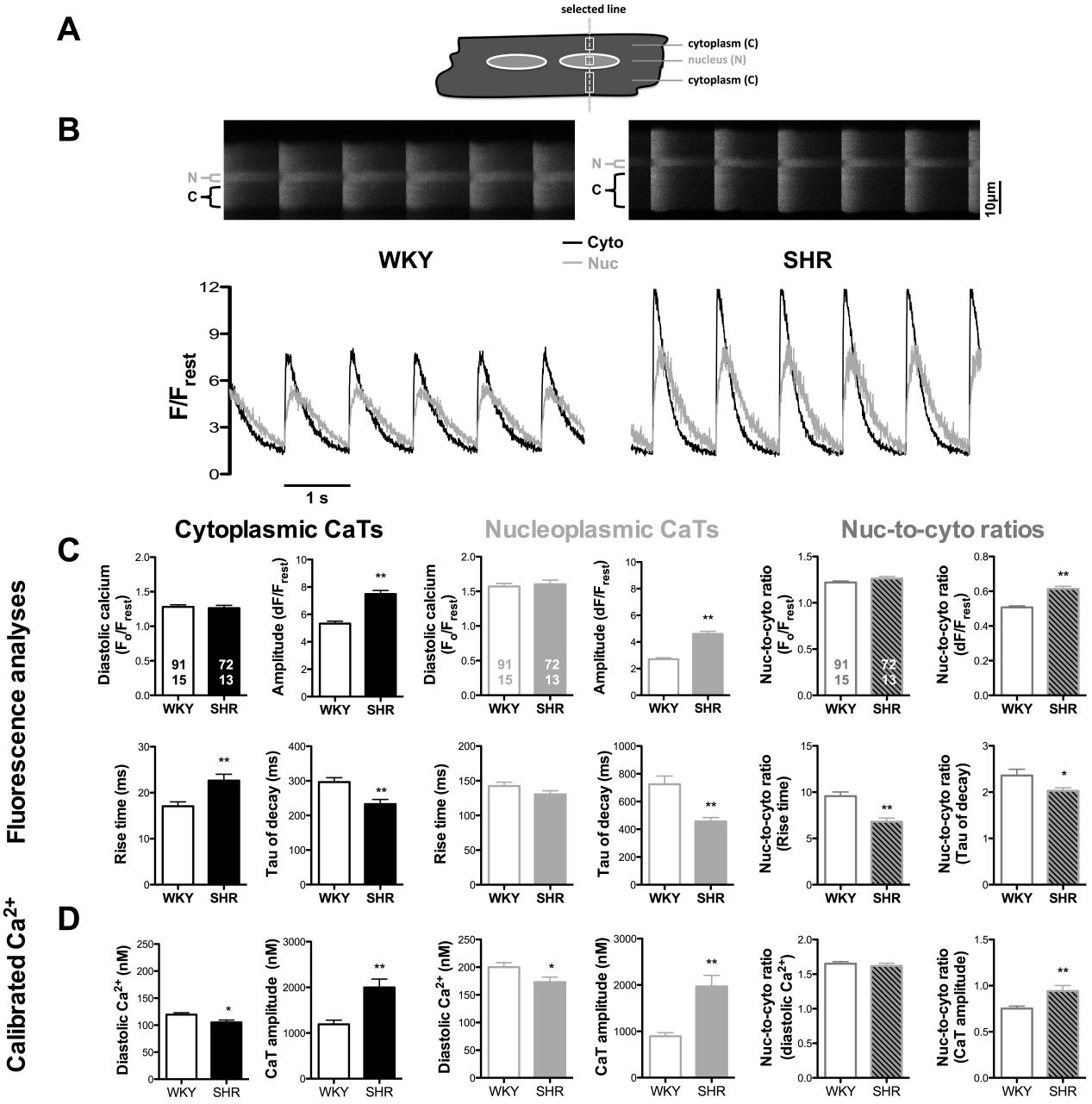

Figure 5-1. Cytoplasmic and nucleoplasmic CaT characteristics of field stimulated ventricular myocytes from 12-14 weeks old WKY and SHR.

(A) Representation of the way of positioning the scanned line in a ventricular myocyte. **(B)** Linescan images of electrically stimulated CaTs in the nucleus (N) vs cytoplasm (C) of typical ventricular myocytes from WKY (left) and SHR (right) and corresponding normalized fluorescence traces. **(C)** Mean fluorescence values of cytoplasmic and nucleoplasmic CaTs: amplitude (dF/F_{rest}), diastolic calcium (F_o/F_{rest}), rise time and time constant (tau) of CaT decay. **(D)** Calibrated [Ca^{2+}] data for diastolic Ca^{2+} and CaT amplitude. Right panels in (C) and (D) show average values of the respective nucleo-to-cytoplasmic ratios. (n=91, N=15 WKY; n=72, N=13 SHR). *P<0.05, **P<0.01.

Normalized fluorescence traces do not report accurate [Ca^{2+}]. Furthermore, it has not been shown before whether Fluo-4 properties differ between WKY and SHR ventricular myocytes. Therefore, for the absolute quantification of [Ca^{2+}] in the cytoplasm and nucleoplasm, we performed in situ calibration of Fluo-4 fluorescence in WKY and SHR ventricular myocytes. The calibration experiments followed protocols explained before (Ljubojevic et al, 2011, Ljubojevic & Bers, 2015). The results of the in situ calibrations are illustrated in Figure 5-2. Figure 5-2A shows overall steps of the calibration procedure. Intact resting myocytes were treated with calibration solutions (marked by the arrows) with free [Ca^{2+}] of 0 nM, 250 nM, 1500 nM, 5000 nM and 2 mM, respectively. Traces for nucleus (Nuc, gray) and cytoplasm (Cyto, black) are shown. Application of the respective solutions leads to stepwise decreases (at 0 nM Ca^{2+}) and increases (at 250 nM to 2 mM Ca^{2+}) in Fluo-4 fluorescence both in the nucleus and cytoplasm. Normalized fluorescence changes (F/F_{rest}) were plotted versus free [Ca^{2+}] and fitted with the Hill equation. Figure 5-2B presents the resulting concentration-response curves for cyto- and nucleoplasmic [Ca^{2+}]. Hill fits yielded apparent dissociation constants for Ca^{2+} binding to Fluo-4 (K_d) of 1404 nM (WKY) and 1389 nM (SHR) in the cytoplasm (Cyto) and of 1039 nM (WKY) and 1086 nM (SHR) in the nucleoplasm (Nuc). Dynamic range (R_f) was 88 (WKY) and 95 (SHR) in the cytoplasm and 42 (WKY) and 54 (SHR) in the nucleoplasm. Resting Ca^{2+} concentrations ($[Ca^{2+}]_{rest}$) (bar graphs shown at the bottom in (B)) were not significantly different between WKY (n=9, N=4) and SHR (n=11, N=4) amounting to 87±17 nM (WKY) and 78±18 nM (SHR) in the cytoplasm and to 106±22 nM (WKY) and 90±20 nM (SHR) in the nucleoplasm. Also, Hill coefficients were not different between WKY (cytoplasm: 1.22±0.40; nucleoplasm: 1.64±0.70; n=9, N=4) and SHR (cytoplasm: 1.30±0.29; nucleoplasm: 1.55±0.44; n=11, N=4). K_d, R_f and $[Ca^{2+}]_{rest}$ values obtained here are in the range of values obtained before in cardiac myocytes: $K_d \approx$ 1100-1400 nM; $R_f \approx$ 40-70; $[Ca^{2+}]_{rest} \approx$ 70-105 nM (Ljubojevic et al, 2011).

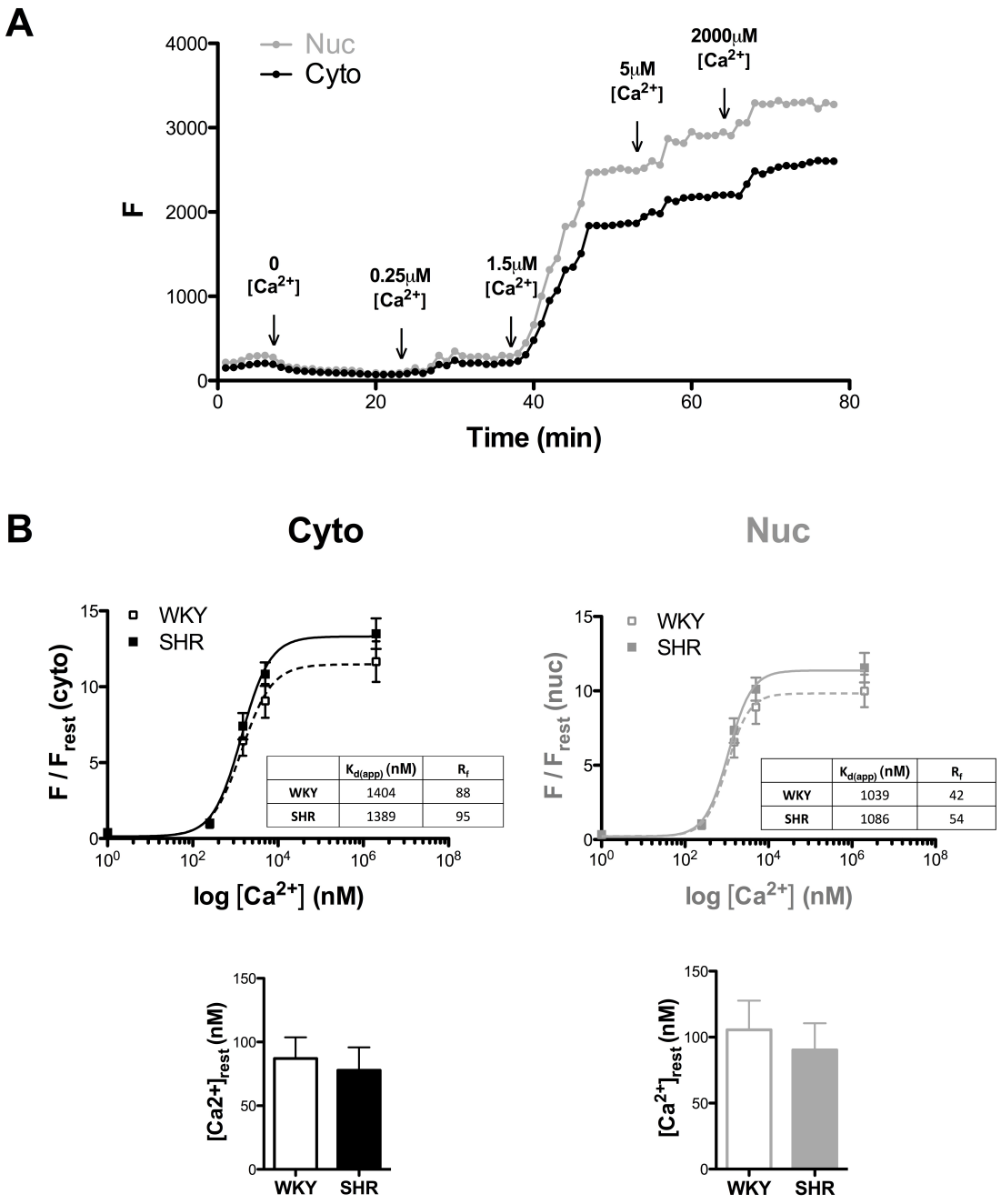

Figure 5-2. In situ calibration of Fluo-4 fluorescence in 12-14 weeks old WKY and SHR ventricular myocytes.

(A) Raw Fluo-4 fluorescence (F) changes in a ventricular myocyte during the calibration protocol. **(B)** The resulting concentration-response curves for cyto- and nucleoplasmic [Ca^{2+}]. Mean values from n=9 myocytes from N=4 WKY and n=11 myocytes from N=4 SHR are shown. Apparent dissociation constants for Ca^{2+} binding to Fluo-4 (K_d) and values for dynamic range (R_f) in cytoplasm and nucleoplasm obtained from the Hill curve fitting are presented in tables next to the curves. Resting Ca^{2+} concentrations ($[Ca^{2+}]_{rest}$) are shown in bar graphs below.

Using the parameters obtained by this method, we calculated cyto- and nucleoplasmic diastolic and systolic [Ca^{2+}] and the amplitude of the CaT for WKY and SHR myocytes (Figure 5-1D). As shown in a previous study on rat cardiomyocytes (Ljubojevic et al, 2011), our normotensive WKY myocytes had cytoplasmic diastolic [Ca^{2+}] in the range of ≈120 nM and a CaT amplitude in the range of ≈1200 nM. Also in line with previous results (Ljubojevic et al, 2011), diastolic [Ca^{2+}] in the nucleus was higher (≈200 nM) and CaT amplitude in the nucleus was smaller (≈900 nM) than in the cytoplasm, yielding a nuc-to-cyto ratio <1 (0.76±0.03, n=91). Compared with WKY, SHR myocytes had slightly decreased diastolic [Ca^{2+}] both in the cyto- (≈105 nM) and nucleoplasm (≈170 nM) (both $P<0.05$ vs WKY) but greatly elevated CaT amplitudes in the range of ≈1900-2000 nM (both $P<0.01$ vs WKY) resulting in the nuc-to-cyto ratio for CaT amplitude approaching unity (0.93±0.06, n=72; $P<0.01$ vs WKY). Thus, in comparison to normotensive WKY, SHR myocytes showed greatly increased cyto- and nucleoplasmic CaTs and enhanced nuclear Ca^{2+} signaling.

Aiming to investigate further whether the enhanced nuclear Ca^{2+} signaling observed in 12-14 weeks old SHR was related to hypertension, we additionally studied cyto- and nucleoplasmic CaTs in WKY and SHR at 6-8 weeks of age, i.e. before the establishment of hypertension in SHR. Experiments and analyses were done in the same way as shown in Figure 5-1 for 12-14 weeks old animals. Figure 5-3 illustrates the results for 6 weeks old animals. At this age point, both Fluo-4 fluorescence analysis and calibrated [Ca^{2+}] analysis yielded the same finding, that there were no big alterations in either cyto- or nucleoplasmic CaTs between WKY and SHR. Cytoplasmic fluorescence CaT amplitude (dF/F_{rest}) was slightly increased (Figure 5-3A), but this difference disappeared when calibrated data were compared (Figure 5-3B). Moreover, Ca^{2+} load data (Figure 5-3C) did not show any differences between WKY and SHR, suggesting that SR and NE Ca^{2+} handling is not altered in SHR at six weeks of age. Interestingly, the nuc-to-cyto ratio for CaT decay was bigger and the nuc-to-cyto ratio for CaT amplitude was smaller in SHR than in WKY. These changes are even opposite to what was found in twelve weeks old animals (Figure 5-1). They argue against enhancement of nuclear Ca^{2+} signaling in SHR at six weeks of age. Furthermore, when we directly compared CaT characteristics of six weeks old SHR

(Figure 5-3) with 12-14 weeks old SHR (Figure 5-1), we found significantly larger cytoplasmic CaT amplitudes, nucleoplasmic CaT amplitudes and nuc-to-cyto ratios for CaT amplitudes for both fluorescence and calibrated [Ca^{2+}] data (all $P<0.01$) in 12-14 weeks old SHR. Thus, cyto- and nucleoplasmic Ca^{2+} handling alterations between WKY and SHR appear to happen only after the development of hypertension in SHR.

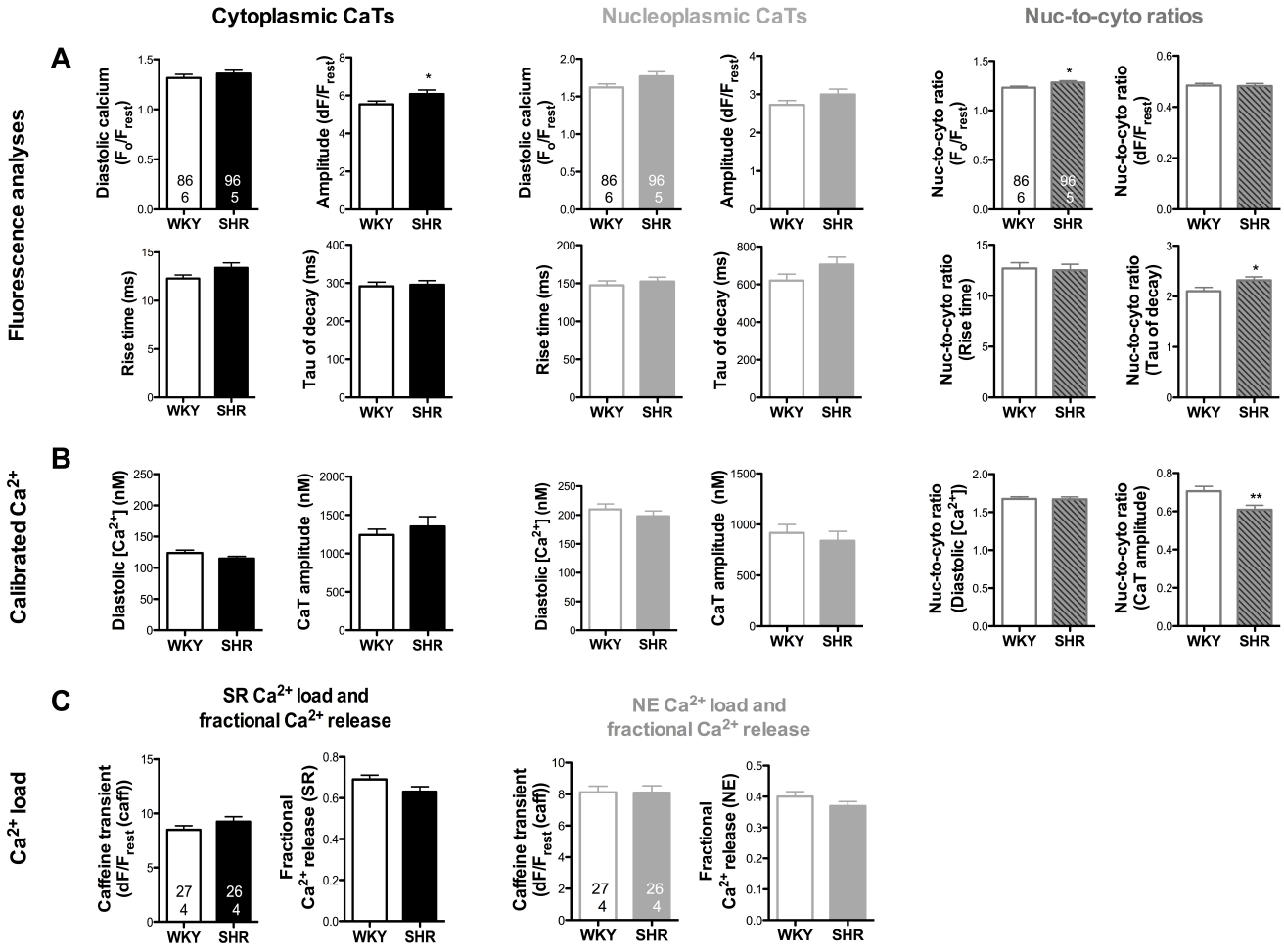

Figure 5-3. Cytoplasmic and nucleoplasmic Ca^{2+} handling in ventricular myocytes from WKY and SHR at 6 weeks of age.

(A) Analyses of Fluo-4 fluorescence changes in electrically stimulated (1 Hz) ventricular myocytes from WKY and SHR at 6 weeks of age. **(B)** Calibrated [Ca^{2+}] for diastolic Ca^{2+} and CaT amplitude in the same myocytes (n=86, N=6 WKY; n=96, N=5 SHR). *P<0.05, **P<0.01 vs WKY. **(C)** Ca^{2+} load and fractional release for SR and NE Ca^{2+} stores. (n=27, N=4 WKY; n=26, N=4 SHR).

Taken together, these data suggested that both cyto- and nucleoplasmic CaTs are augmented in SHR early in HHD. Strikingly, the increase of nucleoplasmic CaTs exceeded the elevation of cytoplasmic CaTs in SHR, suggesting that nucleoplasmic Ca^{2+} signaling must be enhanced by mechanisms other than a simple increase in cytoplasmic Ca^{2+}. We therefore wanted to elucidate the underlying mechanisms involved in enhanced nucleoplasmic Ca^{2+} signaling in SHR and its possible consequences.

5.1.2. Increased SR and NE Ca^{2+} load in SHR

Increased Ca^{2+} content of the intracellular Ca^{2+} stores, i.e. the SR and the NE could lead to the enhanced CaTs in SHR. Therefore, we estimated SR and NE Ca^{2+} load using rapid application of caffeine in cells loaded with Fluo-4 (Figure 5-4A). Caffeine is a RyR2 agonist and quickly releases all Ca^{2+} from the SR and NE. Caffeine-evoked cytoplasmic and nucleoplasmic CaT amplitudes (Figure 5-4B) were larger in SHR than in WKY, implying augmented SR and NE Ca^{2+} load in SHR. Fractional Ca^{2+} release from SR and NE was very similar in both strains amounting to ≈0.65-0.70 for SR and ≈0.45-0.50 for NE, respectively (Figure 5-4B).

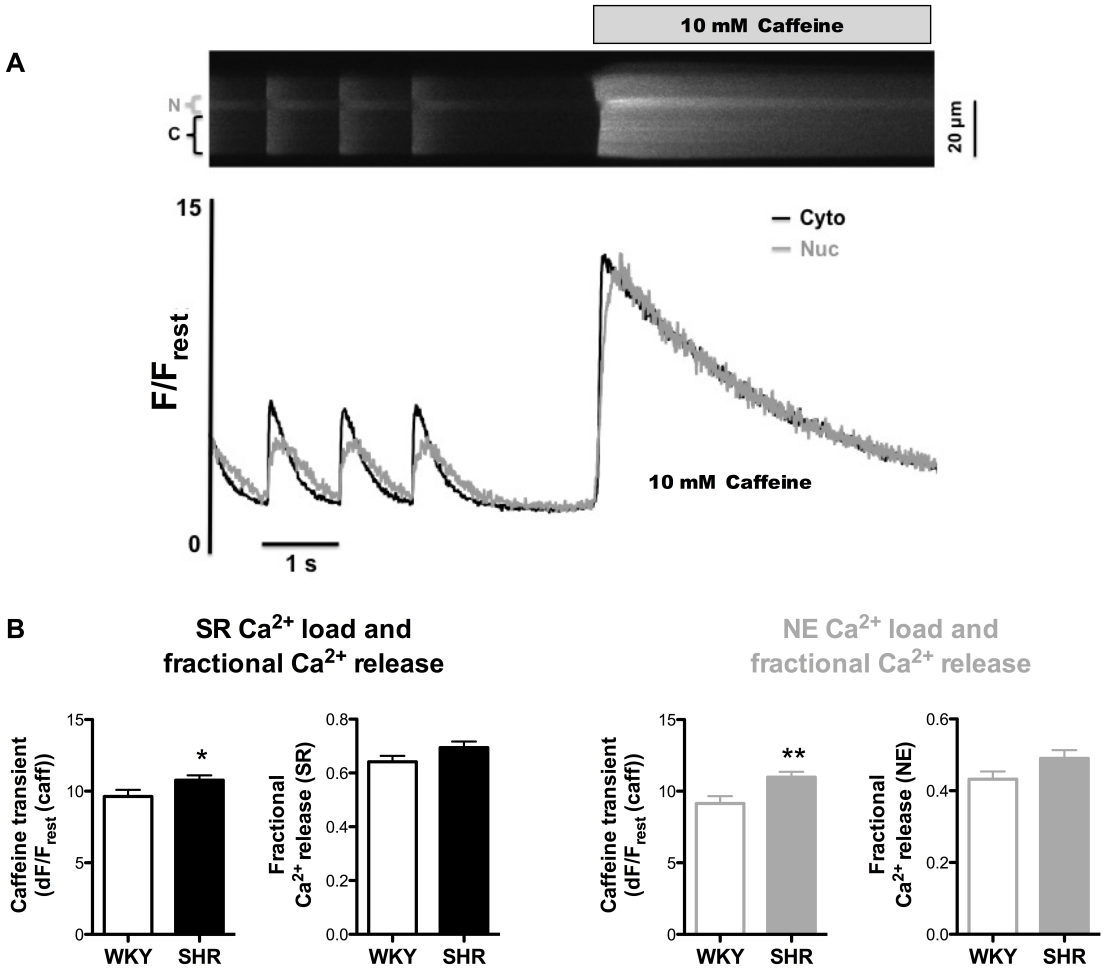

Figure 5-4. SR and perinuclear Ca^{2+} load and fractional release in ventricular myocytes from WKY and SHR at 12-14 weeks of age.

(A) Linescan image from an SHR ventricular myocyte and corresponding normalized nucleoplasmic (N) and cytoplasmic (C) fluorescence traces recorded during caffeine (10 mM) application. **(B)** Average values of caffeine-evoked CaT amplitude (as a measure of Ca^{2+} load) and fractional Ca^{2+} release in cytoplasm (left) and nucleus (right) of ventricular myocytes from WKY and SHR (n=31, N=6 WKY; n=43, N=8 SHR). *P<0.05, **P<0.01.

Fluo-4 is a high affinity Ca^{2+} dye and caffeine-induced CaTs result in large Fluo-4 fluorescence increases, which often fall into the shallow non-linear part of the calibration curve. For that reason, we did not attempt to calibrate these values. We used an additional approach to confirm and validate our findings of increased NE Ca^{2+} load. To address the NE Ca^{2+} store, caffeine was rapidly applied to cells stained with the low affinity Ca^{2+} dye Mag-Fluo-4. Figure 5-5A presents original linescan

images of a ventricular myocyte stained with Mag-Fluo-4. Two lines of bright fluorescence represent the NE (Figure 5-5A, left). After application of caffeine, Mag-Fluo-4 fluorescence decreased consistent with depletion of the NE Ca^{2+} store (Figure 5-5A, middle). After restarting electrical stimulation (1 Hz), Mag-Fluo-4 fluorescence recovered partially, indicating re-accumulation of Ca^{2+} in the NE (Figure 5-5A, right). NE Ca^{2+} load was quantified by normalizing the amplitude of the caffeine-evoked fluorescence decrease (dF_{caff}) to the resting fluorescence of the NE obtained before caffeine application (F_{rest}).

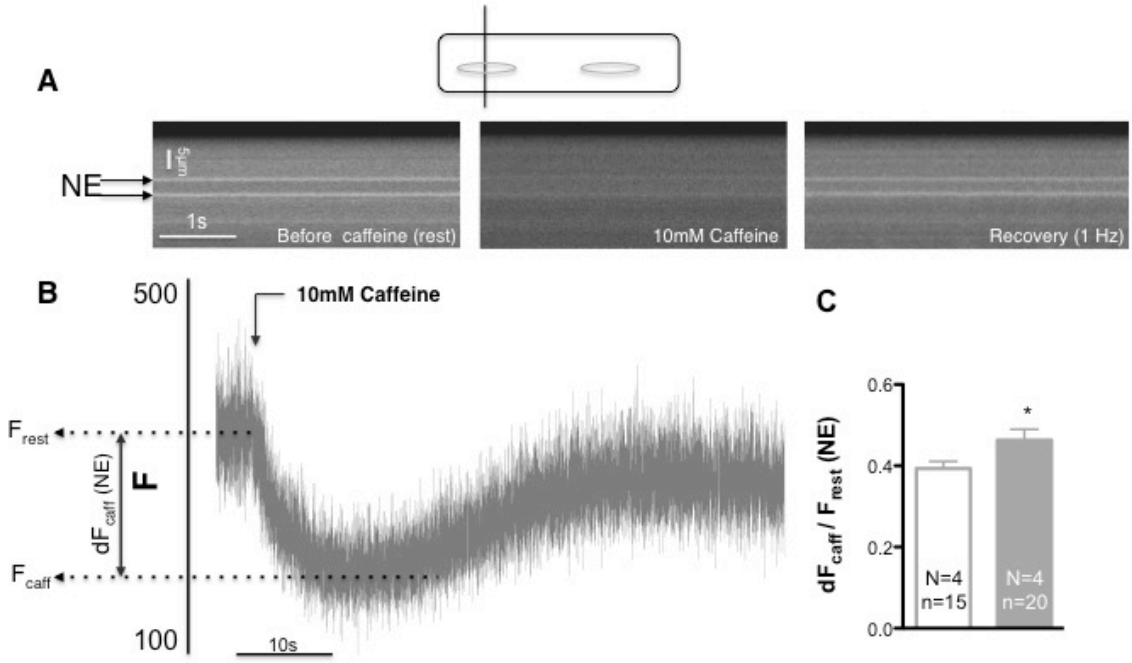

Figure 5-5. NE Ca^{2+} load estimated by caffeine-evoked decrease of Mag-Fluo-4 fluorescence.

(A) Top: Scheme showing position of the scan line. Bottom: Linescan images from a ventricular myocyte loaded with 10 µM Mag-Fluo 4/AM, obtained before (left), during caffeine exposure (middle) and after re-starting of electrical stimulation (right). The two horizontal bright lines represent the NE, as marked by the horizontal arrows. **(B)** Mag-Fluo-4 fluorescence trace of the regions depicted NE in (A). Caffeine bolus application is indicated by the vertical arrow. dF_{caff} refers to the amplitude of the caffeine-induced fluorescence decrease. This was normalized to resting fluorescence (F_{rest}). **(C)** Average values of the amplitude of the caffeine-induced Mag-Fluo-4 fluorescence decrease (dF_{caff}/F_{rest}) as a measure of NE Ca^{2+} load for 12-14 weeks old WKY and SHR (n=15, N=4 WKY; n=20, N=4 SHR). *P<0.05.

NE Ca^{2+} load estimated by this means was larger in SHR than in WKY (Figure 5-5C). Taken together, these results provide strong evidence for increased NE Ca^{2+} load in SHR. Thus, increased nucleoplasmic CaTs in SHR were caused, at least in part, by increased NE Ca^{2+} load at unchanged fractional Ca^{2+} release.

5.1.3. Number and density of nuclear tubules in SHR is not altered

In the nuclei of various cell types, including cardiomyocytes, invaginations of the NE that include deep, branching tubular structures have been identified (Bootman et al, 2009, Alonso & Garsia-Sancho, 2011). As these nuclear tubules contain NPCs, they might facilitate the transport of ions and transcription factors between the cytoplasm and nucleoplasm by decreasing the diffusional delay between the two compartments (Ljubojevic et al, 2014). Therefore, enhanced nucleoplasmic Ca^{2+} signaling in SHR might result from changes in density and function of NTs. To test this hypothesis we compared the morphology of nuclei from WKY and SHR ventricular myocytes loaded with the low affinity Ca^{2+} dye Mag-Fluo-4 using confocal 2D imaging (Figure 5-6A). LV myocytes and nuclei were enlarged in SHR confirming cellular hypertrophy (Figure 5-6B). The nucleus-to-cell area ratio was significantly bigger in SHR (Figure 5-6C). On the other hand, there were no differences in the number or the density of NTs (Figure 5-6D) between the two groups of rats. The number of NTs in both strains was positively correlated with the area of the nuclei (Figure 5-6E) with similar slopes of correlation lines.

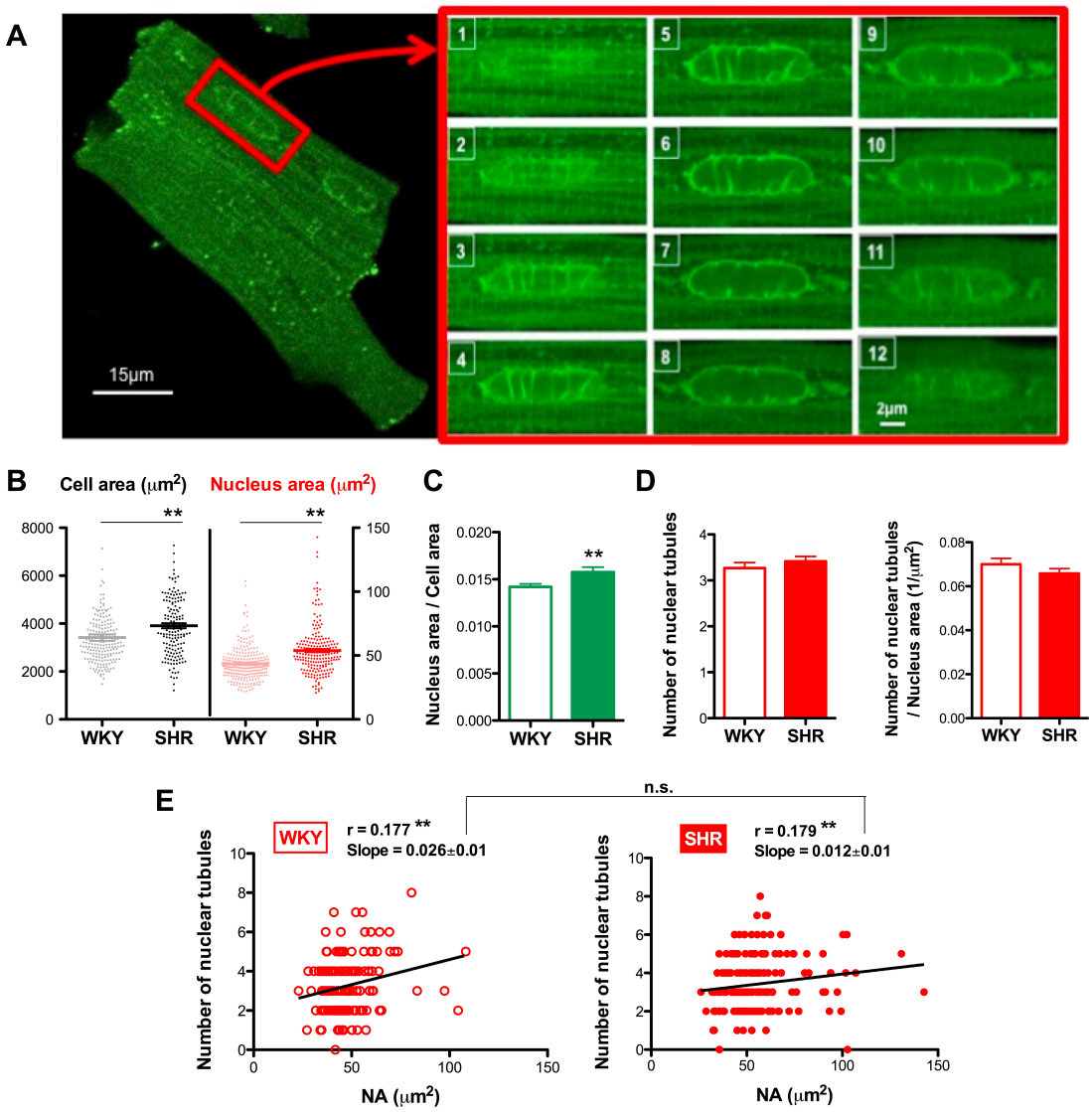

Figure 5-6. Structural characteristics of ventricular myocytes and nuclei from 12-14 weeks old WKY and SHR.

(A) Ventricular myocyte stained with 10 µM Mag-Fluo 4/AM (left) and full z-stack of a nucleus (right) (Δz=0.31 µm; thickness of each confocal plane 0.7 µm) presenting typical features of NTs. **(B)** Hypertrophy of ventricular myocytes and nuclei from SHR as indicated by augmented cell area (n=266, N=15 WKY; n=175, N=8 SHR) and nucleus area (n=313, N=14 WKY; n=227, N=8 SHR) with **(C)** increased nucleus-to-cell area ratio (n=237, N=14 WKY; n=166, N=8 SHR). **(D)** Mean values of the number and density of NTs (n=152, N=8 WKY; n=173, N=6 SHR). **(E)** Correlation between number of NTs and nucleus area (NA). Spearman correlation coefficients (r) indicate positive correlation in both WKY and SHR (n=152 WKY; n=173 SHR). Slopes did not differ between WKY and SHR (P=n.s.). **P<0.01.

5.1.4. Accelerated intranuclear Ca^{2+} propagation in SHR

The presence of NPCs both on the NE and the NTs affects ion diffusion between the cytoplasm and nucleoplasm (Greber & Gerace, 1995). Differences in passive diffusion of Ca^{2+} through NPCs or inside the nucleus might be a reason for the alterations in nucleoplasmic CaTs observed in SHR. To test this, we compared cyto-to-nucleoplasmic Ca^{2+} propagation through the NE (from small cytoplasmic (C) regions close to the NE to subnucleolemmal (SN) regions) and intranuclear Ca^{2+} propagation (from subnucleolemmal (SN) regions to central nuclear (CN) regions) (Figure 5-7A and 5-7B). In both strains, Ca^{2+} propagation from the cytoplasm to the subnucleolemmal region (C-SN) was slower (≈25 µm/s) than Ca^{2+} propagation from the subnucleolemmal to the central nuclear region (SN-CN; ≈50-90 µm/s). This is expected, due to the fact that the NE acts as a diffusion barrier. There was no difference between WKY and SHR in Ca^{2+} propagation through the NE (C-SN), but intranuclear Ca^{2+} propagation (SN-CN) was significantly faster in SHR than in WKY nuclei.

Protein expression was analysed selectively in cardiomyocyte nuclei from LV of WKY and SHR. To achieve this, cardiomyocyte nuclei were isolated from LV from WKY and SHR with an antibody targeting pericentriolar material 1 (PCM1) attached to magnetic beads (Figure 5-8A). High levels of sorting purity were obtained for both WKY (97.1±0.8%, N=4 samples) and SHR (96.2±0.8 %, N=4 samples) nuclei. The degree of ploidy was not different between WKY and SHR cardiomyocyte nuclei (Figure 5-8B). Enrichment of the nuclear fraction was further validated by histone H3 Western blotting (Figure 5-8C).

Employing this method, we determined the nuclear levels of NPC proteins. Using two different antibodies directed against two different components of the NPC, i.e. Nup62, a central core nucleoporin, and Nup106, an essential component of the NPC (Capelson et al, 2010), we performed Western blots with isolated cardiomyocyte nuclei from LV of WKY and SHR (Figure 5-7D) and found increased expression of both nucleoporins in SHR nuclei. These data indicate a higher density of NPCs in the NE and the NTs of SHR nuclei.

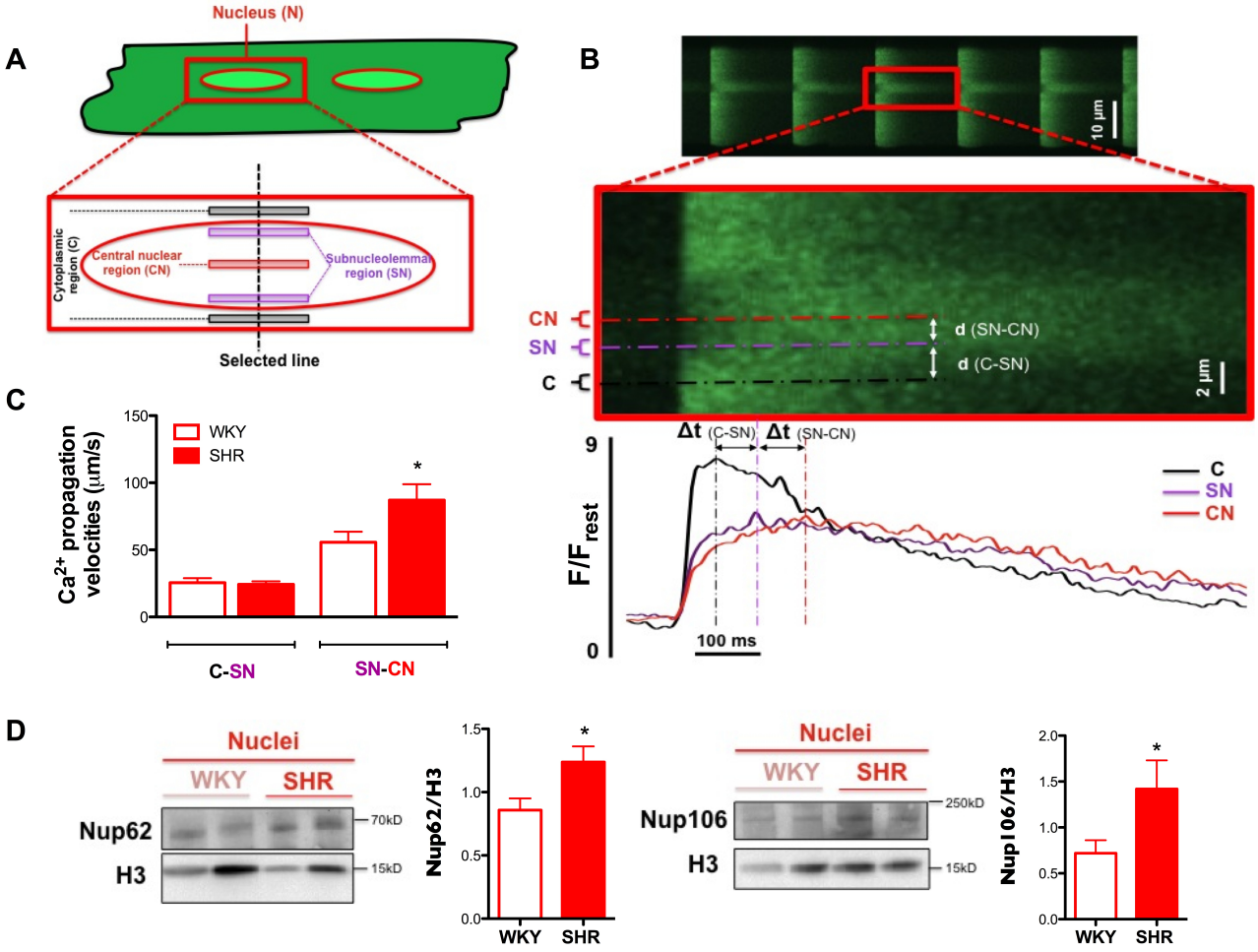

Figure 5-7. Ca^{2+} propagation into and inside of the nucleus.

(A) Scheme of a ventricular myocyte and nucleus (magnification) illustrating positioning of the scanned line and subcellular regions chosen for analysis. **(B)** Linescan image showing cyto- and nucleoplasmic CaTs from an SHR ventricular myocyte. Magnification illustrates nucleoplasmic CaT (smoothed) and corresponding normalized fluorescence traces (averaged over 4-5 CaTs) from a cytoplasmic (C) region adjacent to the nuclear envelope, a subnucleolemmal (SN) region and a central nuclear (CN) region. The distances between cytoplasmic and subnuclear regions (d(C-SN) and d(SN-CN)) and the differences between the time-to-peak of each corresponding CaT (Δt(C-SN) and Δt(SN-CN)) were taken for calculation of Ca^{2+} propagation velocities. **(C)** Average values of Ca^{2+} propagation velocities indicate faster intranuclear Ca^{2+} spread (from SN to CN region) in SHR nuclei. (n=46, N=9 WKY; n=41, N=6 SHR) **(D)** Western Blots and average data showing expression of NPC proteins Nup62 (left) and Nup106 (right) in isolated cardiomyocyte nuclei from LV tissue of WKY and SHR. Histone 3 (H3) was used as loading control. (Nup62: N=10 per group; Nup106: N=8 per group). *P<0.05.

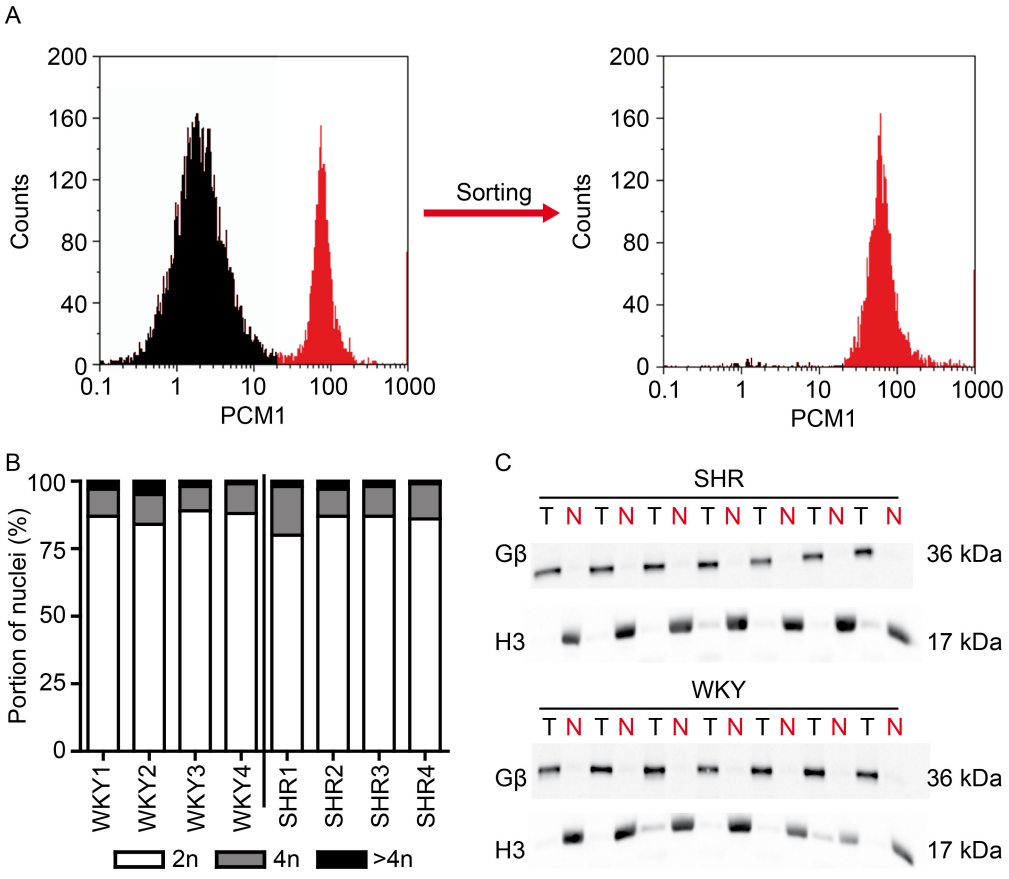

Figure 5-8. Isolation of cardiomyocyte nuclei from left ventricular tissue samples.

(A) Cardiomyocyte nuclei were purified from LV tissue of WKY by MACS with high purity. Left panel: FACS analysis of crude cardiac nuclei. Right panel: FACS analysis of MACS-sorted cardiomyocyte nuclei. Purity after sorting amounted to 97.1±0.8% in WKY (N=4) and to 96.2±0.8% in SHR (N=4). **(B)** Ploidy levels of cardiomyocyte nuclei were not different between SHR and WKY. DNA content was assessed by DAPI staining and analyzed by flow cytometry. **(C)** Western blot with protein lysates from tissue (T) and cardiomyocyte nuclei (N). Purity of the nuclear fraction was validated by antibodies against histone H3 and Gβ. (Isolation of cardiac nuclei, analyses and this figure were kindly done by Sebastian Preißl.)

To confirm that nuclear borders defined for analyses of intranuclear propagation velocities were accurately selected, nuclei of ventricular myocytes loaded with Fluo-4 were stained using the fluorescent nucleic acid dye Syto-16 (Kockskämper et al., 2008). The results are presented in Figure 5-9. From 2D images, it is clear that the two oval areas displaying higher Fluo-4 fluorescence (Figure 5-9A, left) are also stained by Syto-16 (Figure 5-9A, right) indicating that they are indeed the nuclei. From linescan images, it is also clear that the area with the presumed delayed nuclear CaT (Figure 5-9B, left) is also stained by Syto-16 (Figure 5-9B, right) indicating that it is the nucleus. Using the Syto-16 staining as a marker for the nucleus, nuclear borders were depicted by the dashed lines (designated as "Nuc" on the Figure 5-9C, left). The nuclear borders defined with Syto-16 match the nuclear borders defined by the delayed nuclear CaT of Fluo-4 loaded myocytes (Figure 5-9C). For comparison, we have also marked the central cytoplasmic (C), the subnucleolemmal (SN) and the central nuclear (CN) areas in the same way as in previous Figure 5-7B for analysis of Ca^{2+} propagation velocities. According to this definition of the nuclear borders, we have accurately defined and analyzed Ca^{2+} transients and Ca^{2+} propagation in these subcellular areas just outside of and within the nucleus.

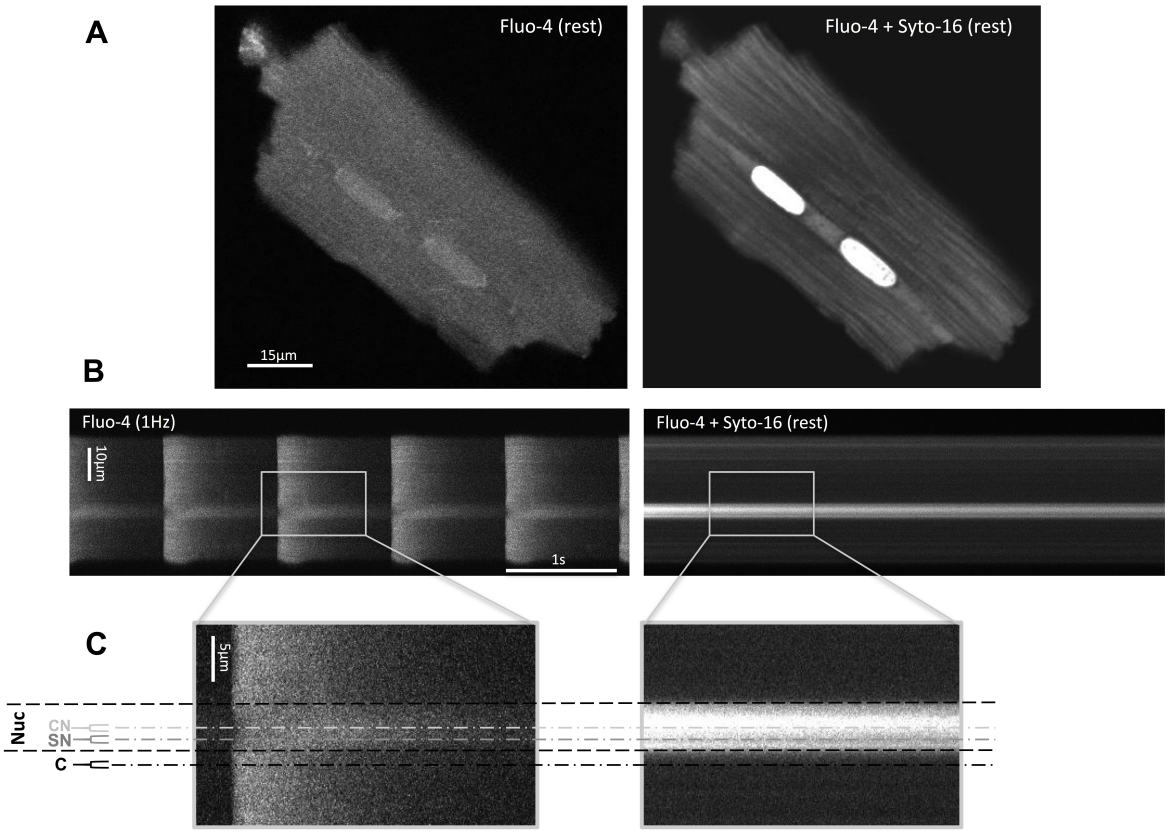

Figure 5-9. Staining of nuclei of ventricular myocytes loaded with Fluo-4 with fluorescent nucleic acid dye Syto-16.

(A) 2D confocal image of a ventricular myocyte loaded with Fluo-4 alone under resting conditions (left) and the same myocyte following additional loading with Syto-16 (5 µM for 4 min, laser power reduced because of bright Syto-16 fluorescence) (right). **(B)** Linescan images of a different ventricular myocyte. On the left, electrically stimulated (1 Hz) CaTs in a Fluo-4-loaded cell are shown with the presumed nuclear transient lagging behind the cytoplasmic transient. Afterwards, the electrical stimulation was stopped and the cell was loaded additionally with Syto-16 (5 µM for 4 min, laser power reduced because of bright Syto-16 fluorescence). The linescan image obtained under these conditions is shown on the right. **(C)** Magnification of one Ca^{2+} transient with the corresponding areas and following Syto-16 staining.

5.1.5. Altered expression of Ca^{2+} handling proteins in SHR nuclei

Altered expression and differential distribution of Ca^{2+}-regulating proteins between cytoplasm and nucleus might contribute to the described alterations in Ca^{2+} signaling in the cyto- and nucleoplasm of SHR. Thus, we analysed the expression of the major Ca^{2+} handling proteins in LV tissue lysates and isolated cardiomyocyte nuclei from WKY and SHR.

Regarding major Ca^{2+} release channels (Figure 5-10A and 5-10B) we observed increased expression of IP3R2 in tissue lysates from SHR. Expression of RyR2 appeared also increased in tissue lysates of SHR, without reaching statistical significance (P=0.07). The higher expression of Ca^{2+} release channel proteins in the tissue lysates might have contributed to the prolongation of the rise time of cytoplasmic CaTs (Figure 5-1C). Nuclear expression of both RyR2 and IP3R2, however, did not differ between WKY and SHR.

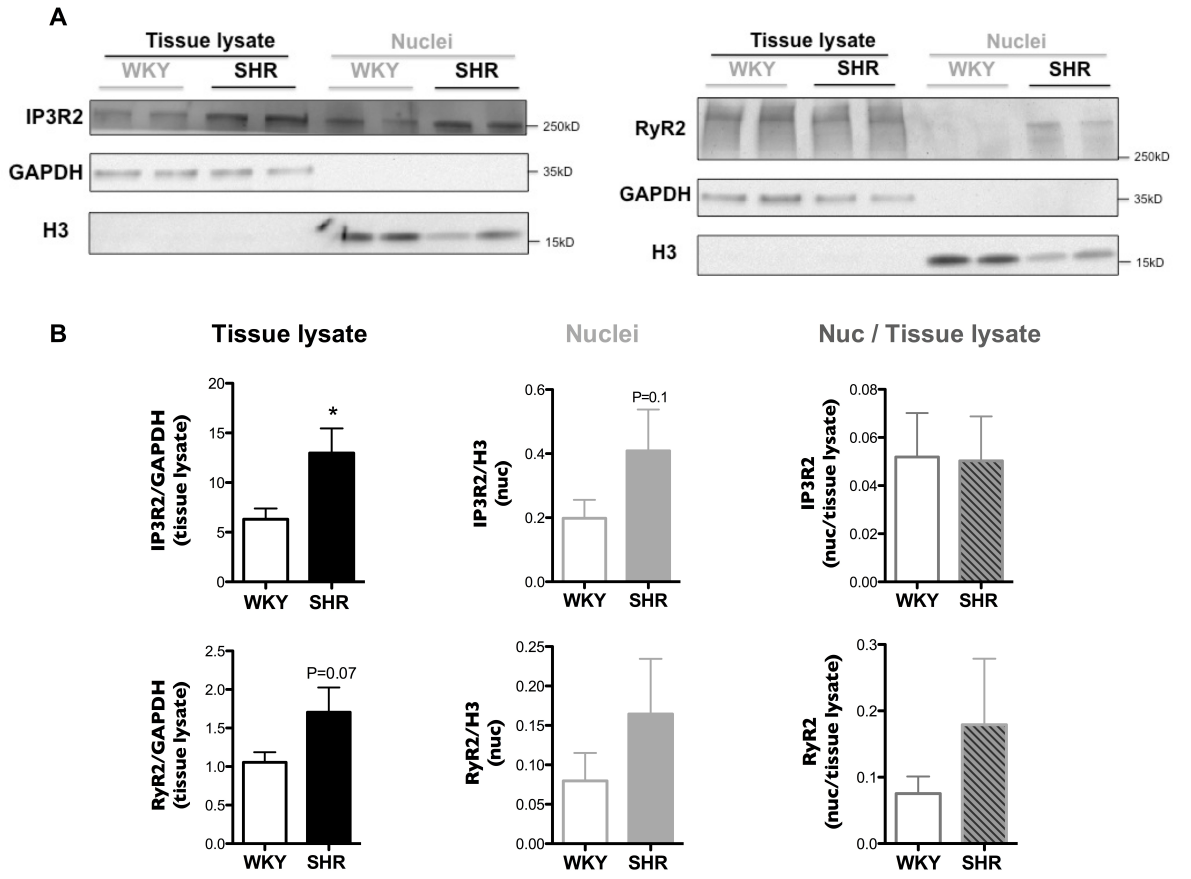

Figure 5-10. Expression of major SR/NE Ca^{2+} release proteins in tissue lysates versus isolated cardiomyocyte nuclei.

(A) Western Blots and **(B)** average data of IP3R2 and RyR2 expression in tissue lysates and isolated cardiomyocyte nuclei from LV tissue of WKY and SHR. GAPDH was used as loading control for tissue lysate samples and H3 as loading control for nuclei samples (N=10 per group). *P<0.05.

Analysis of major proteins involved in Ca^{2+} reuptake into the intracellular Ca^{2+} stores (Figure 5-11A and 5-11B) revealed decreased expression of PLB in tissue lysates of SHR with an increased SERCA2a/PLB ratio. In nuclei of SHR, on the other hand, SERCA2a expression was significantly higher than in WKY. These results suggested increased SERCA2a activity both in the cytoplasm and nuclei of SHR. They are in agreement with the faster decay of cyto- and nucleoplasmic CaTs and increased SR and NE Ca^{2+} load in SHR (Figure 5-1 and 5-3).

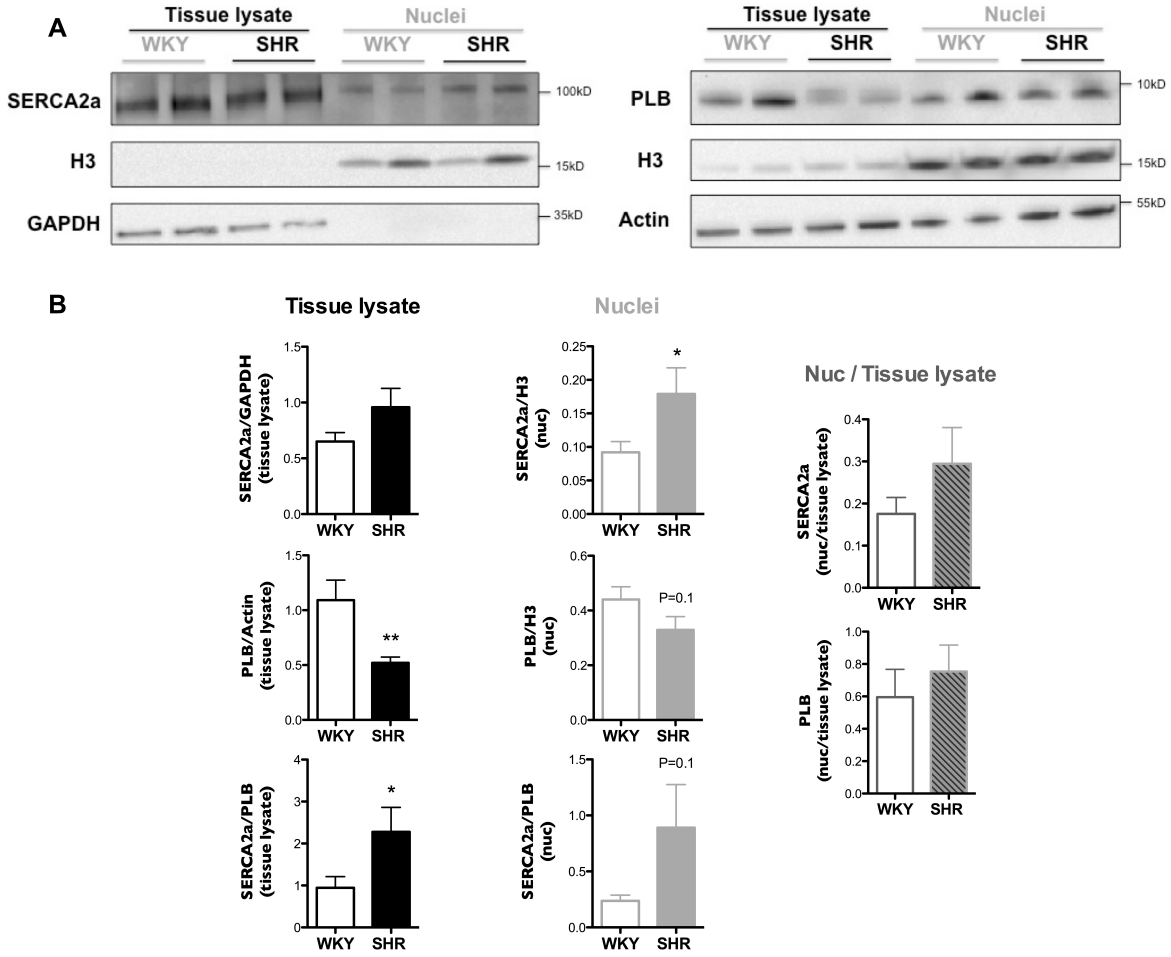

Figure 5-11. Expression of major SR/NE Ca^{2+} reuptake proteins in tissue lysates versus isolated cardiomyocyte nuclei.

(A) Western Blots and **(B)** average data of SERCA2a and PLB expression in tissue lysates and isolated cardiomyocyte nuclei from LV tissue of WKY and SHR. GAPDH or actin was used as loading control for tissue lysate samples and H3 as loading control for nuclei samples (N=10 per group). *P<0.05, **P<0.01.

All together, the data presented so far clearly indicated enhancement of nuclear Ca^{2+} signaling and alterations in Ca^{2+} handling in SHR early after the onset of hypertension. Thus, we aimed at elucidating the potential consequences of the increased nuclear Ca^{2+} signaling for the regulation of transcription.

5.1.6. Altered Ca^{2+}-dependent regulation of transcription in SHR

CaMKII is an important Ca^{2+}-dependent regulator of cardiac hypertrophy activated predominantly by high-amplitude CaTs (at systole) (Frey & Olson, 2000) with CaMKIIδ being the main isoform in the heart (Zhang & Brown, 2004). CaMKIIδ can phosphorylate both HDAC4 and HDAC5 (Back et al, 2008). Phosphorylation of HDAC4/5 leads to the nuclear export of HDAC4/5 and de-repression of MEF2-dependent transcription of hypertrophy genes (Bossuyt et al, 2008, Ha et al, 2010).

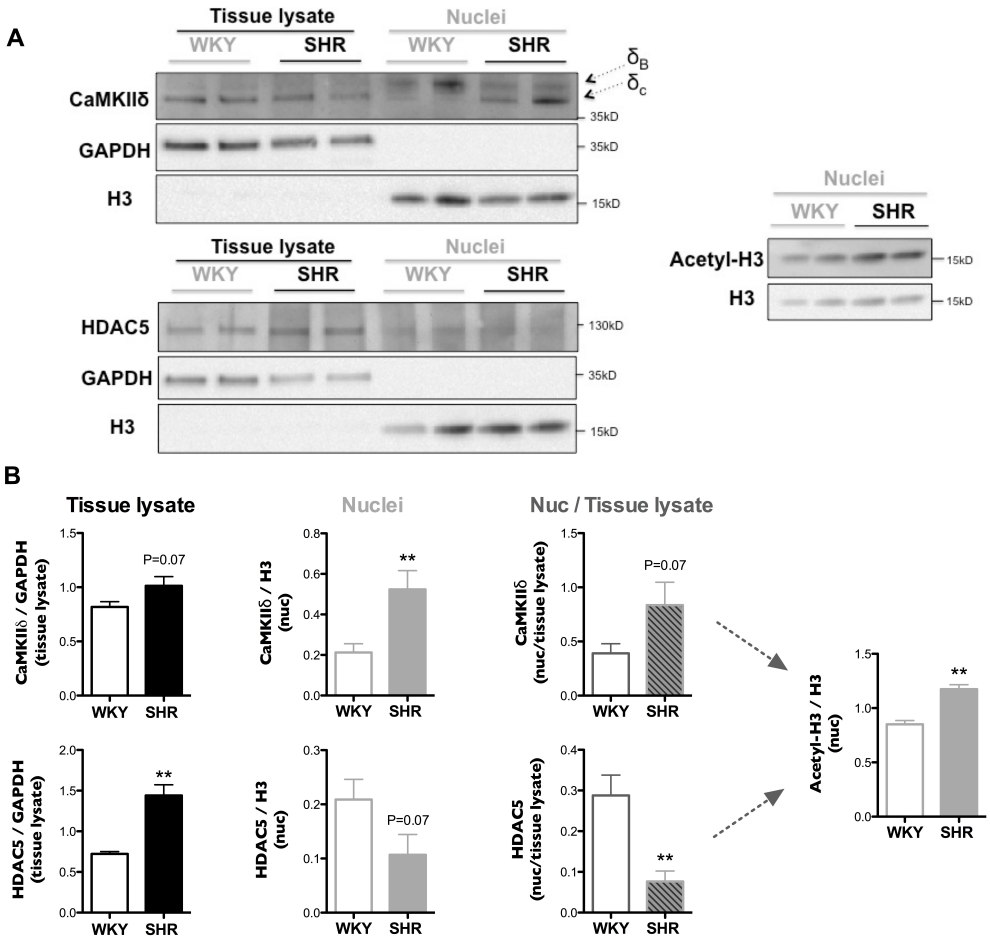

Figure 5-12. Expression of CaMKIIδ, HDAC5 and acetyl-H3 in tissue lysates versus isolated cardiomyocyte nuclei.

(A) Western Blots and **(B)** average data of CaMKIIδ, HDAC5 and acetyl-H3 expression in tissue lysates and isolated cardiomyocyte nuclei from LV tissue of WKY and SHR. GAPDH was used as loading control for tissue lysate samples and H3 as loading control for nuclei samples (N=8 per group). **P<0.01.

We investigated activation of the CaMKII-HDAC pathway to prove that the augmented nuclear Ca^{2+} signaling in SHR ventricular myocytes indeed has an impact on transcriptional regulation. Using antibodies for CaMKIIδ, HDAC5 and acetyl-H3, we performed Western blots with LV tissue lysates and isolated cardiomyocyte nuclei from WKY and SHR (Figure 5-12A and 5-12B). In the nuclei of SHR we found a large increase in the expression of CaMKIIδ, which was caused mainly by a large increase in the CaMKIIδC isoform in the nucleus (Figure 5-13). Importantly, enhanced nuclear CaMKIIδ was accompanied by a redistribution of HDAC5 from the nucleus to the cytoplasm in SHR. The nucleus-to-tissue ratios of CaMKIIδ and HDAC5 expression displayed an increase for CaMKIIδ (P=0.07) and a huge decrease for HDAC5 (P<0.01). Higher levels of acetyl-H3 in SHR nuclei (P<0.01) indicate an increase in histone acetylation, very likely caused by the export of HDAC5 from the nucleus.

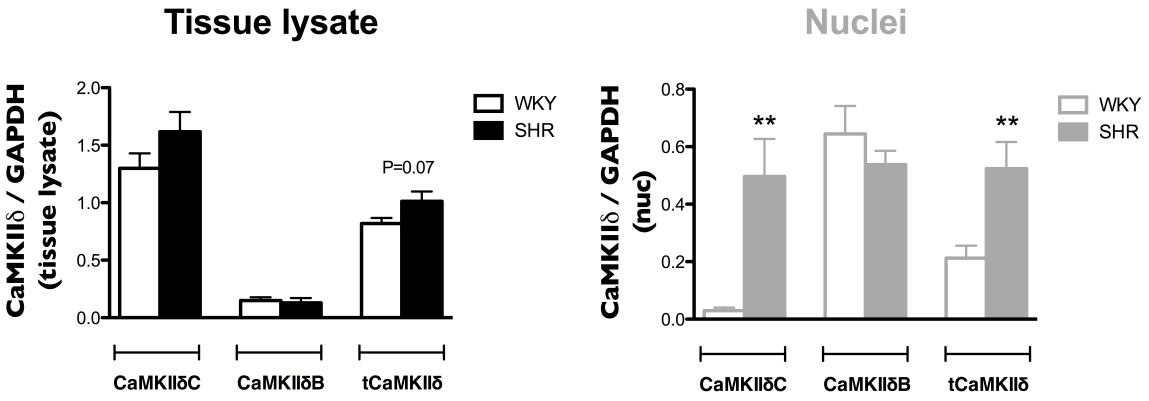

Figure 5-13. Expression of CaMKIIδ isoforms in tissue lysates (left) versus isolated cardiomyocyte nuclei (right).

tCaMKIIδ: total CaMKIIδ (CaMKIIδB + CaMKIIδC). GAPDH was used as loading control for tissue lysate samples and H3 as loading control for nuclei samples (N=8 per group). **P<0.01.

Taken together, these results indicated the following alterations in the left ventricle of SHR in the early stage of the hypertensive heart disease:

- LV myocytes and nuclei from SHR were hypertrophied.
- Cytoplasmic and nucleoplasmic CaTs were enlarged in SHR.
- The increase in nucleoplasmic Ca^{2+} exceeded the increase in cytoplasmic Ca^{2+}, suggesting increased nuclear Ca^{2+} signaling in SHR.
- Ca^{2+} load of SR and perinuclear Ca^{2+} stores was also enlarged in SHR, while fractional release from both stores was unaltered.
- Intranuclear Ca^{2+} propagation was faster in SHR, associated with preserved density of nuclear envelope invaginations and elevated nuclear expression of nucleoporins and SERCA2a.
- Nuclear CaMKIIδ expression was elevated, while histone deacetylases were redistributed from nucleus to cytosol leading to increased histone acetylation in SHR.

The observed remodeling of nuclear Ca^{2+} handling coupled to CaMKII–HDAC-mediated regulation of histone acetylation and transcription might represent an early event in hypertension that contributes to initiation and progression of pathological hypertrophy in hypertensive heart disease.

5.2. ADVANCED STAGE OF HYPERTENSIVE HEART DISEASE – Remodeling of nuclear calcium handling and structure in ventricular myocytes of spontaneously hypertensive rats with heart failure

After the establishment of hypertension in SHR at 8-12 weeks of age, cardiac hypertrophy gradually develops from 3–18 months of age, and HF typically occurs from 15–25 months of age.

Aiming to see whether there are some alterations in nuclear Ca^{2+} handling at the onset of HF, we investigated 15-25 months old SHR at the stage when they gradually develop HF. Similarly as in young hyperetensive rats, we studied subcellular CaTs in the cytoplasm and nucleoplasm, measured SR and perinuclear (PN) calcium load and fractional calcium release and analysed intranuclear calcium propagation velocities in LV myocytes of WKY and SHR. Additionally, we performed structural characterization of ventricular cells and nuclei and Western blot analysis of Ca^{2+}-regulating proteins in LV tissue of WKY and SHR.

5.2.1. Cardiovascular characteristics and incidence of HF in SHR with advanced HHD

We used 15-25 months old male SHR and WKY for our studies, as this is the time when SHR gradually develop HF (Chan et al, 2011, Conrad et al, 1991). Global heart hypertrophy, blood pressure and heart rate measurements were analysed in our laboratory by Drs. Pluteanu and Nikonova. SHR displayed LV, LA and RV hypertrophy, higher diastolic and systolic blood pressure and higher heart rate than WKY. Many SHR exhibited increased lung weight (LW) suggesting the presence of pulmonary edema, a cardinal sign of HF. Many SHR also developed other signs of HF including impaired activity, difficulties breathing and loss of weight. Important to note, not all SHR showed these manifestations of HF. Therefore, SHR were

subdivided into two groups (Figure 5-14) according to the absence or presence of lung congestion: SHR with lung weight higher than the mean plus 2xSD of the value found in age-matched WKY were classified as heart failing group (SHR-HF with LW/TL >50 mg/mm), while SHR with lung weight equal to or below this threshold were defined as the non-failing group (SHR-NF). Using these criteria, lung weight, LA, RA and RV weight of SHR-NF was almost identical to WKY. On the other hand, in comparison to SHR-NF, SHR-HF exhibited increased diastolic and systolic blood pressure and LV, LA, RV and RA weight. Taken together, HF development in SHR was followed by further increases in blood pressure and global heart hypertrophy.

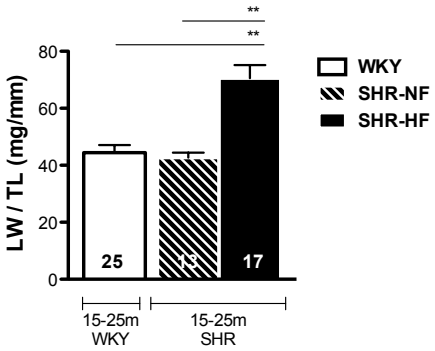

Figure 5-14. Grouping of 15-25 months old SHR into SHR with (HF) and without (NF) heart failure based on the presence or absence of pulmonary edema.

Pulmonary edema was quantified as increased lung wet weight/tibia length (LW/TL). N=25, N=13 and N=17 for WKY, SHR-NF and SHR-HF, respectively. **P<0.01 (One-way ANOVA and Bonferroni's post hoc test).

5.2.2. Augmented cytoplasmic and nucleoplasmic CaTs in old SHR

Using the linescan mode of our confocal microscope (Figure 5-15A), electrically stimulated (1 Hz) cytoplasmic and nucleoplasmic CaTs were simultaneously recorded as Fluo-4 fluorescence changes (Figure 5-15B) in 15-25 months old SHR (at the time of HF development). As previously shown in 12-14 weeks old rats, also here in linescan images, nuclear CaTs (N, Nuc, gray) were obviously slower than cytoplasmic CaTs (C, Cyto, black). This is also evident from the corresponding normalized fluorescence traces (F/F_{rest}) below. Fluorescence traces were analysed and the mean results are presented in Figure 5-15C and 5-15D. Figure 5-15C illustrates comparison between WKY and all SHR, while Figure 5-15D illustrates comparison between WKY and SHR-NF/SHR-HF, emphasising differences between SHR-NF and SHR-HF. When we compare WKY with all SHR, diastolic Ca^{2+} did not differ neither in the cytoplasm nor in the nucleoplasm. On the other hand, CaT amplitudes were significantly bigger in SHR than in WKY. SHR also displayed larger nucleoplasmic-to-cytoplasmic ratio of CaT amplitude compared to WKY. There were also alterations in CaT kinetics between WKY and all SHR. The rise time of CaTs in SHR was slower in the cytoplasm but faster in the nucleoplasm compared with WKY, resulting in significantly smaller nucleoplasmic-to-cytoplasmic ratio of the rise time in SHR. Furthermore, cyto- and nucleoplasmic CaTs of SHR had faster kinetics of decay than WKY. Strikingly, when we compared SHR-NF with SHR-HF, cytoplasmic and nucleoplasmic CaT amplitudes in SHR-HF were significantly larger than in SHR-NF. Additionally, there was gradual acceleration of the kinetics of nucleoplasmic CaTs during progression of HF in the direction (WKY)-(SHR-NF)-(SHR-HF).

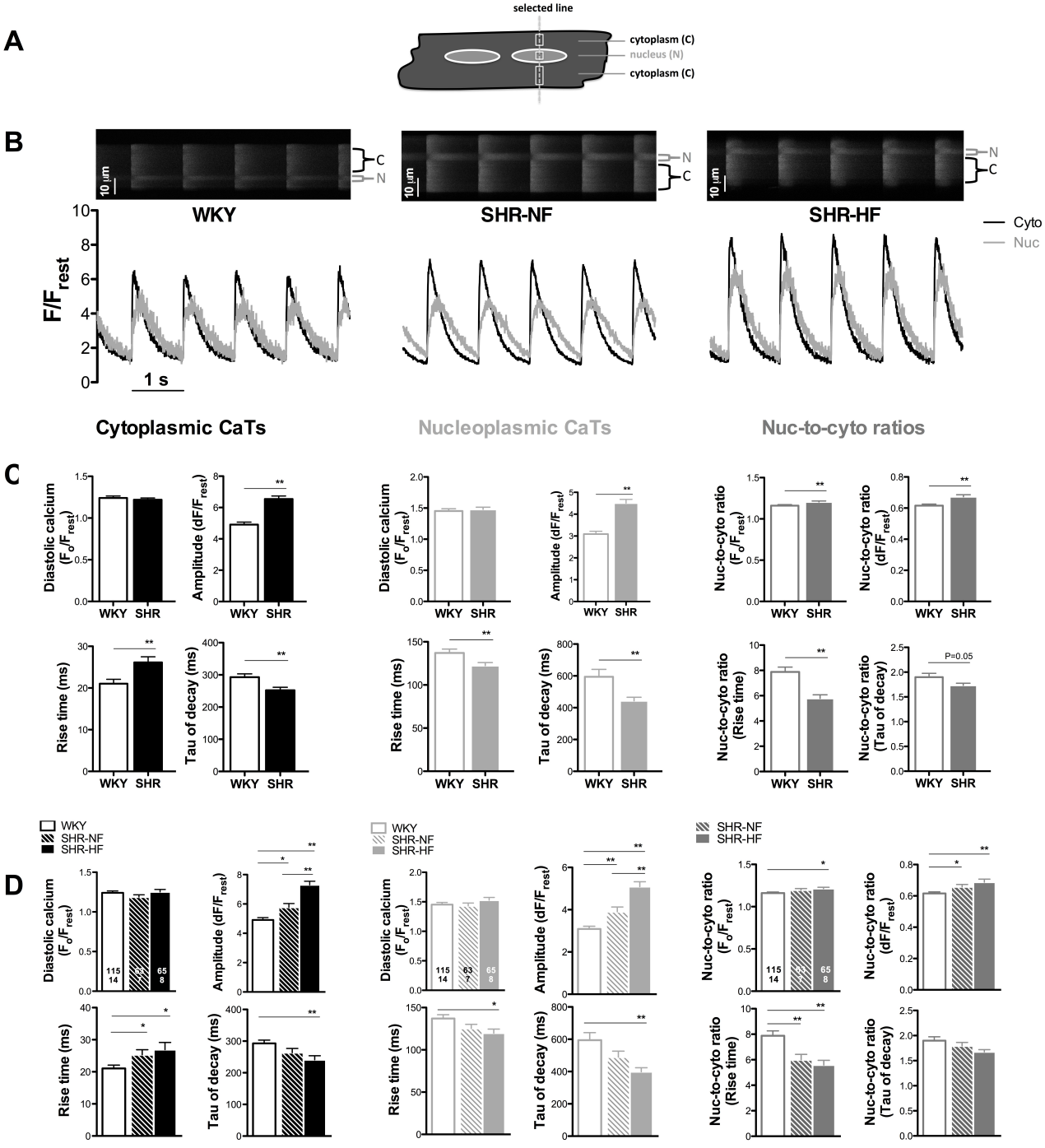

Figure 5-15. Fluo-4 fluorescence analyses of cytoplasmic and nucleoplasmic CaTs in electrically stimulated ventricular myocytes from 15-25 months old WKY and SHR.

(**A**) Scheme illustrating positioning of the scanned line in a ventricular myocyte. (**B**) Linescan images of field stimulated CaTs in the nucleus (N) vs cytoplasm (C) of typical ventricular myocytes from WKY, SHR-NF and SHR-HF and corresponding normalized fluorescence

traces. **(C)** Comparison of average fluorescence values of cytoplasmic and nucleoplasmic CaTs (amplitude (dF/F_{rest}, diastolic calcium (F_o/F_{rest}), rise time and time constant (tau) of CaT decay) between 15-25 months old WKY and 15-25 months old SHR**. (D)** Comparison of average fluorescence values of cytoplasmic and nucleoplasmic CaTs (amplitude (dF/F_{rest}, diastolic calcium (F_o/F_{rest}), rise time and time constant (tau) of CaT decay) between 15-25 months old WKY, SHR-NF and SHR-HF. Right panels in (C) and (D) present average values of the respective nucleo-to-cytoplasmic ratios. (n=115, N=14 WKY; n=128, N=15 SHR; n=63, N=7 SHR-NF; n=65, N=8 SHR-HF). *P<0.05, **P<0.01.

As previously with 12-14 weeks old rats, in 15-25 months old rats we calibrated Fluo-4 fluorescence changes in order to quantify absolute $[Ca^{2+}]$ changes in the cytoplasm and nucleoplasm (Figure 5-16). Calibration of cells not subjected to the in situ calibration protocol is based on the assumption that they have similar $[Ca^{2+}]_{rest}$ as the ones used for in situ calibration. Therefore, we compared F_{rest} between 12-14 weeks old WKY and SHR and 15-25 months old WKY and SHR. Using F_{rest} values and $[Ca^{2+}]_{rest}$ obtained from in situ calibration from 12-14 weeks old WKY and SHR, we have calculated $[Ca^{2+}]_{rest}$ for 15-25 months old rats. Calculated in this way $[Ca^{2+}]_{rest}$ for 15-25 months old WKY, SHR-NF and SHR-HF was as follows: 84, 94 and 73 nM in the cytoplasm and 93, 101 and 78 nM in the nucleoplasm, respectively. Using these $[Ca^{2+}]_{rest}$ values and K_d and R_f values obtained from 12-14 weeks old rats before, we transformed the Fluo-4 fluorescence signals from 15-25 months old rats into absolute $[Ca^{2+}]$. In this way, we calculated cyto- and nucleoplasmic diastolic and systolic $[Ca^{2+}]$ and the CaT amplitude for WKY, SHR-NF and SHR-HF. As for fluorescence traces, Figure 5-16A illustrates comparison between WKY and SHR (pooled SHR-NF and SHR-HF), while in Figure 5-16B we compared WKY with SHR-NF and SHR-HF separately, in order to emphasise differences between SHR-NF and SHR-HF. Compared to 12-14 weeks old WKY, 15-25 months old WKY had slightly lower cytoplasmic diastolic $[Ca^{2+}]$ in the range of ≈110 nM, and a CaT amplitude in the range of ≈1000 nM. Diastolic $[Ca^{2+}]$ in the nucleus in 15-25 months old WKY was higher (≈160 nM) than in the cytoplasm (also a bit lower than in 12-14 weeks old WKY) and CaT amplitude in the nucleus was similar to the cytoplasm in the range ≈1000 nM (a bit higher than in 12-14 weeks old WKY). Slightly lower cytoplasmic CaT amplitude and higher nucleoplasmic CaT amplitude in 15-25 months old WKY

yielded a nuc-to-cyto ratio of 0.89±0.03 (n=115, N=14), which is a bit higher than in 12 weeks old WKY. Compared to 15-25 months old WKY, 15-25 months old SHR myocytes (Figure 5-16A) displayed similar cyto- and nucleoplasmic diastolic [Ca^{2+}], but significantly elevated CaT amplitudes in the range of ≈1500 nM both in the cytoplasm and nucleoplasm, resulting in a nuc-to-cyto ratio for CaT amplitude closer to unity (≈0.95, similar to 12-14 weeks old SHR). However, the nuc-to-cyto ratio of CaT amplitude in old SHR was not significantly higher than in old WKY. Comparing SHR-NF and SHR-HF separately (Figure 5-16B), we additionally found that SHR-HF had significantly lower diastolic [Ca^{2+}] compared to both WKY and SHR-NF, both in the cytoplasm and nucleoplasm. CaT amplitudes were similarly increased in SHR-NF and SHR-HF compared to WKY. However, when SHR was subdivided, SHR-HF displayed increased nuc-to-cyto ratio of CaT amplitude (0.98±0.06; n=65, N=8)) compared to WKY, almost reaching significance (P=0.08).

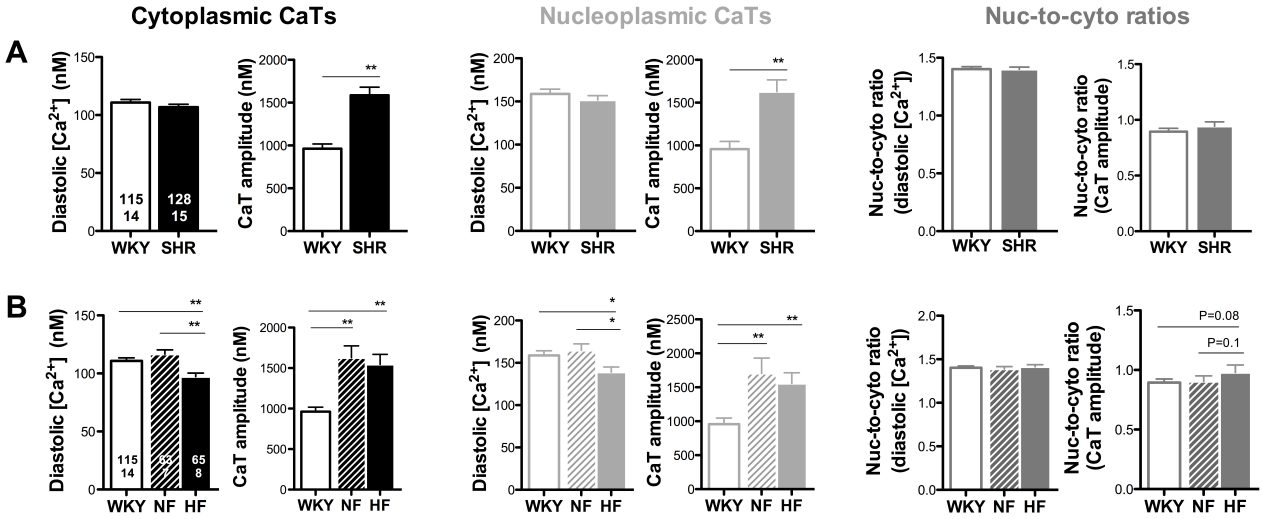

Figure 5-16. Calibrated [Ca^{2+}] data of cytoplasmic and nucleoplasmic CaTs of electrically stimulated ventricular myocytes from 15-25 months old WKY and SHR.

(A) Comparison of calibrated [Ca^{2+}] data for diastolic calcium and CaT amplitude between 15-25 months old WKY and 15-25 months old SHR**. (B)** Comparison of calibrated [Ca^{2+}] data for diastolic calcium and CaT amplitude between 15-25 months old WKY, SHR-NF and SHR-HF. Right panels in (A) and (B) illustrate average values of the respective nucleo-to-cytoplasmic ratios. (n=115, N=14 WKY; n=128, N=15 SHR; n=63, N=7 SHR-NF; n=65, N=8 SHR-HF). *P<0.05, **P<0.01.

Additionally, in all groups, there was a direct positive correlation between the tau of decay of nucleoplasmic CaT and cytoplasmic CaT (Figure 5-17). The slope of the linear regression line in SHR-HF was significantly smaller than in WKY and SHR-NF. In constrast to CaT decay, the rise time of the nucleoplasmic CaT was not correlated with the rise time of the cytoplasmic CaT in all groups.

Taken together, these data suggested that both cytoplasmic and nucleoplasmic CaTs were augmented in SHR with advanced HHD, similarly as in 12 weeks old SHR. Interestingly, in all groups kinetics of the rise of nucleoplasmic CaT did not follow kinetics of the rise of cytoplasmic CaT, while kinetics of nucleoplasmic CaT decay followed kinetics of cytoplasmic CaT decay, with a significantly less steep slope in SHR-HF compared to WKY and SHR-NF. These data indicated that HF development might be associated with alterations of nuclear Ca^{2+} handling in SHR. Further on, our goal was to try to elucidate which factors contribute to these alterations.

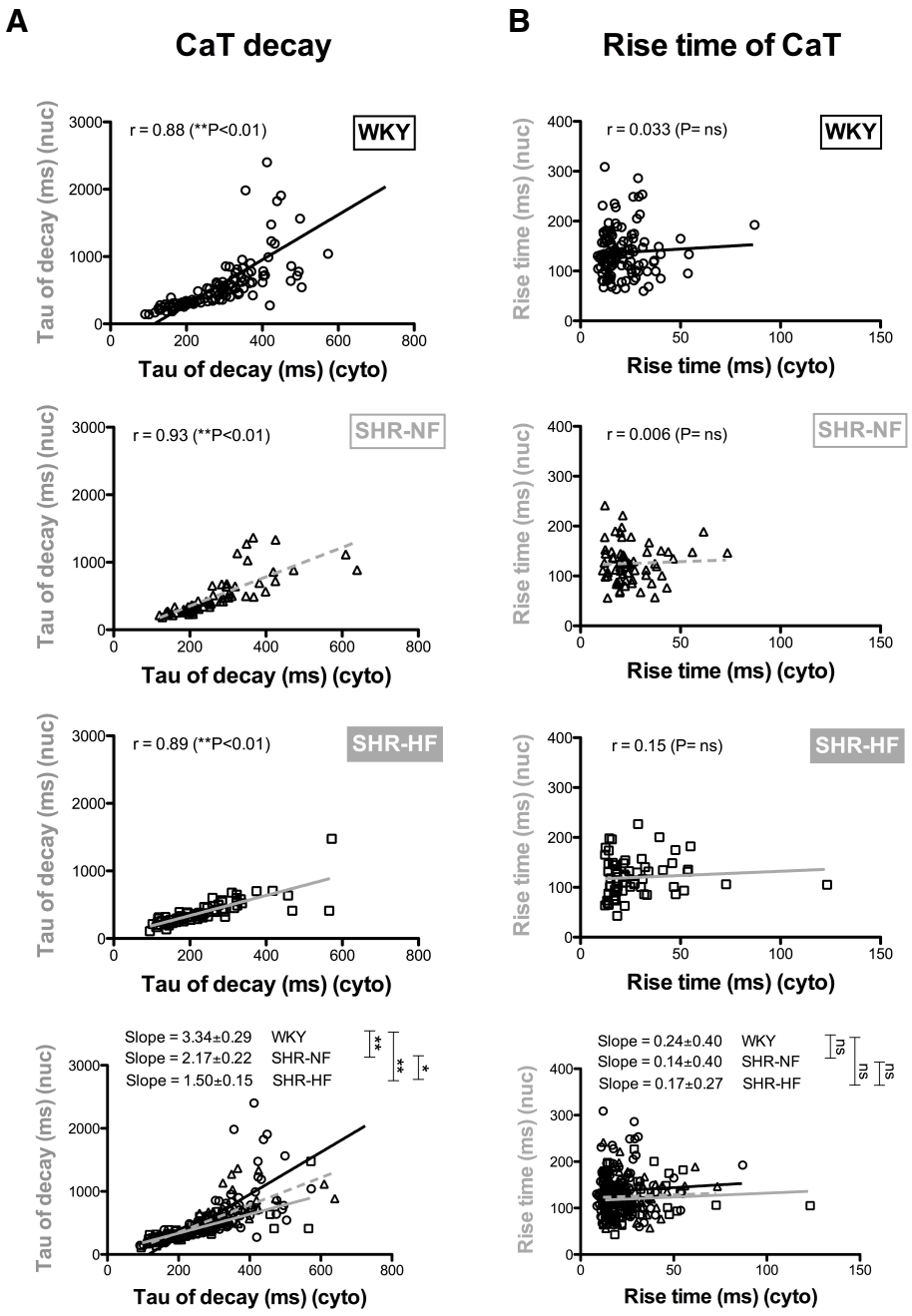

Figure 5-17. Correlation between the tau of decay and the rise time of cytoplasmic and nucleoplasmic CaTs in WKY, SHR-NF and SHR-HF left ventricular cells.

(A) The tau of decay of nucleoplasmic CaTs was positively correlated with the tau of decay of cytoplasmic CaTs in WKY, SHR-NF and SHR-HF, as indicated from Spearman correlation coefficients (r). The slope of correlation line in SHR-HF was significantly smaller than in WKY and SHR-NF. **(B)** The rise time of nucleoplasmic CaTs was not correlated with the rise time of cytoplasmic CaTs, as indicated from Spearman correlation coefficients (r) (P= ns). (n=115, N=14 WKY; n=63, N=7 SHR-NF; n=65, N=8 SHR-HF). *P<0.05, **P<0.01.

5.2.3. Increased SR and NE Ca^{2+} load and fractional Ca^{2+} release in old SHR

The Ca^{2+} content of the SR and NE, as an important factor determining the amplitude of CaTs, was further evaluated by rapid application of caffeine in cells loaded with Fluo-4 (Figure 5-18). Amplitudes of cytoplasmic and nucleoplasmic caffeine-evoked CaTs, as a measure of SR and NE Ca^{2+} load, were smaller in old WKY and SHR compared to 12 weeks old WKY and SHR, indicating lower Ca^{2+} loading with age. However, both SR and NE Ca^{2+} loads were larger in SHR-NF and SHR-HF than in old WKY. Fractional Ca^{2+} release from both SR and NE were also significantly bigger in SHR-NF and SHR-HF compared to old WKY, amounting to ≈0.70-0.75 for SR and ≈0.50-0.55 for NE, a little higher than in 12 weeks old SHR. Therefore, increased SR/NE Ca^{2+} content and, on top of it, higher fractional Ca^{2+}release from SR/NE could explain higher CaTs both in SHR-NF and SHR-HF.

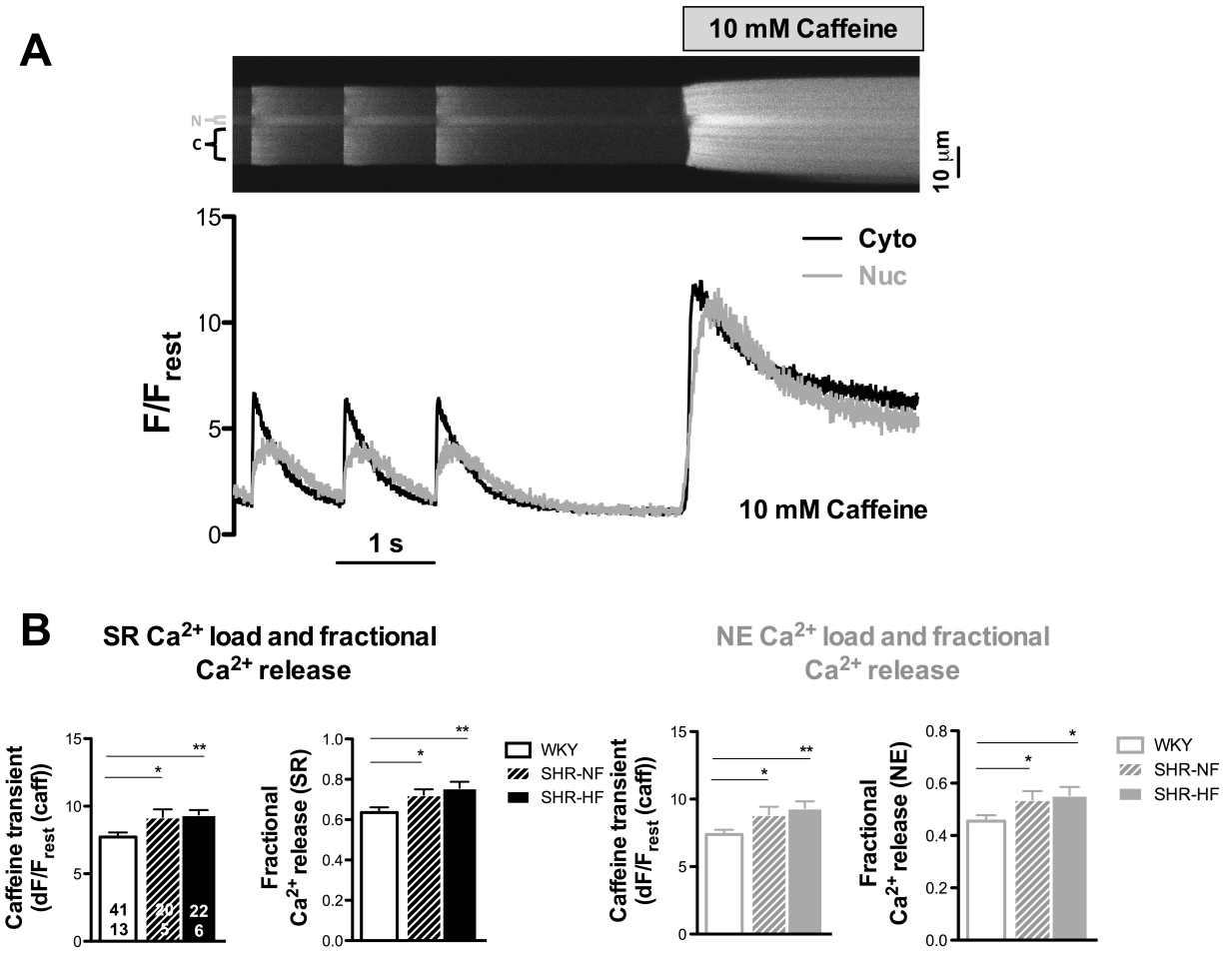

Figure 5-18. SR and perinuclear Ca^{2+} load and fractional Ca^{2+} release in ventricular myocytes from 15-25 months old WKY, SHR-NF and SHR-HF.

(A) Linescan image from WKY ventricular myocyte and corresponding normalized fluorescence traces of nucleoplasmic (N, Nuc, grey) and cytoplasmic (C, Cyto, black) CaTs recorded before and during caffeine (10 mM) application. **(B)** Average values of caffeine-evoked CaT amplitude (as a measure of Ca^{2+} load) and fractional Ca^{2+} release in cytoplasm (left) and nucleus (right) of ventricular myocytes from WKY, SHR-NF and SHR-HF (n=41, N=13 WKY; n=20, N=5 SHR-NF; n=22, N=6 SHR-HF). *P<0.05, **P<0.01.

5.2.4. Increased number and density of nuclear tubules in SHR-HF

As mentioned before, the presence of deep branching tubular structures of the NE (Bootman et al, 2008, Alonso & Garsia-Sancho, 2011) which contain NPCs might influence diffusion of ions and transcription factors between the cytoplasm and nucleoplasm (Ljubojevic et al, 2014). Alterations in the kinetics of nucleoplasmic CaTs, especially in SHR-HF, might result from alterations in the density of NTs. Therefore, using confocal 2D imaging, we compared nuclear morphology from WKY, SHR-NF and SHR-HF ventricular myocytes loaded with the low affinity Ca^{2+} dye Mag-Fluo-4 (Figure 5-19).

Firstly, our results showed that ventricular cells and nuclei from control 15-25 months old WKY were significantly bigger compared to 12-14 weeks old WKY, suggesting further growth of myocytes and nuclei with age. Compared to 15-25 months old WKY and also to 12-14 weeks old SHR, ventricular myocytes and nuclei from SHR-NF and SHR-HF (Figure 5-19B) were significantly enlarged to a similar extent, indicating that the later stages of HHD are associated with further hypertrophy of the left ventricle. The number of NTs in 15-25 months old WKY was similar as in 12-14 weeks old WKY and SHR. On the other hand, there was a clear gradual increase of the number of NTs of SHR-NF and SHR-HF (Figure 5-19D), with SHR-NF having a slightly higher number of NTs compared to WKY, and SHR-HF having significantly more NTs compared to both WKY and SHR-NF. After calculating density of NTs, SHR-NF displayed the same value as WKY, while SHR-HF showed a pronounced increase in the density of NTs compared to both WKY and SHR-NF. These results suggest that the transition from compensated LV hypertrophy to HF in the old SHR is associated with structural remodeling of the nucleus.

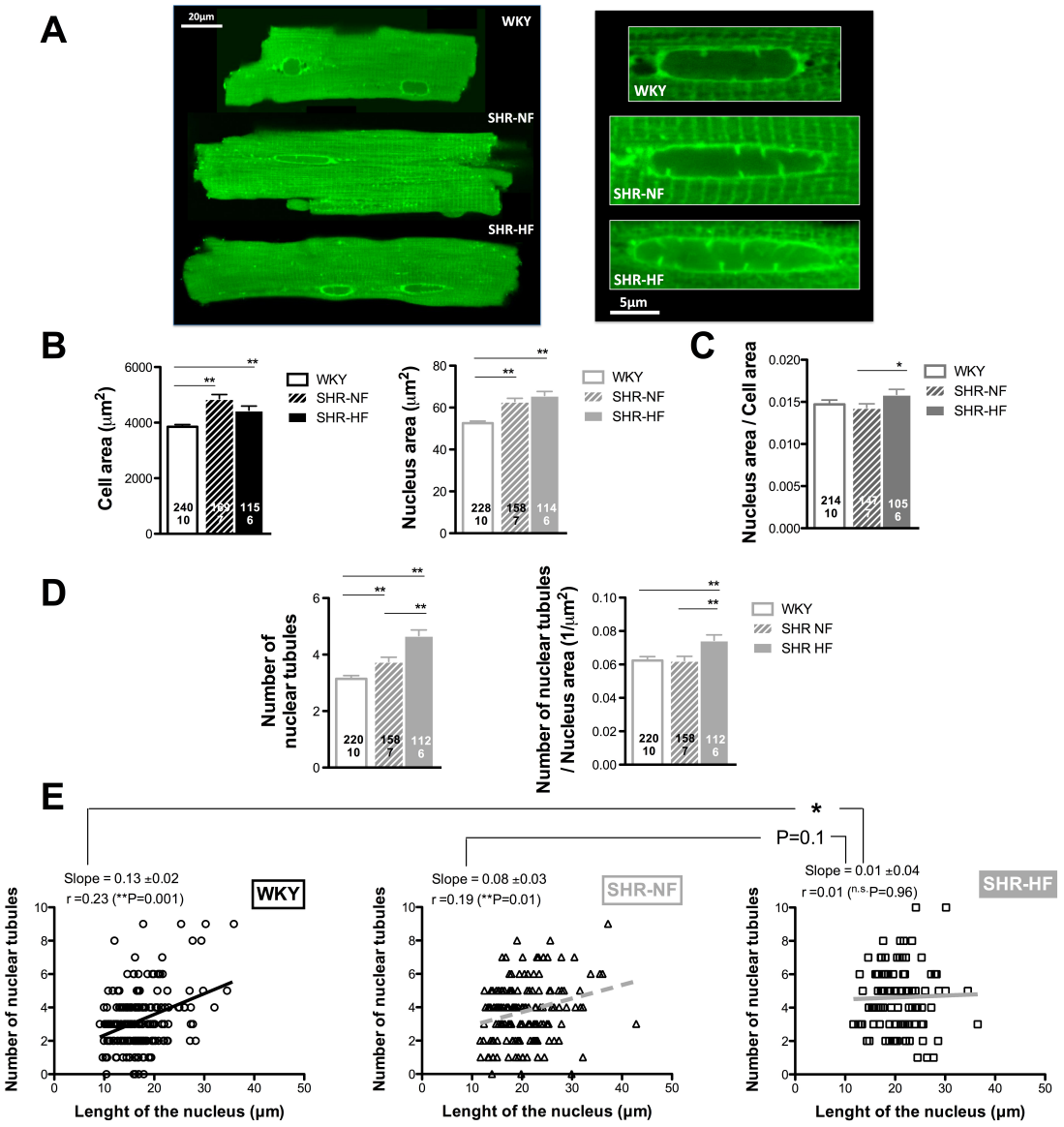

Figure 5-19. Morphology of ventricular myocytes and nuclei from 15-25 months old WKY, SHR-NF and SHR-HF.

(A) Representative images of ventricular myocytes (left) and nuclei (right) from WKY, SHR-NF and SHR-HF. Cells were loaded with 10 µM Mag-Fluo 4/AM. **(B)** Average values of cell area (n=240, N=10 WKY; n=169, N=7 SHR-NF; n=115, N=6 SHR-HF) and nucleus area (n=228, N=10 WKY; n=158, N=7 SHR-NF; n=114, N=6 SHR-HF). **(C)** Mean values of nucleus-to-cell area ratio (n=214, N=10 WKY; n=147, N=7 SHR-NF; n=105, N=6 SHR-HF). **(D)** Average values of the number and density of NTs (n=220, N=10 WKY; n=158, N=7 SHR-NF; n=112, N=6 SHR-HF). **(E)** Correlation of NTs with the length of the nucleus. Spearman correlation coefficients (r) indicated positive correlation in WKY and SHR-NF (n=197 WKY; n=158 SHR-NF; n=108 SHR-HF). Slope was lower in SHR-HF compared to WKY (P=0.1) and SHR-NF (*P<0.05). **P<0.01.

The number of NTs was positively correlated with the length of the nuclei in both WKY and SHR-NF (Figure 5-19E), while in SHR-HF this correlation was lost. This means that in SHR-HF many nuclei had a higher density of NTs, no matter how long they were. Or in other words, many smaller nuclei in SHR-HF already exhibited a high number of NTs, yielding a higher density in SHR-HF overall. Increased density of NTs in SHR-HF could contribute to the faster rise and decay time of nucleoplasmic CaTs.

Since we observed more NTs with development of HF in SHR and a cardinal sign of HF is lung congestion, we also tried to correlate the density of NTs with the lung weight in WKY and SHR. While in WKY there was no correlation at all, in SHR there was a slight tendency, which did not reach statistical significance (P=0.1).

To test our hypothesis that increased density of NTs indeed contributes to the faster kinetics of nucleoplasmic CaTs, we performed correlation of rise time and tau of decay of nucleoplasmic CaTs with the density of NTs in WKY and SHR (Figure 5-20). Mean values of rise time and tau of decay for each WKY and SHR were correlated with the mean value of the density of NTs obtained for each rat on the same day of experiments. In both WKY and SHR, rise time was decreasing with an increase in the density of NTs. Correlation coefficients indicated that rise time was much better negatively correlated with the density of NTs in SHR (r=-0.70, P<0.01)) than in WKY (r=-0.41, P=n.s.). With regard to CaT decay, in WKY tau of decay was decreasing with the increase in the density of NTs, but not in SHR.

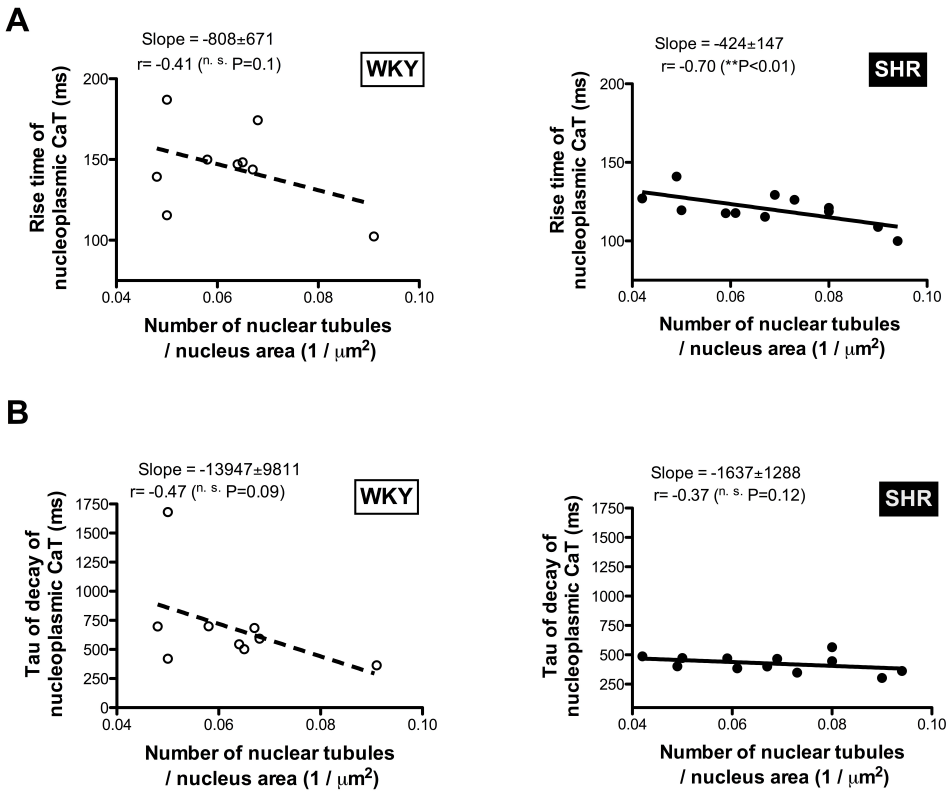

Figure 5-20. Correlation of kinetic parameters of nucleoplasmic CaTs with the density of nuclear tubules in 15-25 months WKY and SHR.

(A) Rise time of nucleoplasmic CaTs as a function of the density of NTs in WKY and SHR. Slopes of correlation lines did not differ (P=n.s.). Pearson correlation coefficients (r) indicated better negative correlation in SHR (**P<0.01). **(B)** Tau of decay of nucleoplasmic CaTs as a function of the density of NTs in WKY and SHR. Slopes of correlation lines differed almost significantly (P=0.1). Pearson correlation coefficients (r) indicated lower negative correlation in SHR. (n=9 WKY; n=12 SHR).

These data could partially explain why we have lower nuc-to-cyto ratio of the rise time of nucleoplasmic CaTs in SHR-HF than in WKY. On the other hand, tau of decay of nucleoplasmic CaTs in SHR-HF clearly better follows kinetics of decay of cytoplasmic CaTs. Existence of lower nuc-to-cyto ratio of the rise time of nuclear CaTs in SHR-NF clearly needs to be further studied, and might result from differential expression of NPCs in SHR-NF. The question why kinetics of decay do not correlate with the density of NTs in old SHR might be answered by comparing the expression of NPCs and Ca^{2+} handling proteins in the nuclei of WKY and SHR.

5.2.5. Faster intranuclear Ca^{2+} propagation in SHR-HF

To test if faster kinetics of nucleoplasmic CaTs observed in SHR are brought about by differences in passive diffusion of Ca^{2+} through the NPCs on the NE or inside the nucleus, we compared Ca^{2+} propagation velocity through the NE (from small cytoplasmic (C) regions close to the NE to subnucleolemmal (SN) regions) and intranuclear Ca^{2+} propagation (from subnucleolemmal (SN) regions to central nuclear (CN) regions) in the same way as in 12-14 weeks old rats (Figure 5-21).
Compared to 12-14 weeks old WKY, old WKY displayed similar Ca^{2+} propagation velocities both through the NE (≈25 µm/s) and from subnucleolemmal (SN) regions to central nuclear (CN) regions (≈50 µm/s). SHR-NF behaved similarly. Propagation of Ca^{2+} through NE in SHR-HF was also similar to both SHR-NF and WKY. Importantly, however, Ca^{2+} propagation inside the nucleus from subnucleolemmal (SN) regions to central nuclear (CN) regions was much faster in SHR-HF (≈125 µm/s, P=0.05) than in both WKY and SHR-NF (and also faster than in 12-14 weeks old SHR). These results are in agreement with the increased density of NTs and the accelerated rise time of CaTs in SHR-HF.

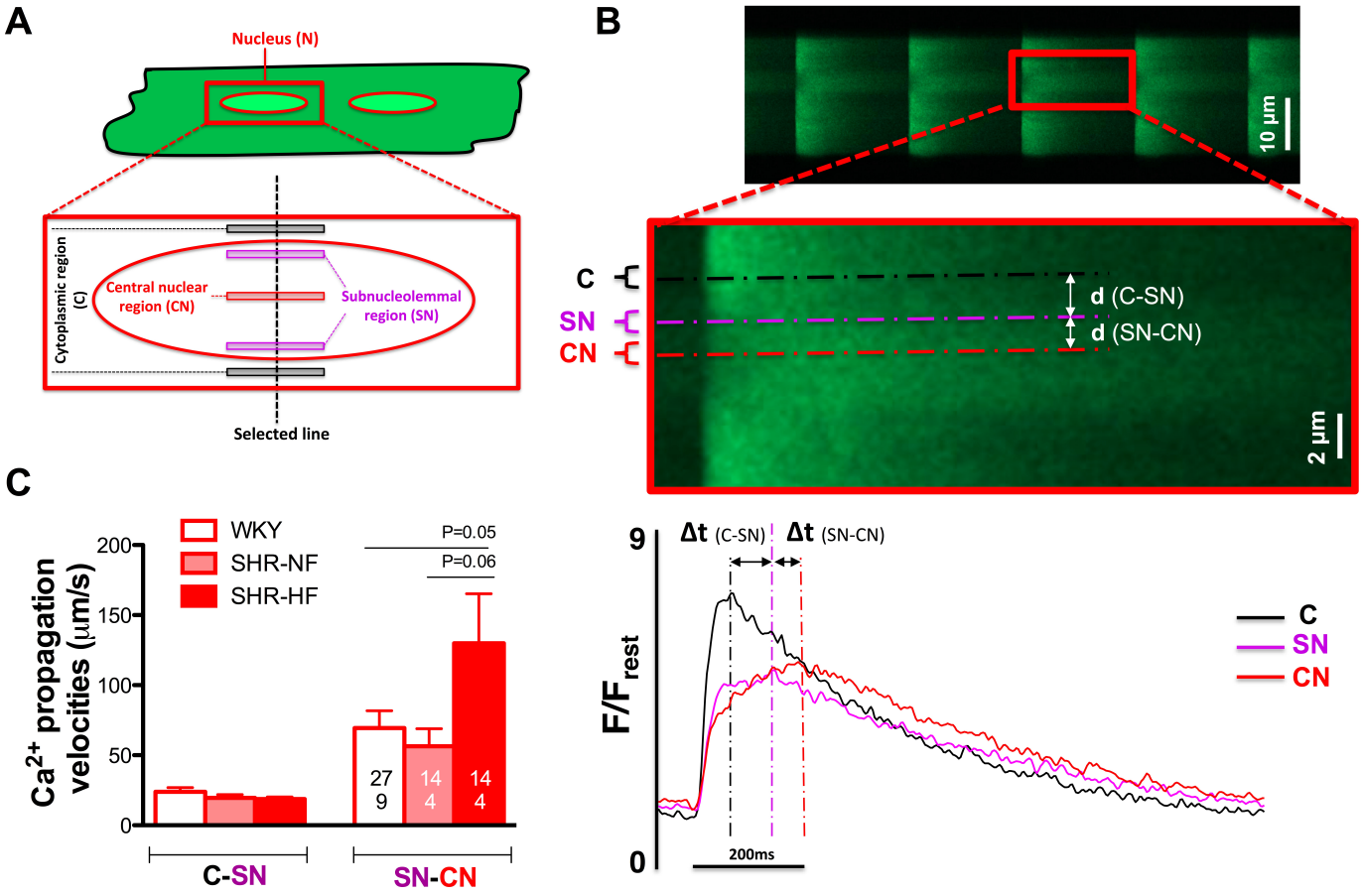

Figure 5-21. Ca^{2+} propagation into and inside of the nucleus in left ventricular myocytes from 15-25 months old WKY, SHR-NF and SHR-HF.

(A) Schematic representation of a ventricular myocyte and nucleus (magnified) illustrating positioning of the scanned line and definition of subcellular regions chosen for analysis. **(B)** Linescan image of cyto- and nucleoplasmic CaTs from an SHR-NF ventricular myocyte. Magnification illustrates nucleoplasmic CaT (smoothed) and corresponding normalized fluorescence traces (averaged over 4-5 CaTs) from a cytoplasmic (C) region adjacent to the nuclear envelope, a subnucleolemmal (SN) region and a central nuclear (CN) region. The distances between cytoplasmic and subnuclear regions (d(C-SN) and d(SN-CN)) and the differences between the time to peak of each corresponding CaT (Δt (C-SN) and Δt (SN-CN)) were taken for calculation of Ca^{2+} propagation velocities. **(C)** Average values of Ca^{2+} propagation velocities indicate faster intranuclear Ca^{2+} spread (P=0.05) (from SN to CN region) in SHR-HF nuclei (n=27, N=9 WKY; n=14, N=4 SHR-NF; n=14, N=4 SHR-HF).

5.2.6. Altered expression of Ca^{2+} handling proteins in left ventricular tissue of SHR-HF

Since we managed to elucidate some factors contributing to the faster and augmented nuclear CaTs in SHR-HF, and since nuclear CaTs mainly depend on cytoplasmic CaTs, our next goal was to investigate global cytoplasmic Ca^{2+} handling. Therefore, we compared expression of Ca^{2+}-regulating proteins in the LV tissue of WKY and SHR-HF.

Regarding major sarcolemmal Ca^{2+} handling channels (Figure 5-22), Western blot analyses revealed unaltered expression of the α1C subunit of LTCC and increased expression of NCX1 in SHR-HF LV tissue

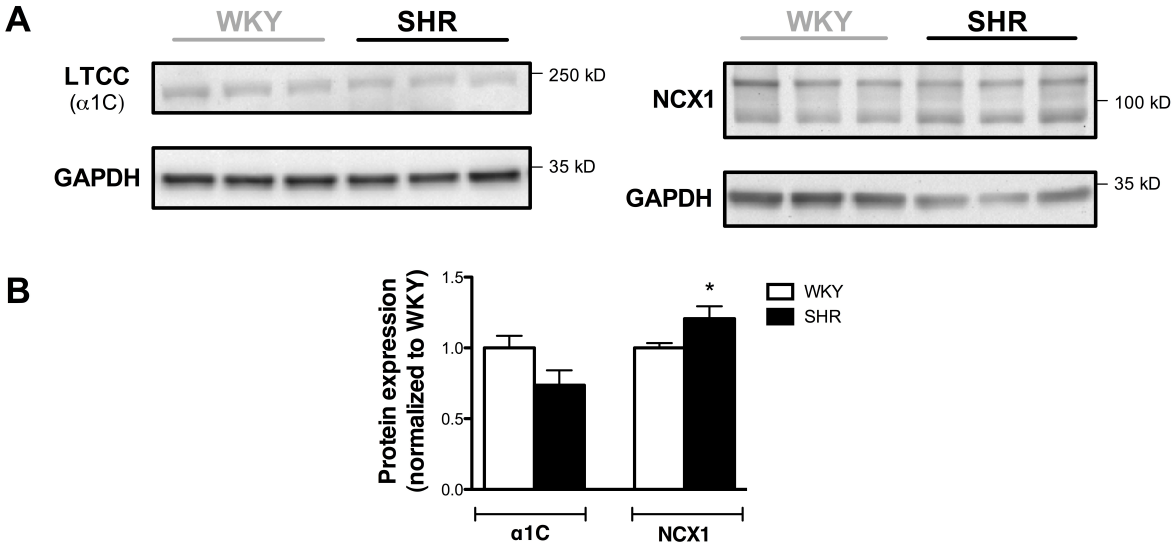

Figure 5-22. Expression of major sarcolemmal Ca^{2+} handling proteins in left ventricular tissue lysates from 15-25 months old WKY and SHR-HF.

(A) Western Blots and **(B)** average data of LTCC (α1C) and NCX1 expression in LV tissue lysates from WKY and SHR-HF. After normalization to GAPDH, values were normalized to control WKY expression level (N=8 WKY, N=7 SHR-HF). *P<0.05.

We next analysed the most important proteins involved in SR Ca^{2+} release (Figure 5-23). The protein levels of RyR2 did not differ between WKY and SHR-HF. RyR2 function is regulated through phosphorylation by PKA (at Ser2808) and CaMKII (at Ser2814). Phosphorylation leads to higher open probability and increased Ca^{2+} leak through RyR2 (Huke & Bers 2008). Western blot analysis revealed unaltered phosphorylation at the PKA site and decreased phosphorylation at the CaMKII site in SHR-HF, suggesting that RyR2 might be less leaky in SHR-HF. Protein expression of IP3R2, the other SR Ca^{2+} release channel, was unchanged or increased. Using an antibody from Abcam, there was no change, while using the custom made CLG antibody (kindly provided by Dr. H. L. Roderick, Cambridge) we found much higher expression in SHR-HF than in WKY ($P<0.01$). So, it might be necessary to use a third antibody in order to make a final statement. CSQ is a major intra SR Ca^{2+} buffering protein involved in regulation of RyR gating. There was no change of CSQ expression between WKY and SHR-HF.

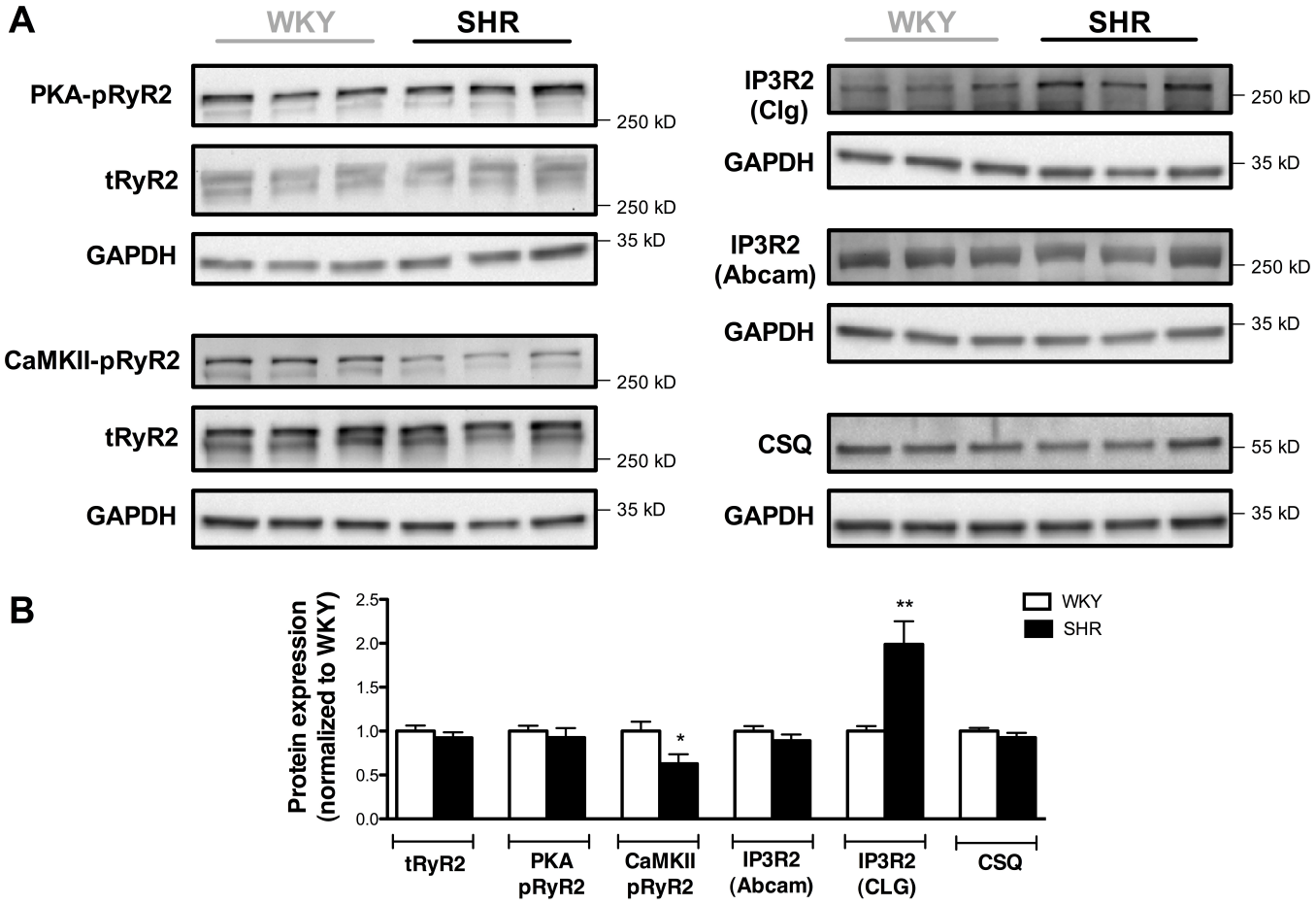

Figure 5-23. Expression of major SR Ca^{2+} release proteins in LV tissue lysates from WKY vs SHR-HF.

(A) Western Blots and **(B)** average data of tRyR2, pRyR2S2808 (PKA phosphorylation), pRyR2S2814 (CaMKII phosphorylation), IP3R2 (using two different antibodies: Abcam and custom made CLG) and calsequestrin (CSQ) protein expression in LV tissue lysates from WKY and SHR-HF. GAPDH was used as loading control. After normalization to GAPDH, values were normalized to control WKY expression level (N=8 WKY, N=7 SHR-HF). *P<0.05,**P<0.01.

Western blot analyses of SR Ca^{2+} reuptake proteins (Figure 5-24) revealed significantly lower protein levels of SERCA2a in SHR-HF. The most important endogenous regulator of SERCA2a function is the small protein PLB. In dephosphorylated form, PLB is binding to and inhibiting SERCA2a activity. Upon phosphorylation, PLB dissociates from SERCA2a and the inhibitory effect is removed (Kranias & Hajjar, 2012). The most important kinases, which regulate PLB activity, are PKA (phosphorylates PLB at Ser16) and CaMKII (phosphorylates PLB at Thr17). LV tissue from SHR-HF had lower levels (P=0.07) of PLB phosphorylated at Thr17 (CaMKII-pPLB), unchanged levels of PLB phosphorylated at Ser16 (PKA-pPLB) and unchanged levels of total PLB (tPLB). Lower expression of SERCA2a and unchanged expression of tPLB yielded a higher tPLB/SERCA2a ratio in SHR-HF. Increased tPLB/SERCA2a ratio together with lower levels of CaMKII-pPLB in SHR-HF indicated a bigger inhibitory effect of PLB on SERCA2a, which would suggest decreased activity of SERCA2a in SHR-HF.

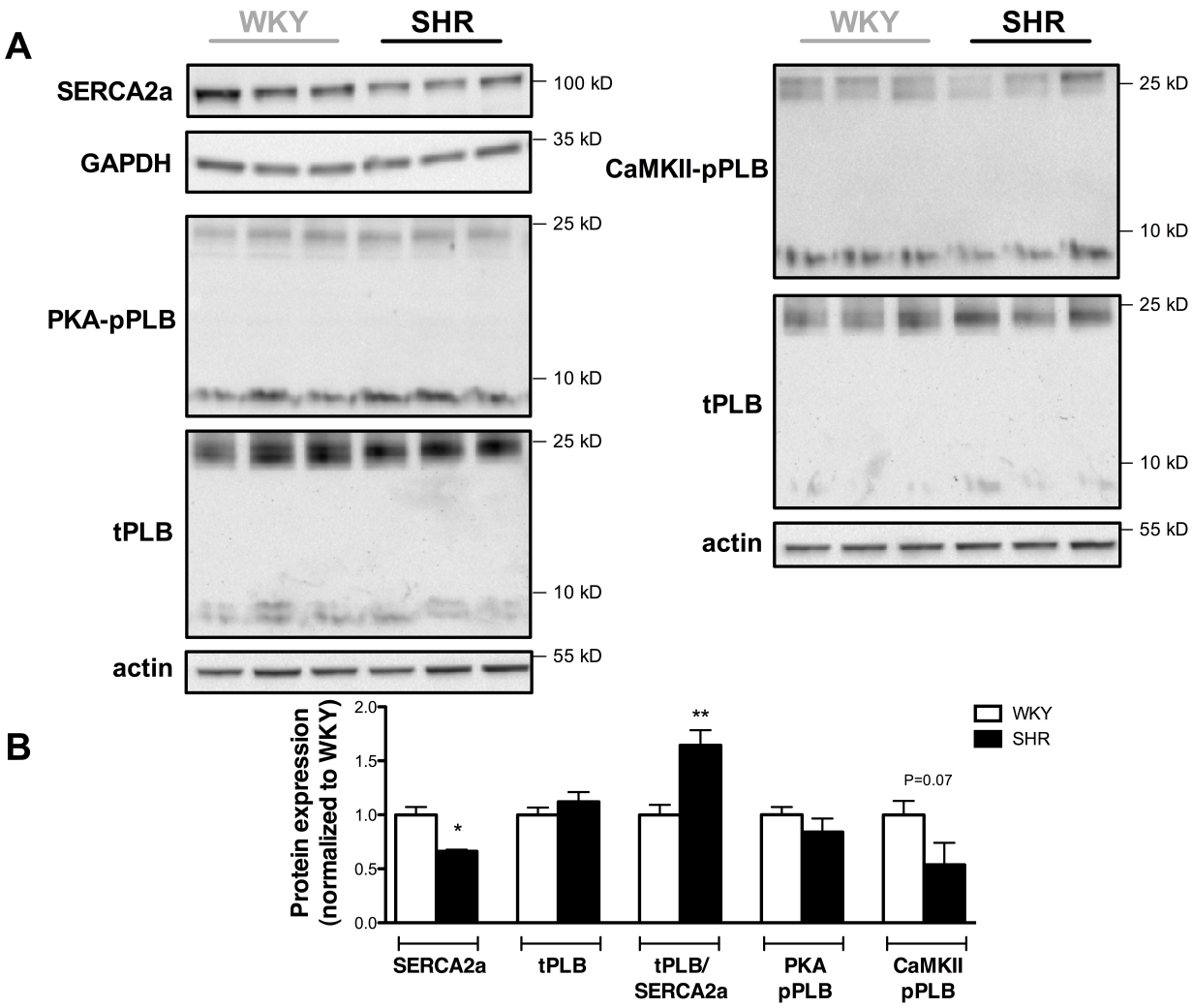

Figure 5-24. Expression of major SR Ca^{2+} reuptake proteins in LV tissue lysates from WKY vs SHR-HF.

(A) Western Blots and **(B)** average data of SERCA2a, total phospholamban (tPLB), pPLBS16 (PKA phosphorylation), pPLBT17 (CaMKII phosphorylation) expression and tPLB/SERCA2a ratio in LV tissue lysates from WKY and SHR-HF. GAPDH or actin was used as loading control. After normalization to GAPDH or actin, values were expressed relative to the WKY expression levels (N=8 WKY; N=7 SHR-HF). *P<0.05, **P<0.01.

So, the Western blot data suggested that during development of HF in SHR CaMKII activity might be decreased. Thus, we compared global CaMKII protein expression and the autophosphorylation state at T286 between WKY and SHR-HF (Figure 5-25). Levels of pCaMKII-T286 of each sample were normalized to the total CaMKII protein levels of that sample and expressed relative to control WKY. Interestingly, SHR-HF displayed increased levels of autophosphorylated CaMKII (pCaMKII-T286), but at the same time greatly reduced expression of total CaMKII. This would indicate that SHR-HF had a higher proportion of active CaMKII in a globally lower amount of CaMKII protein levels, which could explain lower CaMKII activity overall in SHR-HF, as we observed.

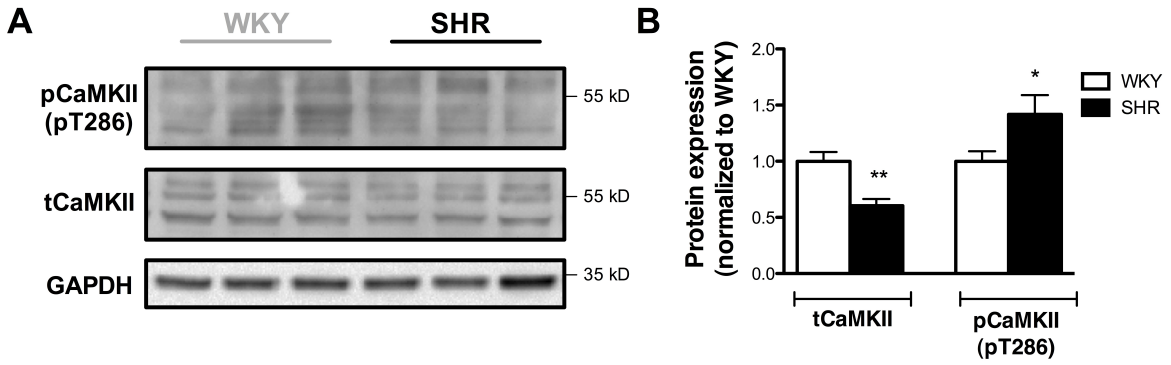

Figure 5-25. Protein levels of total CaMKII and the autophosphorylated form of CaMKII (pCaMKII-T286) in LV tissue lysates from WKY vs SHR HF.

(A) Western Blots and **(B)** average data of tCaMKII and pCaMKII-T286/tCaMKII expression in LV tissue lysates from WKY and SHR-HF. GAPDH was used as loading control. After normalization to the GAPDH, values were normalized to control WKY expression levels (N=8 WKY; N=7 SHR-HF). *P<0.05,**P<0.01.

Taken together, our results suggested decreased activity of CaMKII in SHR during HF development. Therefore, we performed correlations between CaMKII phosphorylation of RyR2 or PLB and lung weight in SHR (as an indicator of HF). Since SERCA2a and IP3R2 expression (using CLG antibody) was also changed in SHR-HF, we plotted expression of tPLB/SERCA2a and IP3R2 as a function of lung weight, too. Correlation coefficients (Figure 5-26A) indicated direct negative

correlation between phosphorylation of RyR2 at Ser2808 (P=0.09) or PLB at Thr17 (P<0.05) and lung weight in SHR. On the other hand, there were good positive correlations between tPLB/SERCA2a ratio (P=0.1) or IP3R2 expression (P<0.01) and lung weight (Figure 5-26B).

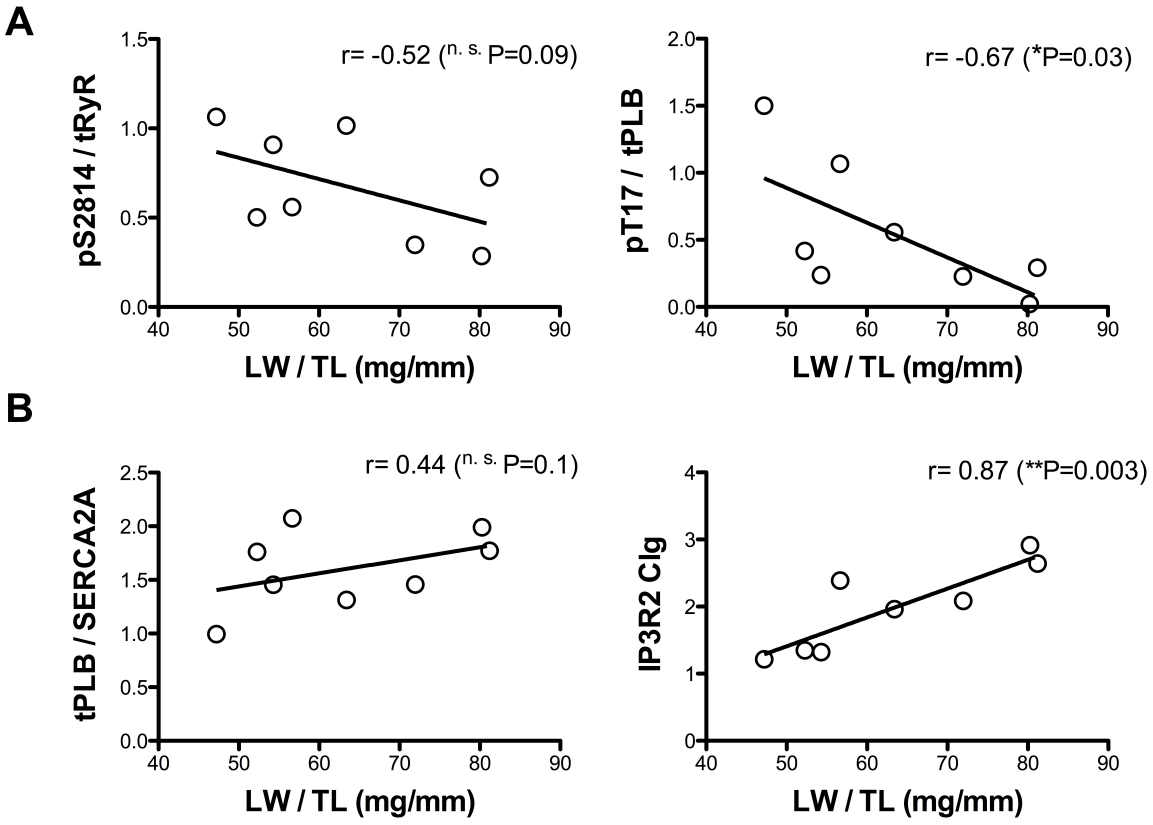

Figure 5-26. Expression and CaMKII phosphorylation of major Ca^{2+} handling proteins, tPLB/SERCA2a and IP3R2 expression in LV tissue from SHR as a function of lung weight (LW) (normalized to tibia length, TL).

(A) CaMKII phosphorylation of RyR2 at Ser2814 and PLB at Thr17 as a function of lung weight (LW) (normalized to tibia length, TL). Pearson correlation coefficients (r) indicated negative correlation**. (B)** tPLB/SERCa2a (as a measure of SERCA2a inhibition by PLB) and IP3R2 expression as a function of lung weight (LW) (normalized to tibia length, TL). Pearson correlation coefficients (r) indicated positive correlation**.** *P<0.05,**P<0.01.

To summarize, the following changes in the left ventricle of SHR at the late stage of hypertensive heart disease were found:

- LV myocytes and nuclei were larger compared to young hypertrophic SHR, suggesting further growth of the ventricle with progression of HHD.
- Cytoplasmic and nucleoplasmic CaTs were augmented (as in young hypertrophic SHR).
- SR and perinuclear (PN) Ca^{2+} load was increased (as in young hypertrophic SHR) and additionally fractional Ca^{2+} release of SR and NE was also increased.
- The decay of cytoplasmic and nucleoplasmic CaTs was accelerated (tau of decay of nuclear CaTs was positively correlated with the tau of decay of cytoplasmic CaTs).
- The rise time of CaTs was prolonged in the cytosol and shortened in the nucleus (the rise time of nuclear CaTs was not correlated with the rise time of cytoplasmic CaTs).
- Rise time, but not tau of decay, of nuclear CaTs was negatively correlated with the density of NTs in SHR.

In the LV, development of heart failure in old SHR was associated with:

- increased density of NTs in SHR-HF nuclei,
- faster intranuclear Ca^{2+} propagation in SHR-HF and
- shortening of both rise time and tau of decay of nuclear CaTs in SHR-HF.

The major changes in SHR during the transition to HF were related to nuclear structure and Ca^{2+} handling. Alterations of global Ca^{2+} handling observed by Western Blotting (increased NCX1 expression, lower SERCA2a expression, lower CaMKII phosphorylation of PLB and RyR2) could not easily explain our functional data. Therefore, for better understanding of mechanisms of regulation of cytoplasmic and nucleoplasmc Ca^{2+}, it will be necessary to compare the expression of Ca^{2+} handling proteins separately in cytosolic fraction and isolated nuclei.

6. Discussion

6.1. Early hypertension

Hypertension is the most common stimulus for the development of pathological hypertrophy and HF (Heineke et al, 2006). The aim of the first part of this thesis was to investigate the mechanisms of nuclear Ca^{2+} signaling regulation in the early stage of HHD and its potential role for the initiation and progression of cardiac hypertrophy. Shortly after the establishment of hypertension LV myocytes from young SHR (3 months) had increased nucleoplasmic Ca^{2+} signaling associated with altered nuclear expression of Ca^{2+} handling proteins, activation of the CaMKIIδ–HDAC5 pathway and increased histone acetylation. This data presents the first evidence for augmented nucleoplasmic Ca^{2+} signaling in early hypertension as a putative cause of epigenetic alterations contributing to the development of hypertrophy.

6.1.1. Structural remodeling of LV myocytes and nuclei in early hypertension

In agreement with previous studies (Brooksby et al,1993, Cerbai et al, 1994, Okayama et al, 1998, Pluteanu et al, 2015), already in early hypertension SHR displayed LV hypertrophy. Both LV myocytes and nuclei were hypertrophic with increased nucleus-to-cell area ratio in SHR. Although the mechanisms that control nuclear size remain unclear, the ratio between nuclear and cytoplasmic volumes is important for cell function. Disturbance of this ratio is associated with certain types of cancers, suggesting that this ratio is crucial for cell integrity. There is a strong correlation between nuclear size, RNA transcription levels and cell size, so the larger nuclei facilitate the increase in transcription that is required in larger cells (Webster et al, 2009). There was no change in the density of NTs in SHR. Nuclear tubules seem to be involved in regulation of diffusible substances (including Ca^{2+}) deep within the nucleus (Alonso et al, 2011, Escobar et al, 2011, Malhas et al, 2011). Containing NPCs (Ljubojevic et al, 2014) they could enable and facilitate diffusional exchange between cytosol and nucleoplasm. The presence of Ca^{2+} pumps (SERCA2a) on NTs (Echevarria et al, 2003, Ljubojevic et al, 2014) suggests their potential involvement in

regulation of nucleoplasmic CaT decay and Ca^{2+} loading of the perinuclear Ca^{2+} stores. Reduction of the density of NTs has been reported in mouse and rabbit models of pressure overload-induced hypertrophy and HF and in failing human hearts and has been related to impaired nuclear Ca^{2+} regulation (Ljubojevic et al, 2014). The preserved density of NTs shown here indicates a different situation in early hypertension. In addition to the preserved density of NTs in SHR, nuclear expression of Nup62 and Nup106, two essential components of NPCs, was increased suggesting an increased density of NPCs in SHR. An earlier study has reported an increased level of nucleoporin Nup62 in patients with ischemic and dilated cardiomyopathy (Cortes et al, 2010). An other study has shown an increase in different nucleoporins (Nup160, Nup153 and Nup93) in HF patients (Tarazón et al, 2012). Both studies suggested a relationship between changes in nucleoporin levels and the alterations of the nucleocytoplasmic transport.

The combination of preserved density of NTs and increased density of NPCs in SHR is assumed to maintain or even facilitate diffusion of Ca^{2+} into and out of the nucleus and, in that way, also systolic and diastolic regulation of nucleoplasmic CaTs.

6.1.2. Remodeling of nuclear Ca^{2+} handling in early hypertension

In early HHD, this study found elevated nucleoplasmic CaTs and lower diastolic Ca^{2+} levels in LV myocytes from SHR. SHR displayed pronounced elevation of nucleoplasmic CaTs with amplitudes doubling the amplitudes in WKY (≈1900 nM in SHR vs ≈900 nM in WKY). Consistent with previous reports on cytoplasmic Ca^{2+} signaling and EC coupling in SHR (Chen-Izu et al, 2007, Fowler et al, 2005, Shorofsky et al, 1999), CaTs in the cytosol were also augmented in SHR, exhibiting decreased diastolic Ca^{2+} and increased amplitudes. Cytoplasmic CaT amplitudes in SHR reached ≈2000 nM (vs ≈1200 nM in WKY). This finding of enhanced cytoplasmic CaTs was confined to the left ventricle, since left atrial myocytes from SHR of the same age did not exhibit any changes in cytoplasmic CaTs (Pluteanu et al, 2015). Since the cytoplasmic Ca^{2+} increase is a major determinant of the nucleoplasmic Ca^{2+} increase in systole (Ljubojevic et al, 2011), the increase in

cytoplasmic CaTs will certainly contribute to the observed elevation of nucleoplasmic CaTs in SHR. However, based on the observation that the ratio of the nucleo-to-cytoplasmic CaT amplitude was increased in SHR, there must be additional mechanisms contributing to the increase in nucleoplasmic CaTs in SHR.

The increase in NE Ca^{2+} load observed here could be one additional mechanism leading to larger nucleoplasmic CaTs in SHR. At unaltered fractional release increased NE Ca^{2+} load will lead to larger perinuclear Ca^{2+} elevations. Perinuclear Ca^{2+} elevations will be further augmented by the increased cytoplasmic CaTs (triggering even more Ca^{2+} release from perinuclear stores) and by the prolonged cytoplasmic Ca^{2+} increases (increased rise time of cytoplasmic CaTs) in SHR. Together, these factors will cause enlarged and prolonged Ca^{2+} increases in the perinuclear area, which, in turn, will augment the Ca^{2+} increases within the nucleus.

Another mechanism that represents an important contributing factor to larger nucleoplasmic CaTs in SHR is the accelerated intranuclear Ca^{2+} propagation. Nucleoplasmic Ca^{2+} increases depend mainly on diffusion of Ca^{2+} from the cytoplasm through NPCs into the nucleus. Ca^{2+} increases in the central core of the nucleus depend on Ca^{2+} propagation via diffusion from subnucleolemmal to central nuclear sites and on the presence and density of NTs extending deep into the nucleus (Ljubojevic and Bers, 2015). Augmented and prolonged Ca^{2+} increase in the perinuclear area and the increased density of NPCs at preserved density of NTs could explain the increase in Ca^{2+} propagation velocity from subnucleolemmal to central nuclear regions in SHR. While the former enhances subnucleolemmal CaTs, the latter will accelerate the central nuclear Ca^{2+} increase.

Remodeling of nuclear Ca^{2+} handling in early hypertension was clearly evident also as alterations in the protein levels of major Ca^{2+}-regulating proteins in LV myocyte nuclei from SHR. Regarding Ca^{2+} release channels, RyR2 and IP3R2 expression was unaltered. On the other side, expression of SERCA2a, which has been identified on the NE and on the NTs (Ljubojevic et al, 2014), was greatly up-regulated (doubled) and PLB showed a trend toward less nuclear expression. Thus, the major

finding in SHR nuclei was increased expression and activity of SERCA2a. This is in line with the increased Ca^{2+} load of the perinuclear Ca^{2+} stores and with the faster decay of the nucleoplasmic CaT. A recent study of Wu et al nicely demonstrated that PLB is present at relatively high levels in the NE compared to the SR, and exhibits regulation of nuclear SERCA2a, and in such way represents an important regulator of nuclear Ca^{2+} handling (Wu et al, 2016). An additional factor leading to the accelerated Ca^{2+} decay in the nucleus is the accelerated Ca^{2+} decay in the cytosol, as the faster reduction in cytoplasmic Ca^{2+} will speed up Ca^{2+} diffusion out of the nucleus, too.

Interestingly, our findings differ from what was found before in pressure-overload models of hypertrophy. Ljubojevic et al have compared the structural and functional changes of the NE and nuclear Ca^{2+} handling in ventricular myocytes at the hypertrophic phase and in HF from pressure-overload animal models and human HF (Ljubojevic et al, 2014). Firstly, they reported a progressive decrease in the density of NTs with the progression of cardiac disease (while early in HHD, we see no change in the density of NTs and higher expression of NPCs, that would even facilitate diffusion of Ca^{2+} into and out of the nucleus). Secondly, they showed reduced expression of SERCA2a and RyR2s, with increased expression of IP3Rs in the nuclei of hypertrophic and failing cardiomyocytes (while we have found higher expression of SERCA2a and unaltered expression of RyR and IP3Rs). Thirdly, the changes they observed were associated with diminished and prolonged nuclear CaTs and increased nucleoplasmic diastolic [Ca^{2+}]. In contrast, the changes that we observed here in early HHD were associated with elevated nucleoplasmic CaTs, lower nucleoplasmic diastolic [Ca^{2+}] and faster kinetics of nuclear CaTs. So, there might be differential regulation of nuclear Ca^{2+} handling depending on the model used.

6.1.3. Activation of CaMKIIδ–HDAC5 signaling and elevated histone acetylation in early hypertension

In the situation of increased cyto- and nucleoplasmic CaTs CaMKII is expected to be activated (Frey et al, 2000). CaMKIIδ is the predominant isoform in the heart. The main splice variants in adult mammalian cardiomyocytes are δB and δC (Zhang et al, 2004). δB contains a nuclear localization sequence and is located predominantly in the nucleus, whereas δC is located predominantly in the cytoplasmic compartment. Localization in a particular cellular compartment, however, is not exclusive and both splice variants are also found in significant amounts in other cellular compartments (Mishra et al, 2011). In line with these previous findings, our results revealed also higher expression of CaMKIIδB in ventricular myocyte nuclei and stronger expression of CaMKIIδC in tissue lysates. While expression of total CaMKIIδ (δB plus δC) was unchanged in SHR (or maybe slightly increased, P=0.07 vs WKY), there was a huge increase (2.5-fold) in nuclear expression of CaMKIIδ in SHR, which resulted from a massive translocation of CaMKIIδC from the cytoplasm to the nucleus. The reason for this redistribution in SHR is unknown at present. The consequence, however, is increased abundance of CaMKIIδ in myocyte nuclei. Increased nuclear CaTs observed in SHR are expected to cause increased activity of CaMKIIδ and increased phosphorylation of CaMKIIδ targets.

Nuclear CaMKIIδ phosphorylates histone deacetylase 5 (HDAC5), one of the major HDAC isoforms in ventricular myocytes and an important factor for the initiation of pathological cardiac hypertrophy (Backs et al, 2006). Phosphorylation of HDAC5 drives nuclear export of HDAC5 and leads to increased histone acetylation. Since the repression of transcription of hypertrophy genes is mediated via direct interaction of HDAC5 with myocyte enhancer factor 2 (MEF2), the dissociation of HDAC5 from MEF2 leads to de-repression of MEF2-dependent transcription (Backs et al, 2006). According to this sequence of events, we found redistribution of HDAC5 from nucleus to cytosol and, as a consequence, increased histone acetylation in SHR. Taken together, our results show that, in early HHD, there is remodeling of nuclear Ca^{2+} handling with enhanced nucleoplasmic CaTs that stimulate nuclear CaMKIIδ

activity, which, in addition, shows increased abundance in the nucleus. Nuclear CaMKIIδ phosphorylates HDAC5, the nuclear export of which initiates increased histone acetylation and MEF2-dependent transcription of hypertrophy genes.

In a previous study the increase in nucleoplasmic diastolic [Ca^{2+}] in hypertrophied and failing cardiomyocytes was also associated with activation of gene transcription via the nuclear CaMKII-HDAC pathway (Ljubojevic et al, 2014). Similarly, we have shown here the link between increased nucleoplasmic CaT amplitude and activation of CaMKII–HDAC-mediated regulation of histone acetylation as an early event in hypertension-induced cardiac remodeling (summarized in Figure 6-1). So, similar mechanisms are involved in the regulation of transcription during development of hypertrophy in pressure overload and hypertension, despite differences in the regulation of nuclear CaTs.

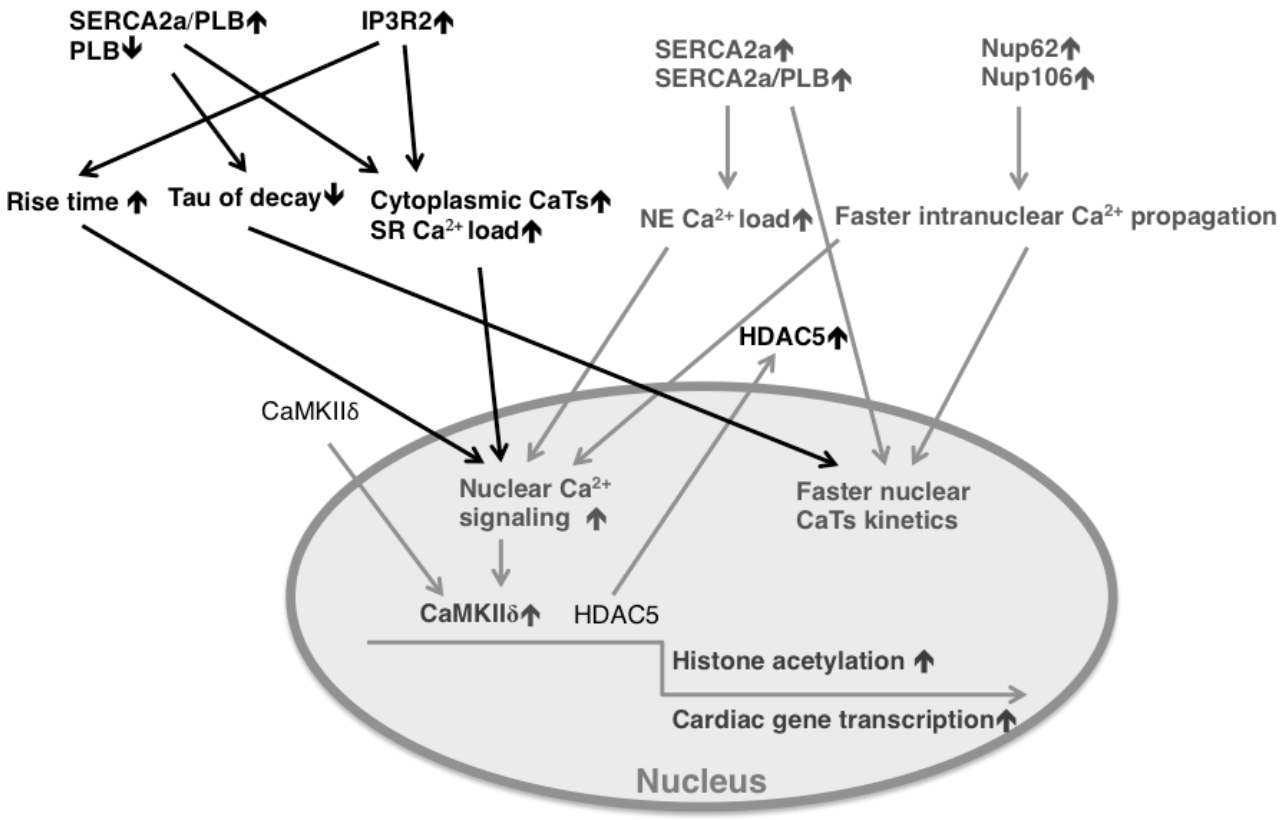

Figure 6-1. Alterations of Ca^{2+} signaling and gene transcription in LV myocytes from SHR in early HHD.

Black color indicates cytoplasmic Ca^{2+} signaling changes, while gray color indicates nucleoplasmic Ca^{2+} signaling changes in SHR. Arrows indicate connection between different findings. Briefly, prolonged and higher cytoplasmic CaTs, higher NE Ca^{2+} load and faster intranuclear calcium propagation are all expected to contribute to enhanced nuclear Ca^{2+} signaling observed in SHR. Faster cytoplasmic CaT decay, faster intranuclear calcium propagation and higher nuclear SERCA activity are expected to accelerate nuclear CaTs. Increased nuclear Ca^{2+} signaling leads to the increased activity of CaMKIIδ, which phosphorylates HDAC5 causing its export to the cytosol. Translocation of HDAC5 to the cytosol results in the increase in histone acetylation, which indicates higher cardiac gene transcription.

6.2. Advanced hypertension

Hypertension is an important risk factor for the development of LV hypertrophy. Initially, hypertrophy can be beneficial reducing myocardial stress, but chronic hypertension may lead to progression from compensated hypertrophy to HF. Very little is understood regarding factors that may trigger the transition from compensated LV hypertrophy to HF in HHD.

The present study has revealed profound remodeling of nuclear structure and Ca^{2+} handling in LV myocytes of SHR during transition to HF. Interestingly, SHR with HF exhibited higher CaTs in both cytosol and nucleoplasm, faster nuclear CaTs and intranuclear Ca^{2+} propagation associated with increased density of NTs in SHR-HF nuclei. Nuclear Ca^{2+} signaling and mechanisms of nuclear Ca^{2+} regulation in SHR with advanced HHD has not been investigated before. The current data, therefore, present the first evidence of alterations in structure and Ca^{2+} regulation in the ventricular myocyte nuclei of SHR during development of HF.

6.2.1. Structural remodeling of LV myocytes and nuclei from SHR in advanced HHD

According to the lung congestion as a sign of LV failure and in line with previous studies (Conrad et al, 1995, Boluyt et al, 1995), ≈60% of 15-25 months old SHR developed HF. Grouping old SHR into SHR-NF and SHR-HF and comparing these groups enabled identification of ventricular remodeling associated with the development of HF. Transition to HF in SHR was characterized – like in other reports (Ward et al, 2003, Chen-Izu et al, 2007) – by progression of hypertension and further growth of the whole heart (LV, RV, LA and RA).

In line with other reports (Ward et al, 2003, Cerbai et al, 1994), the current study showed that LV myocytes from old SHR were enlarged compared to both old WKY and young hypertrophic SHR, suggesting further growth of the LV with chronic

hypertension in advanced HHD. SHR nuclei in both SHR-NF and SHR-HF were also increased compared to WKY. It is important to note that on the cellular level the size of LV myocytes and nuclei were not different between SHR-NF and SHR-HF, suggesting that the growth of the LV observed on the tissue level in the period of decompensation and development of overt HF could result from the growth of other components of the heart. Indeed, many studies (Boluyt et al, 1995, Bing et al, 1991, Ward et al, 2003) reported increased levels of major components of the interstitial fibrillar network (like fibronectin and collagen I and III) and of key components regulating extracellular matrix (ECM) remodeling processes (like transforming growth factor-β1 (TGF-β1) and tissue inhibitor of matrix metalloproteinases (TIMPs)), with down-regulation of components involved in ECM degradation (like matrix metalloproteinases (MMPs) and plasminogen activator (PA)). Taken together, there is an increase in fibrosis in the LV of SHR-HF. Therefore, during transition to HF, the LV appears to be growing due to the increase of fibrosis and not due to the increase in cardiomyocyte size. In addition, there is evidence (Boluyt et al, 1995, Conrad et al, 1995) of myocyte loss and an increase in myocyte apoptosis during transition to HF in SHR.

Interestingly, our results revealed dramatic structural nuclear remodeling in SHR-HF. The current data showed a larger density of NTs in SHR-HF nuclei compared to both SHR-NF and WKY. This was unexpected, since previously a reduction of the density of NTs has been reported in pressure overload-induced HF and has been linked to impaired intranuclear Ca^{2+} regulation and slowed intranuclear Ca^{2+} diffusion (Ljubojevic et al, 2014). In SHR with HF, however, we have found a different situation and our data suggest that with the progression of cardiac remodeling in HHD, the size of nuclei stays the same, but the number of NE invaginations increases.

As mentioned before, NE invaginations penetrating deep into the nucleoplasm could have several important functional consequences. Increased density of NTs in SHR-HF is expected to facilitate diffusion of Ca^{2+} into and out of the nucleus, especially in deep nuclear regions, which might be critical for the regulation of gene transcription by local subnuclear Ca^{2+}. The presence of NPCs on the NTs facilitate also transport

of cargo in areas that would otherwise be hardly accessible from the nuclear periphery. The presence of SERCA pumps on the NTs (Ljubojevic et al, 2014) enables Ca^{2+} removal deep within the nucleus, which may play a key role in regulation of nucleoplasmic CaTs kinetics. The dramatic increase of NT density in SHR-HF is, therefore, expected to be a contributing factor in accelerating nucleoplasmic CaTs. The altered nuclear CaTs, in turn, might contribute to altered Ca^{2+}-dependent regulation of transcription and development of HF.

6.2.2. Functional remodeling – Alterations of subcellular Ca^{2+} handling in SHR with advanced HHD

Impaired Ca^{2+} homeostasis is a hallmark of HF. Many studies reported alterations of cytoplasmic Ca^{2+} handling in the LV of failing SHR (Kapur et al, 2010, Ward et al, 2010, Ward et al, 2003, Song et al, 2006, Bing et al, 1991). There is, however, discrepancy between different studies depending on the approach or the preparation analysed (intact whole heart, trabeculae, papillary muscles or isolated myocytes). Although widely studied, it is controversial whether or not abnormal myocardial Ca^{2+} handling indeed plays a role in the genesis of end-stage contractile failure in this animal model, since very few studies examined force and Ca^{2+} together in failing SHR (Ward et al, 2003, Ward et al, 2010). On the other hand, consistent findings in human HF and many other experimental models of HF (Beuckelmann et al, 1992, Piacentino et al, 2003, Briston et al, 2011, Gomez et al, 1997) are the reduction and prolongation of cytoplasmic CaTs. Much less is known about nuclear Ca^{2+} regulation, although it might play a crucial role in triggering the onset of HF.

6.2.2.1. Altered cytoplasmic Ca^{2+} handling in SHR with advanced HHD

In line with some previous reports of increased cytoplasmic Ca^{2+} signaling in SHR-HF (Ward et al, 2003, Ward et al, 2010), and in contrast to some other studies reporting reduced contractility in conjunction with diminished CaTs in SHR-HF (Song et al, 2006, Kapur et al, 2010), cytoplasmic CaTs observed here were augmented in SHR in advanced HHD. Grouping of SHR into HF and NF revealed no difference in CaT amplitude, but lower diastolic Ca^{2+} levels in the cytosol of SHR-HF. Cytoplasmic CaT amplitudes in SHR reached ≈1500 nM (vs ≈1000 nM in WKY). Enhanced cytoplasmic CaTs were confined to the left ventricle, since left atrial myocytes from SHR of the same age exhibited a trend toward a reduction of cytoplasmic CaTs (unpublished data from our laboratory). Additionally, we also observed alterations in kinetics of cytoplasmic CaTs in SHR, characterized as prolongation in the rise time and acceleration of the CaT decay.

Remodeling of cytoplasmic Ca^{2+} handling in HF was clearly evident as alterations in the protein levels of major Ca^{2+}-regulating proteins in LV from SHR-HF. Regarding Ca^{2+} release channels, our data revealed a possible increase in IP3R2 expression. Increased expression of IP3R2 might contribute to the prolongation of the rise time of cytoplasmic CaTs, increased fractional SR Ca^{2+} release and higher CaTs in SHR-HF. Elevated IP3R2 expression was detected in hearts from SHR before, as well as in hypertrophic mouse hearts and in human patients with HF (Go et al, 1995, Harzheim et al, 2009). Hence, increased IP3R expression was proposed as a general mechanism that underlies remodelling of Ca^{2+} signalling during hypertrophy and HF (Harzheim et al, 2009). Prolongation of Ca^{2+} release (increased rise time of cytoplasmic CaTs) in old SHR could be also the result of the disruption of T-tubule organizations (Kapur et al, 2010) and reduced colocalization of LTCC and RyRs, characterized by orphaned RyRs (Song et al, 2006). As consistently observed in many HF studies (Schillinger et al, 1996, Sainte Beuve et al, 1997), there was no change in RyR protein levels in SHR-HF. However, RyR function appeared to be changed in HF. In contrast to many studies showing elevation in PKA- and CaMKII-dependent phosphorylation of RyR that increases RyR open probability and in that

way contributes to progression of HF and arrhythmias (Marks A. R., 2000, Chen-Izu et al, 2007), we observed no change in PKA-dependent phosphorylation of RyR and a reduction in CaMKII-dependent phosphorylation of RyR, suggesting reduced RyR-mediated Ca^{2+} leak in SHR-HF.

Regarding SR Ca^{2+} reuptake proteins, our results revealed lower expression of SERCA2a. The increased tPLB/SERCA2a ratio together with the reduction of CaMKII-dependent phosphorylation of PLB in SHR-HF indicated lower activity of SERCA2a. This finding was made before in failing human myocardium (Pieske et al, 1995, Schwinger RH, 1995) and also in SHR (Kapur et al, 2010, Ward et al, 2010, Boluyt et al, 1994). Important to note, Hasenfuss et al. showed that SERCA expression might depend on the region of the LV tissue analysed. For instance, in the subepicardial region it was lower, while in the subendocardial region of the failing heart it was higher (Hasenfuss, 2002). The question is whether the observed increase of SR Ca^{2+} load can be explained despite reduced SERCA activity. Reduced SERCA activity did not always result in reduction of SR Ca^{2+} load, but increased RyR leak always affected SR load (Eisner and Trafford, 2002, Ward et al, 2010). SR Ca^{2+} load depends on the balance between SR Ca^{2+} uptake (by SERCA) and SR Ca^{2+} release (leak) mainly mediated by RyR. Hence, the reduced open probability of RyR observed here could be an important factor for preventing lowering of SR Ca^{2+} load due to reduced SERCA activity. Importantly, one study illustrated that selective reduction of the open probability of RyR in adult rat ventricular myocytes did not only abolish diastolic Ca^{2+} release (leak), but at the same time potentiated systolic Ca^{2+} release (Venetucci et al, 2006).

For sarcolemmal Ca^{2+} handling proteins, our analyses showed that the LV of SHR-HF displayed increased expression of NCX1. Increased NCX levels in combination with lower Ca^{2+} leak of RyR might explain lower diastolic Ca^{2+} levels in SHR-HF. Li et al reported that already at 12 months of age SHR exhibited SERCA2a downregulation and NCX upregulation (Li et al, 2005). They showed that inhibition of SERCA2a has a smaller effect on contractile function and CaTs in SHR than in WKY, indicating reduced contribution of SERCA2a to Ca^{2+} decay in cardiac

myocytes in spontaneous hypertension (Li et al, 2005). They suggested that SERCA2a plays the main role in the maintenance of normal cardiac mechanical function, while in pathological conditions NCX might play an important role as a compensatory mechanism (Lammerich et al, 1995, Li et al, 2005). It was shown also (Fowler et al, 2007) that the proportion of Ca^{2+} extrusion via NCX1 in the total Ca^{2+} removal during the relaxation period with aging is increasing, while the proportion of Ca^{2+} extrusion from cytoplasm to the SR via SERCA2a is decreasing in both WKY and SHR. So, as a speculation, although SERCA2a is the major Ca^{2+} reuptake protein in general, maybe in old rats the increase in the expression of NCX1 might contribute to the acceleration of cytoplasmic CaT decay.

Reduction of SERCA2a activity in combination with increased expression of NCX1 in SHR-HF is expected to lower the SR Ca^{2+} load and indirectly cytoplasmic CaTs. However, our results show different observations. Regulation of NCX activity is very complex and several factors could affect NCX function: age, activity of other Ca^{2+}-regulatory proteins and pathological factors (Fowler et al, 2006, Terraciano et al, 2001). In one study, a transgenic mouse model with cardiac overexpression of NCX displayed higher SR Ca^{2+} load, whereas in another study rabbit myocytes with cardiac NCX overexpression exhibited reduced SR Ca^{2+} load (Terracciano et al, 2001, Terracciano C, 2002, Schillinger et al, 2000). Bers nicely described that there might be differences between small and large mammals regarding NCX function. Overexpression of NCX in rabbit, human and canine myocardium led to a reduction of SR Ca^{2+} load, while in mice and rats it did not (Bers DM. 2001). On the contrary, they displayed higher Ca^{2+} load and enlarged electrically stimulated CaTs. These differences might be explained by significant differences in excitation-contraction coupling between these two groups of species. Small mammals have very high heart rates, very short action potentials, low expression of NCX and relatively high $[Na^+]$ in the cells. The high $[Na^+]$ favours reverse-mode of NCX and Ca^{2+} entry, that might be more pronounced in conditions of increased NCX expression. Moreover, NCX function is regulated by local $[Na^+]$ in the immediate vicinity of the transporter. Thus, a slight increase of subsarcolemmal $[Na^+]$ could affect NCX function drastically favouring Ca^{2+} influx. Many previous studies described elevated $[Na^+]$ in ventricular

myocytes in human HF and in various animal models (Pogwizd et al, 2003, Pieske & Houser, 2003, Despa & Bers 2013, Clancy et al. 2015). However, data from our laboratory (Nikonova, 2016) did not reveal any significant changes in global [Na^+] in ventricular myocytes from old SHR. Ward et al. found increased CaTs with increased SR Ca^{2+} load and also reduction of SERCA2a activity in LV trabeculae from failing SHR (Ward et al, 2003). They identified a sarcolemmal origin for the increased CaTs and emphasized the contribution of reduced Ca^{2+} extrusion capacity of sarcolemmal (SL) Ca^{2+}-ATPase to the increased SR Ca^{2+} content.

Electrophysiological studies have shown prolongation of the action potential (AP) with age in SHR (Cerbai et al, 1994), due to the reduction in the repolarising transient outward potassium current (I_{to}) density. Increased AP duration alone increases SR Ca^{2+} load (Terracciano et al, 1997). It has long been recognised that action potential duration is an important regulator of the amount of calcium released from the SR. Prolonged depolarization during the plateau of extended action potentials enhances calcium entry via the LTCC and retards calcium extrusion via the NCX, thereby loading the cell with calcium and increasing the amplitude of the calcium transient in cardiac myocytes (Wickenden,1998).

6.2.2.2. Altered nucleoplasmic Ca^{2+} handling in SHR with advanced HHD

In advanced HHD, our data showed that SHR exhibited augmented nucleoplasmic CaTs with amplitudes ≈50% higher than the amplitudes in WKY (≈1500 nM in SHR vs ≈1000 nM in WKY). Grouping SHR into HF and NF revealed lower diastolic Ca^{2+} levels in LV nuclei from SHR-HF. The elevation of cytoplasmic CaTs, as the key determinant of the nucleoplasmic Ca^{2+} increase (Ljubojevic et al, 2011), is expected to contribute to the observed elevation of nucleoplasmic CaTs in SHR.

Additional mechanisms leading to larger perinuclear Ca^{2+} elevations in SHR are certainly the increase in NE Ca^{2+} load and, on top of it, increased fractional Ca^{2+} release. Perinuclear Ca^{2+} elevations will be further enlarged by higher and prolonged (increased rise time of cytoplasmic CaTs) cytoplasmic CaTs in SHR. NE Ca^{2+} load

and fractional Ca^{2+} release were, however, similarly increased both in SHR-NF and SHR-HF.

An important mechanism that is potentially responsible for higher nuclear CaTs and the decreased nuc-to-cyto ratio of the rise time of CaTs in SHR-HF is the accelerated intranuclear Ca^{2+} propagation. Prolonged and higher cytoplasmic CaTs (augmenting subnucleolemmal CaTs) and accelerated Ca^{2+} propagation from subnucleolemmal to central nuclear sites will accelerate central nuclear Ca^{2+} increases and subsequently lead to larger and faster nuclear CaTs in SHR-HF. Ca^{2+} propagation via diffusion from subnucleolemmal to central nuclear sites depends on the presence and density of NTs extending deep into the nucleus (Ljubojevic and Bers, 2015). Thus, the increased density of NTs may explain the increase in Ca^{2+} propagation velocity from subnucleolemmal to central nuclear regions in SHR-HF.

Suprisingly, nuclear CaT kinetics (faster upstroke of nucleoplasmic CaT) did not follow cytoplasmic CaT kinetics in SHR (slower upstroke of cytoplasmic CaT). The rise time of nucleoplasmic CaTs was not correlated with the rise time of cytoplasmic CaTs in all three groups, i.e. WKY, SHR-NF and SHR-HF. Therefore, our data suggested that the faster rise time of nuclear CaTs in SHR-HF was due to the increase in the density of NTs.

On the other hand, there was a direct positive correlation between the tau of decay of nucleoplasmic CaT and cytoplasmic CaT in all three groups, suggesting that faster reduction in cytoplasmic Ca^{2+} will speed up Ca^{2+} diffusion out of the nucleus, too. This would suggest that the acceleration of the CaT decay in the nucleus of SHR is mainly the result of the acceleration of CaT decay in the cytosol.

So, our study showed that with development of HF the density of NTs is increased, associated with acceleration of nuclear CaTs. Figure 6-2 summarizes alterations of Ca^{2+} signaling in old SHR emphasizing changes observed in SHR-HF.

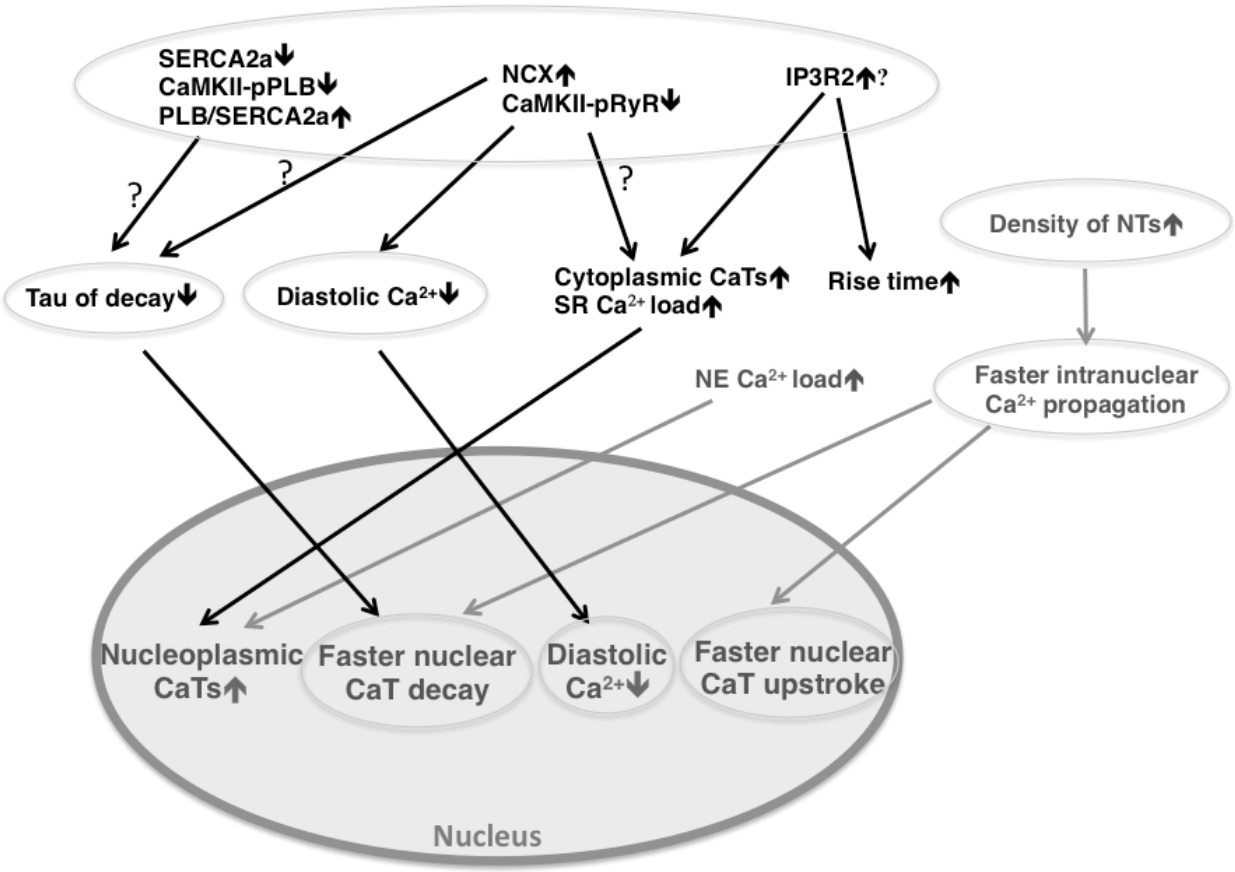

Figure 6-2. Alterations of Ca^{2+} signaling in LV myocytes from SHR in advanced HHD.

Black color indicates cytoplasmic Ca^{2+} signaling changes, while gray color indicates nucleoplasmic Ca^{2+} signaling changes in old SHR compared to old WKY. Arrows indicate connection between different findings. Circled findings illustrate changes typical only for SHR-HF compared to WKY or SHR-NF. Briefly, prolonged and increased cytoplasmic CaTs and increased NE Ca^{2+} load are expected to increase nuclear Ca^{2+} signaling observed both in SHR-NF and SHR-HF. In addition, increased density of NTs and faster intranuclear calcium propagation in SHR-HF are expected to contribute to the decrease in the nuc/cyto ratio of the rise time of nuclear CaTs. Decay time of nuclear CaTs in SHR-HF is following kinetics of cytoplasmic CaTs.

6.3. Conclusions

Many previous studies have elucidated the role of altered cytoplasmic Ca^{2+} handling in the pathogenesis of hypertrophy and HF. The current study presents the first evidence for altered nucleoplasmic Ca^{2+} handling in the early stage of HHD. Whether altered nucleoplasmic Ca^{2+} handling is also found in other models of hypertension and may be a general feature of hypertension-induced LV remodeling remains to be determined. In conjunction with a previous study (Ljubojevic et al, 2014), however, our study suggests that remodeling of nucleoplasmic Ca^{2+} handling coupled to CaMKII–HDAC-mediated regulation of histone acetylation and transcription is an early event in hypertension that contributes to initiation and progression of pathological hypertrophy and HF.

The transition from compensated hypertrophy to HF in HHD is poorly understood. Although the SHR model has been widely studied, it remains unclear whether disturbed myocardial Ca^{2+} handling indeed plays a role in the genesis of end-stage contractile failure in this animal model. In agreement with previous studies (Ward et al, 2003, 2010), our study revealed high cytoplasmic CaTs in failing SHR that were accompanied by alterations in the expression and phosphorylation of Ca^{2+} handling proteins. Furthermore, our data present the first evidence for altered nucleoplasmic Ca^{2+} handling in advanced HHD. Importantly, we identified distinct alterations in nuclear structure and Ca^{2+} handling during transition from compensated hypertrophy to HF in SHR, providing new insights into mechanisms of nuclear Ca^{2+} regulation in cardiac pathology.

Thus, normalization of nucleoplasmic Ca^{2+} handling may represent a novel target for the treatment of hypertrophy and HF in hypertensive heart disease.

7. References

Akpunonu, B. E., Mulrow, P. J., & Hoffman, E. A. (1996). Secondary hypertension: evaluation and treatment. *Disease-a-Month: DM*, *42*(10), 609–722.

Allen, B. G., Hebert, T. E. (2015). Chapter 12, Methods in molecular biology: Nuclear G-protein coupled receptors, Methods and protocols

Alonso, M. T., & García-Sancho, J. (2011). Nuclear Ca^{2+} signalling. *Cell Calcium*, *49*(5), 280–289.

Anderson, M. E., Brown, J. H., Bers, D. M. (2011). CaMKII in myocardial hypertrophy and heart failure. *J Mol Cell Cardio,* 51(4), 468-73.

Authors/Task Force Members: Mancia, G. et al. (2013). 2013 ESH/ESC Guidelines for the management of arterial hypertension. *European Heart Journal*, *34*(28), 2159–2219.

Authors/Task Force Members. (2005). Guidelines for the diagnosis and treatment of chronic heart failure: executive summary (update 2005): The Task Force for the Diagnosis and Treatment of Chronic Heart Failure of the European Society of Cardiology. *European Heart Journal*, *26*(11), 1115–1140.

Authors/Task Force Members. (2016). Guidelines for the diagnosis and treatment of chronic heart failure: The Task Force for the Diagnosis and Treatment of Chronic Heart Failure of the European Society of Cardiology. *European Heart Journal*, *37 (27),* 2129–2200.

Backs, J., & Olson, E. N. (2006). Control of cardiac growth by histone acetylation/deacetylation. *Circulation Research*, *98*(1), 15–24.

Backs, J., Backs, T., Bezprozvannaya, S., McKinsey, T. A., Olson, E. N. (2008). Histone deacetylase 5 acquires calcium/calmodulin-dependent kinase II responsiveness by oligomerization with histone deacetylase 4. *Mol Cell Biol,* 28, 3437-45.

Backs, J., Backs, T., Neef, S., Kreusser, M. M., Lehmann, L. H., Patrick, D. M., et al. (2009). The delta isoform of CaM kinase II is required for pathological cardiac hypertrophy and remodeling after pressure overload. *Proc Natl Acad Sci U S A*, *106*, 2342-7.

Bell, R. M., Mocanu, M. M., & Yellon, D. M. (2011). Retrograde heart perfusion: The Langendorff technique of isolated heart perfusion. *Journal of Molecular and Cellular Cardiology*, *50*(6), 940–950.

Bénitah, J. P., Gómez, A. M., Bailly, P., Da Ponte, J. P., Berson, G., Delgado, C., & Lorente, P. (1993). Heterogeneity of the early outward current in ventricular cells isolated from normal and hypertrophied rat hearts. *The Journal of Physiology*, *469*, 111–138.

Berridge, M. J., Bootman, M. D., & Roderick, H. L. (2003). Calcium signalling: dynamics, homeostasis and remodelling. *Nature Reviews Molecular Cell Biology*, *4*(7), 517–529.

Bers, D. M. (2001). Eccitation-contraction coupling and cardiac contractile force. *Dodrecht: Kluwer Academic Publishers.*

Bers, D. M. (2002). Cardiac excitation-contraction coupling. *Nature*, *415*(6868), 198–205.

Bers, D. M. (2003). Sarcoplasmic Reticulum Ca^{2+} and Heart Failure: Roles of Diastolic Leak and Ca^{2+} Transport. *Circulation Research*, *93*(6), 487–490.

Bers, D. M. (2008). Calcium cycling and signaling in cardiac myocytes. *Annual Review of Physiology*, *70*, 23–49.

Bers, D. M., & Despa, S. (2006). Cardiac Myocytes Ca^{2+} and Na^{+} Regulation in Normal and Failing Hearts. *Journal of Pharmacological Sciences*, *100*(5), 315–322.

Beuckelmann, D. J., Nabauer, M., Erdmann, E. (1992). Intracellular Calcium Handling in Isolated Ventricular Myocytes from Patients with Terminal Heart-Failure. *Circulation*, 85(3):1046-1055.

Bianchi, G. et al., (1974). Blood Pressure Changes Produced by Kidney Cross-Transplantation between Spontaneously Hypertensive Rats and Normotensive Rats. *Clinical Science*, 47(5), 435–448.

Bing, O. H., Brooks, W. W., Conrad, C. H., Sen, S., Perreault, C. L., & Morgan, J. P. (1991). Intracellular calcium transients in myocardium from spontaneously hypertensive rats during the transition to heart failure. Circulation Research, 68(5), 1390–1400.

Boknik, P., Heinroth-Hoffmann, I., Kirchhefer, U., Knapp, J., Linck, B., Luss, H., et al. (2001). Enhanced protein phosphorylation in hypertensive hypertrophy. *Cardiovascular Research*, *51*(4), 717–728.

Boluyt, M. O., Bing, O. H., & Lakatta, E. G. (1995). The ageing spontaneously hypertensive rat as a model of the transition from stable compensated hypertrophy to heart failure. *European Heart Journal*, 16 Suppl N, 19–30.

Boluyt, M. O., O'Neill, L., Meredith, A. L., Bing, O. H., Brooks, W. W., Conrad, C. H., et al. (1994). Alterations in cardiac gene expression during the transition from stable hypertrophy to heart failure. Marked upregulation of genes encoding extracellular matrix components. *Circulation Research*, 75(1), 23–32.

Bootman, M. D., Fearnley, C., SMYRNIAS, I., MacDonald, F., & Roderick, H. L. (2009). An update on nuclear calcium signalling. *Journal of Cell Science*, *122*(14), 2337–2350.

Bossuyt, J., Helmstadter, K., Wu, X., Clements-Jewery, H., Haworth, R. S., Avkiran M, et al. (2008). Ca^{2+}/Calmodulin-Dependent Protein Kinase II delta and Protein Kinase D Overexpression Reinforce the Histone Deacetylase 5 Redistribution in Heart Failure. *Circ Res.*

Briston, S. J., Caldwell, J. L., Horn, M. A., Clarke, J. D., Richards, M. A., Greensmith, D. J., et al. (2011). Impaired beta-adrenergic responsiveness accentuates dysfunctional excitation-contraction coupling in an ovine model of tachypacing-induced heart failure. *Journal of Physiology*, 589(6):1367-1382.

Brock, J. A., Van Helden, D. F., Dosen, P., & Rush, R. A. (1996). Prevention of high blood pressure by reducing sympathetic innervation in the spontaneously hypertensive rat. *Journal of the Autonomic Nervous System*, *61*(2), 97–102.

Brooksby, P., Levi, A. J., Jones, J. V. (1993). Investigation of the mechanisms underlying the increased contraction of hypertrophied ventricular myocytes isolated from the spontaneously hypertensive rat. *Cardiovasc Res*, 27, 1268-77.

Calaghan, S. C., White, E., Bedut, S., & Le Guennec, J.-Y. (2000). Cytochalasin D reduces Ca(2+) sensitivity and maximum tension via interactions with myofilaments in skinned rat cardiac myocytes. *The Journal of Physiology*, *529*(Pt 2), 405–411.

Capelson, M., Doucet, C., Hetzer, M. W. (2010). Nuclear pore complexes: guardians of the nuclear genome. *Cold Spring Harb Symp Quant Biol,* 75, 585-97.

Cappola, T. P. (2008). Molecular Remodeling in Human Heart Failure. *Journal of the American College of Cardiology*, *51*(2), 137–138.

Carretero, O. A., & Oparil, S. (2000). Essential Hypertension: Part I: Definition and Etiology. *Circulation*, *101*(3), 329–335.

Carvalho, B. M. R., Bassani, R. A., Franchini, K. G., & Bassani, J. W. M. (2006). Enhanced calcium mobilization in rat ventricular myocytes during the onset of pressure overload-induced hypertrophy. *American Journal of Physiology. Heart and Circulatory Physiology*, *291*(4), H1803–13.

Cerbai, E., Barbieri, M., Li, Q., & Mugelli, A. (1994). Ionic basis of action potential prolongation of hypertrophied cardiac myocytes isolated from hypertensive rats of different ages. *Cardiovascular Research*, 28(8), 1180–1187.

Chan, V., Fenning, A., Levick, S. P., Loch, D., Chunduri, P., Iyer, A., Teo, Y. L., Hoey, A., Wilson, K., Burstow, D., Brown, L. (2011). Cardiovascular changes during maturation and ageing in male and female spontaneously hypertensive rats. *Journal of cardiovascular pharmacology*, 57(4), 469–478.

Chen-Izu, Y., Chen, L., Banyasz, T., McCulle, S. L., Norton, B., Scharf, S. M., et al. (2007). Hypertension-induced remodeling of cardiac excitation-contraction coupling in ventricular myocytes occurs prior to hypertrophy development. *Am J Physiol Heart Circ Physiol.* 293, H3301-10.

Chen-Izu, Y., Ward, C. W., Stark W. Jr., Banyasz, T., Sumandea, M. P., Balke, C. W., Izu, L. T., Wehrens, X. H. T. (2007). Phosphorylation of RyR2 and shortening of RyR2 cluster spacing in spontaneously hypertensive rat with heart failure. *American Journal of Physiology - Heart and Circulatory Physiology*, 293(4), H2409-H2417.

Clancy, C. E., Chen-Izu, Y., Bers, D. M., Belardinelli, L., Boyden, P. A., Csernoch, L., et al. (2015). Deranged sodium to sudden death. *The Journal of Physiology*, 593(6), 1331–1345.

Claxton, N.S., Fellers, T. J., Davidson, M. W. Laser scanning confocal microscopy, www.aptechnologies.co.uk

Conrad, C. H., Brooks, W. W, Robinson, K. G., Bing, O. H. (1991). Impaired myocardial function in spontaneously hypertensive rats with heart failure. *Am J Physiol*, 260, H136-145.

Conrad, C. H., Brooks, W. W., Hayes, J. A., Sen, S., Robinson, K. G., & Bing, O. H. (1995). Myocardial fibrosis and stiffness with hypertrophy and heart failure in the spontaneously hypertensive rat. *Circulation*, 91(1), 161–170.

Cortes, R., Roselló-Lletí, E., Rivera, M., Martinez-Dolz, L., Salvador, A., Azorin, I., & Portolés, M. (2010). Influence of heart failure on nucleocytoplasmic transport in human cardiomyocytes. *Cardiovascular Research*, *85*(3), 464–472.

Coulombe, A., Momtaz, A., Richer, P., Swynghedauw, B., & Coraboeuf, E. (1994). Reduction of calcium-independent transient outward potassium current density in DOCA salt hypertrophied rat ventricular myocytes. *Pflugers Archiv-European Journal of Physiology*, 427(1-2), 47–55.

Denton, R. M., & McCormack, J. G. (1990). Ca^{2+} as a second messenger within mitochondria of the heart and other tissues. *Annual Review of Physiology*, *52*, 451–466.

Despa, S., & Bers, D. M. (2013). Na^{+} transport in the normal and failing heart - remember the balance. *Journal of Molecular and Cellular Cardiology*, *61*, 2–10.

Diamond, J. A., & Phillips, R. A. (2005). Hypertensive heart disease. *Hypertension Research: Official Journal of the Japanese Society of Hypertension*, *28*(3), 191–202.

Dobrev, D., & Wehrens, X. H. T. (2014). Role of RyR2 Phosphorylation in Heart Failure and Arrhythmias: Controversies Around Ryanodine Receptor Phosphorylation in Cardiac Disease. *Circulation Research*, *114*(8), 1311–1319.

Doggrell, S. A., Brown, L. (1998). Rat models of hypertension, cardiac hypertrophy and failure. *Cardiovasc Res*, *39*, 89-105.

Dolmetsch, R. E., Xu, K., Lewis, R. S. (1998). Calcium oscillations increase the efficiency and specificity of gene expression. *Nature*, 392(6679), 933-936.

Domínguez-Rodríguez, A., Ruiz-Hurtado, G., Benitah, J.-P., & Gómez, A. M. (2012). The other side of cardiac Ca^{2+} signaling: transcriptional control. *Frontiers in Physiology*, *3*, 452.

Drazner, M. H. (2011). The Progression of Hypertensive Heart Disease. *Circulation*, *123*(3), 327–334.

Echevarría, W., Leite, M. F., Guerra, M. T., Zipfel, W. R., & Nathanson, M. H. (2003). Regulation of calcium signals in the nucleus by a nucleoplasmic reticulum. *Nature Cell Biology*, *5*(5), 440–446.

Eisner, D. A, Trafford, A. V. (2002). Heart Failure and the Ryanodine Receptor: Does Occam's Razor Rule? *Circulation Research*, 91(11), 979–981.

Escobar, M., Cardenas, C., Colavita, K., Petrenko, N. B., & Franzini-Armstrong, C. (2011). Structural evidence for perinuclear calcium microdomains in cardiac myocytes. *Journal of Molecular and Cellular Cardiology*, *50*(3), 451–459.

Felker, G. M., Adams, K. F. J., Konstam, M. A., O'Connor, C. M., & Gheorghiade, M. (2003). The problem of decompensated heart failure: nomenclature, classification, and risk stratification. *American Heart Journal*, *145*(2 Suppl), S18–25.

Fowler, M. R., Naz, J. R., Graham, M. D., Bru-Mercier, G., Harrison, S. M., Orchard, C. H. (2005). Decreased Ca2+ extrusion via Na+/Ca2+ exchange in epicardial left ventricular myocytes during compensated hypertrophy. *Am J Physiol Heart Circ Physiol*, 288, H2431-8.

Fowler, M. R., Orchard, C. H., & Harrison, S. M. (2006). Cellular distribution of calcium current is unaltered during compensated hypertrophy in the spontaneously hypertensive rat. *Pflügers Archiv*, 453(4), 463–469.

Fowler, R. M., Graham, J. R., Orchard, C. H., Harrison, S. M. (2007). Age and hypertrophy alter the contribution of sarcoplasmic reticulum and Na+/Ca2+ exchange to Ca2+ removal in rat left ventricular myocytes. *Journal of Molecular and Cellular Cardiology*, 42 (3), 582-589.

Frey, N., McKinsey, T. A., Olson, E. N. (2000). Decoding calcium signals involved in cardiac growth and function. *Nat Med,* 6, 1221-7.

Galva, C., Artigas, P., & Gatto, C. (2012). Nuclear Na^{+}/K^{+}-ATPase plays an active role in nucleoplasmic Ca^{2+} homeostasis. *Journal of Cell Science*, *125*(24), 6137–6147.

Gee, K. R., Brown, K. A., Chew, W. N., Bishop-Stewart, J., Grey, D., Johnson, I. (2000). Chemical and physiological characterisation of fluo-4 Ca2+-indicator dyes. *Cell Calcium*, *27*(2), 97-106.

General Electric Company. (2011). Western Blot, Principles and methods, Handbook from GE Healthcare Bio-Sciences

Gerasimenko, O. (2004). New aspects of nuclear calcium signalling. *Journal of Cell Science*, *117*(15), 3087–3094.

Gilsbach, R., Preissl, S., Gruning, B. A., Schnick, T., Burger, L., Benes, V., et al. (2014). Dynamic DNA methylation orchestrates cardiomyocyte development, maturation and disease. *Nat Commun.* 5, 5288.

Go, L. O., Moschella, M. C., Watras, J., Handa, K. K., Fyfe, B. S., Marks, A. R. (1995). Differential Regulation of 2 Types of Intracellular Calcium-Release Channels during End-Stage Heart-Failure. *J Clin Invest*, 95(2):888-894.

Gomez, A. M., Valdivia, H. H., Cheng, H., Lederer, M. R., Santana, L. F., Cannell, M. B., et al. (1997). Defective excitation-contraction coupling in experimental cardiac hypertrophy and heart failure. *Science*, 276(5313):800-806.

Greber, U. F., Gerace, L. (1995). Depletion of calcium from the lumen of endoplasmic reticulum reversibly inhibits passive diffusion and signal-mediated transport into the nucleus. *J Cell Biol.* 128, 5-14.

Ha, C. H., Kim, J. Y., Zhao, J., Wang, W., Jhun, B. S., Wong, C, et al. (2010). PKA phosphorylates histone deacetylase 5 and prevents its nuclear export, leading to the inhibition of gene transcription and cardiomyocyte hypertrophy. *Proc Natl Acad Sci U S A,* 107, 15467-72.

Hagen, B. M., Boyman, L., Kao, J. P., Lederer, W. J. (2012). A comparative assesment of fluo Ca2+ indicators in rat ventricular myocytes. *Cell Calcium, 52* (2), 170-181.

Harzheim, D., Movassagh, M., Foo, R. S., Ritter, O., Tashfeen, A., Conway, S. J., et al. (2009). Increased InsP3Rs in the junctional sarcoplasmic reticulum augment Ca^{2+} transients and arrhythmias associated with cardiac hypertrophy. *Proc Natl Acad Sci*, 106(27):11406-11411.

Hasenfuss, G. (2002). Calcium Cycling in Congestive Heart Failure. Journal of Molecular and *Cellular Cardiology*, 34(8), 951–969.

Heineke, J., & Molkentin, J. D. (2006). Regulation of cardiac hypertrophy by intracellular signalling pathways. *Nature Reviews Molecular Cell Biology*, *7*(8), 589–600.

Heineke, J., & Ritter, O. (2012). Cardiomyocyte calcineurin signaling in subcellular domains: From the sarcolemma to the nucleus and beyond. *Journal of Molecular and Cellular Cardiology*, *52*(1), 62–73.

Huke, S., Bers, D. M. (2008). Ryanodine receptor phosphorylation at Serine 2030, 2808 and 2814 in rat cardiomyocytes. *Biochemical and Biophysical Research Communications*, 376(1), 80–85.

Johnson, I. and Spence, M. (2010). The molecular probes handbook. :Life Technologies

Kahan, T., & Bergfeldt, L. (2005). Left ventricular hypertrophy in hypertension: its arrhythmogenic potential. *Heart (British Cardiac Society)*, *91*(2), 250–256.

Kapur, S., Aistrup, G. L., Sharma, R., Kelly, J. E., Arora, R., Zheng, J., et al. (2010). Early development of intracellular calcium cycling defects in intact hearts of spontaneously hypertensive rats. *American Journal of Physiology. Heart and Circulatory Physiology*, 299(6), H1843–H1853.

Kehat, I., & Molkentin, J. D. (2010). Molecular Pathways Underlying Cardiac Remodeling During Pathophysiological Stimulation. *Circulation*, *122*(25), 2727–2735.

Kemp, C. D., & Conte, J. V. (2012). The pathophysiology of heart failure. *Cardiovascular Pathology: the Official Journal of the Society for Cardiovascular Pathology*, *21*(5), 365–371.

Kockskämper, J, Seidlmayer, L., Walther, S., Hellenkamp, K., Maier, L. S., Pieske, B. (2008). Endothelin-1 enhances nuclear Ca2+ transients in atrial myocytes through Ins (1,4,5)P3-dependent Ca2+ release from perinuclear Ca2+ stores. *Journal of Cell Science*, *121*(2):186-195.

Kodavanti, U.P. et al. (2000). The Spontaneously Hypertensive Rat as a Model of Human Cardiovascular Disease: Evidence of Exacerbated Cardiopulmonary Injury and Oxidative Stress from Inhaled Emission Particulate Matter. *Toxicology and Applied Pharmacology*, 164(3), 250–263.

Kokubo, M., Uemura, A., Matsubara, T., Murohara, T. (2005). Noninvasive evaluation of the time course of change in cardiac function in spontaneously hypertensive rats by echocardiography. *Hypertens Res*, *28*, 601-9.

Kranias, E. G., Hajjar, R. J. (2012). Modulation of cardiac contractility by the phospholamban/SERCA2a regulatome. *Circ Res,* 110(12):1646-60.

Lammerich, A., Gunther, J., Pfitzer, G., Storch, E., & Vetter, R. (1995). Alterations of cardiac contractile function are related to changes in membrane calcium transport in spontaneously hypertensive rats. *Journal of Hypertension*, 13(11), 1313–1324.

Ledeen, R. W., & Wu, G. (2007). Sodium-calcium exchangers in the nucleus: an unexpected locus and an unusual regulatory mechanism. *Ann N Y Acad Sci*, *1099*, 494–506.

Lee, C. S., & Tkacs, N. C. (2008). Current concepts of neurohormonal activation in heart failure: mediators and mechanisms. *AACN Advanced Critical Care*, *19*(4), 364-386.

Li, S.-Y., Golden, K. L., Jiang, Y., Wang, G.-J., Privratsky, J. R., Zhang, X., et al. (2005). Inhibition of sarco(endo)plasmic reticulum Ca2+-ATPase differentially regulates contractile function in cardiac myocytes from normotensive and spontaneously hypertensive rats. *Cell Biochemistry and Biophysics*, 42(1), 1–12.

Liew, C.-C., & Dzau, V. J. (2004). Molecular genetics and genomics of heart failure. *Nature Reviews. Genetics*, *5*(11), 811–825.

Ljubojevic, S, Bers, D. M. (2015). Measuring intranuclear and nuclear envelope [Ca^{2+}] vs. cytosolic [Ca^{2+}]. *Methods Mol Biol,* 1234, 135-47.

Ljubojevic, S., & Bers, D. M. (2015). Nuclear calcium in cardiac myocytes. *Journal of Cardiovascular Pharmacology*, *65*(3), 211–217.

Ljubojevic, S., Radulovic, S., Leitinger, G., Sedej, S., Sacherer, M., Holzer, M., et al. (2014). Early remodeling of perinuclear Ca2+ stores and nucleoplasmic Ca2+ signaling during the development of hypertrophy and heart failure. *Circulation*, 130(3), 244-255.

Ljubojevic, S., Walther, S., Asgarzoei, M., Sedej, S., Pieske, B., Kockskamper, J. (2011). In situ calibration of nucleoplasmic versus cytoplasmic Ca^{2+} concentration in adult cardiomyocytes. *Biophys J.*, 100(10), 2356-2366.

Louch, W. E., Sheehan, K. A., & Wolska, B. M. (2011). Methods in cardiomyocyte isolation, culture, and gene transfer. *Journal of Molecular and Cellular Cardiology*, *51*(3), 288–298.

Lunde, I. G., Kvaloy, H., Austbo, B., Christensen, G., & Carlson, C. R. (2011). Angiotensin II and norepinephrine activate specific calcineurin-dependent NFAT transcription factor isoforms in cardiomyocytes. *Journal of Applied Physiology*, *111*(5), 1278–1289.

Maier, L. S., & Bers, D. M. (2002). Calcium, calmodulin, and calcium-calmodulin kinase II: heartbeat to heartbeat and beyond. *Journal of Molecular and Cellular Cardiology*, *34*(8), 919–939.

Malhas, A., Goulbourne, C., Vaux, D. J. (2011). The nucleoplasmic reticulum: form and function. *Trends Cell Biol*, 21(6), 362-373.

Marius, P., Guerra, M. T., Nathanson, M. H., Ehrlich, B. E., & Leite, M. F. (2006). Calcium release from ryanodine receptors in the nucleoplasmic reticulum. *Cell Calcium*, *39*(1), 65–73.

Marks, A. R. (2000). Cardiac intracellular calcium release channels: role in heart failure. *Circulation Research*, 87(1), 8–11.

McMurray, J. J., Pfeffer, M. A. (2005). Heart failure. *Lancet*, *365*(9474), 1877-1889.
Millane, T., Jackson, G., Gibbs, C. R., & Lip, G. Y. H. (2000). Acute and chronic management strategies. *BMJ: British Medical Journal*, *320*(7234), 559–562.

Mishra, S., Gray, C. B., Miyamoto, S., Bers, D. M., Brown, J. H. (2011). Location matters: clarifying the concept of nuclear and cytosolic CaMKII subtypes. *Circ Res*, 109, 1354-62.

Molkentin, J. D. (2000). Calcineurin and beyond: cardiac hypertrophic signaling. *Circulation Research*, *87*(9), 731–738.

Molkentin, J. D. (2004). Calcineurin-NFAT signaling regulates the cardiac hypertrophic response in coordination with the MAPKs. *Cardiovascular Research*, *63*(3), 467–475.

Nikonova, Y. (2016). Atrial remodelling in hypertensive heart disease: Role of Na+ homeostasis and contractility, Philipps-Universität Marburg.

Okamoto, K. & Aoki, K., (1963). Development of a strain of spontaneously hypertensive rats. *Japanese circulation journal*, 27, 282–293.

Okayama, H., Hamada, M., Kawakami, H., Ikeda, S., Hashida, H., Shigematsu, Y., et al. (1998). Increased contraction of myocytes isolated from the young spontaneously hypertensive rat: relationship between systolic and diastolic function. *Am J Hypertens,* 11, 349-56.

Paddock, S. W. (2000). Principles and Practices of Laser Scanning Confocal Microscopy, *Molecular Biotechnology*, *16* (2), 127-149.

Paredes, R. M., Etzler, J. C., Watts, L. T., Lechleiter, J. D. (2009). Chemical calcium indicators. *NIH*, *46*(3), 143–151.

Paris, J. B., Bootman, M. D., Yule, D. I., Bultynck, G. (2014). Calcium techniques: a laboratory manual. *Cold Spring Harbour Laboratory Press*, New York

Passier, R., Zeng, H., Frey, N., Naya, F. J., Nicol, R. L., McKinsey, T. A., et al. (2000). CaM kinase signaling induces cardiac hypertrophy and activates the MEF2 transcription factor in vivo. *Journal of Clinical Investigation*, *105*(10), 1395–1406.

Piacentino, V., Weber, C. R., Chen, X. W., Weisser-Thomas, J., Margulies, K. B., Bers, D. M., et al. (2003). Cellular basis of abnormal calcium transients of failing human ventricular myocytes. *Circ Res,* 92(6):651-658.

Pieske, B. & Houser, S. R. (2003). [Na+]i handling in the failing human heart. *Cardiovascular Research*, 57(4), pp.874–886.

Pieske, B., Kretschmann, B., Meyer, M., Holubarsch, C., Weirich, J., Posival, H., et al. (1995). Alterations in intracellular calcium handling associated with the inverse force-frequency relation in human dilated cardiomyopathy. *Circulation*, 92(5), 1169–1178.

Pluteanu, F., Hess, J., Plackic, J., Nikonova, Y., Preisenberger, J., Bukowska, A., et al. (2015). Early subcellular Ca2+ remodelling and increased propensity for Ca^{2+} alternans in left atrial myocytes from hypertensive rats. *Cardiovasc Res,* 106, 87-97.

Pogwizd, S. M., & Bers, D. M. (2004). Cellular basis of triggered arrhythmias in heart failure. *Trends in Cardiovascular Medicine*, *14*(2), 61–66.

Pogwizd, S. M., Sipido, K. R., Verdonck, F., & Bers, D. M. (2003). Intracellular Na^{+} in animal models of hypertrophy and heart failure: contractile function and arrhythmogenesis. *Cardiovascular Research*, 57(4), 887–896.

Preissl, S., Schwaderer, M., Raulf, A., Hesse, M., Gruning, B. A., Kobele, C., et al. (2015). Deciphering the Epigenetic Code of Cardiac Myocyte Transcription. *Circ Res,117*(5):413-423.

Rivera, D. M., & Lowes, B. D. (2005). Molecular remodeling in the failing human heart. *Current Heart Failure Reports*, *2*(1), 5–9.

Sainte Beuve, C., Allen, P. D., Dambrin, G., Rannov, F., Marty, I., Trouvé, P., Bors, V., Pavie, A., Gandgjbakch, I., Charlemagne, D. (1997). Cardiac calcium release channel (ryanodine receptor) in control and cardiomyopathic human hearts: mRNA and protein contents are differentially regulated. *J Mol Cell Cardiol,* 29:1237–1246.

Salazar, N. C., Chen, J., Rockman, H. A. (2007). Cardiac GPCRs: GPCR signaling in healthy and failing hearts. *Biochimica Et Biophysica Acta-Biomembranes*, 1768(4):1006-1018.

Schägger, H., (2006). Tricine-SDS-PAGE. *Nature Protocols*, *1*(1), 16-22.

Schillinger, W., Janssen, P. M., Emami, S., Henderson, S. A., Ross, R. S., Teucher, N., et al. (2000). Impaired contractile performance of cultured rabbit ventricular myocytes after adenoviral gene transfer of Na(+)-Ca(2+) exchanger. *Circulation Research*, 87(7), 581–587.

Schillinger, W., Meyer, M., Kuwajima, G., Mikoshiba, K., Just, H., Hasenfuss, G. (1996). Unaltered ryanodine receptor protein levels in ischemic cardiomyopathy. *Mol Cell Biochem*, 161:297–302.

Schwinger, R. H. G., Böhm, M., Schmidt, U., Karczewski, P., Bavendiek, U., Flesch, M., Krause, E. G. and Erdmann, E. (1995). Unchanged Protein Levels of SERCA II and Phospholamban but Reduced Ca^{2+} Uptake and Ca2+-ATPase Activity of Cardiac Sarcoplasmic Reticulum From Dilated Cardiomyopathy Patients Compared With Patients With Nonfailing Hearts. *Circulation*, 92, 3220-3228.

Scoote, M. (2002). The cardiac ryanodine receptor (calcium release channel) Emerging role in heart failure and arrhythmia pathogenesis. *Cardiovascular Research*, *56*(3), 359–372.

Shanks, J. & Herring, N., (2013). Peripheral cardiac sympathetic hyperactivity in cardiovascular disease: role of neuropeptides. *AJP: Regulatory, Integrative and Comparative Physiology*, 305(12), R1411–R1420.

Shorofsky, S. R., Aggarwal, R., Corretti, M., Baffa, J. M., Strum, J. M., Al-Seikhan, B. A., et al. (1999). Cellular mechanisms of altered contractility in the hypertrophied heart: big hearts, big sparks. *Circ Res*, 84, 424-34.

Sipido, K. R., Volders, P. G., de Groot, S. H., Verdonck, F., Van de Werf, F., Wellens, H. J., & Vos, M. A. (2000). Enhanced Ca(2+) release and Na/Ca exchange activity in hypertrophied canine ventricular myocytes: potential link between contractile adaptation and arrhythmogenesis. *Circulation*, *102*(17), 2137–2144.

Song, L.-S., Sobie, E. A., McCulle, S., Lederer, W. J., Balke, C. W., & Cheng, H. (2006). Orphaned ryanodine receptors in the failing heart. *Proceedings of the National Academy of Sciences of the United States of America*, 103(11), 4305–4310.

Tadevosyan, A., Vaniotis, G., Allen, B. G., Hébert, T. E., & Nattel, S. (2012). G protein-coupled receptor signalling in the cardiac nuclear membrane: evidence and possible roles in physiological and pathophysiological function. *The Journal of Physiology*, *590*(6), 1313–1330.

Tarazón, E., Rivera, M., Roselló-Lletí, E., Molina-Navarro, M. M., Sánchez-Lázaro, I. J., España, F., et al. (2012). Heart Failure Induces Significant Changes in Nuclear Pore Complex of Human Cardiomyocytes. *PLoS ONE*, *7*(11)

Terracciano, C. (2002). Functional consequences of Na/Ca exchanger overexpression in cardiac myocytes. *Ann N Y Acad Sci*, 976, 520–527.

Terracciano, C., Philipson, K. D., & MacLeod, K. T. (2001). Overexpression of the Na+/Ca2+ exchanger and inhibition of the sarcoplasmic reticulum Ca2+-ATPase in ventricular myocytes from transgenic mice. *Cardiovascular Research*, 49, 38–47.

Terracciano, C., Tweedie, D., & MacLeod, K. T. (1997). The effects of changes to action potential duration on the calcium content of the sarcoplasmic reticulum in isolated guinea-pig ventricular myocytes. *Pflugers Archiv-European Journal of Physiology*, 433, 542–544.

Thomas, D., Tovey, S. C., Collins, T. J., Bootman, M. D., Berridge, M. J., & Lipp, P. (2000). A comparison of fluorescent Ca^{2+} indicator properties and their use in measuring elementary and global Ca^{2+} signals. *Cell Calcium*, *28*(4), 213–223.

Tomanek, R. J, Hovanec, J. M. (1981). The effects of long-term pressure-overload and aging on the myocardium. *J Mol Cell Cardiol*, *13*, 471-88.

Tomaselli, G. (1999). Electrophysiological remodeling in hypertrophy and heart failure. *Cardiovascular Research*, *42*(2), 270–283.

Tomita, F., Bassett, A. L., Myerburg, R. J., & Kimura, S. (1994). Diminished transient outward currents in rat hypertrophied ventricular myocytes. *Circulation Research*, *75*(2), 296–303.

Vanecková, I. et al. (2002). Function of the isolated perfused kidney in young and adult spontaneously hypertensive and dahl salt-sensitive rats. *Kidney & blood pressure research*, 25(5), pp.315–321.

Venetucci, L. A. (2006). Reducing Ryanodine Receptor Open Probability as a Means to Abolish Spontaneous Ca2+ Release and Increase Ca2+ Transient Amplitude in Adult Ventricular Myocytes. *Circulation Research*, 98(10), 1299–1305.

Walker , J.M. (1994). The bicinchonic acid (BCA) assay for protein quantification. *Methods in Molecular Biology*, 32, 5-8.

Wang, Z. (2001). Na^{+}-Ca^{2+} Exchanger Remodeling in Pressure Overload Cardiac Hypertrophy. *Journal of Biological Chemistry*, *276*(21), 17706–17711.

Wang, Z., Kutschke, W., Richardson, K. E., Karimi, M., & Hill, J. A. (2001). Electrical Remodeling in Pressure-Overload Cardiac Hypertrophy: Role of Calcineurin. *Circulation*, *104*(14), 1657–1663.

Ward, M. L., Pope, A. J., Loiselle, D. S., Cannell, M. B. (2003). Reduced contraction strength with increased intracellular [Ca2+] in left ventricular trabeculae from failing rat hearts. *J Physiol,* 546(2), 537-550.

Ward, M.-L., Crossman, D. J., Loiselle, D. S., & Cannell, M. B. (2010). Non-steady-state calcium handling in failing hearts from the spontaneously hypertensive rat. *Pflügers Archiv*, 460(6), 991–1001.

Webster, M., Witkin, K. L., & Cohen-Fix, O. (2009). Sizing up the nucleus: nuclear shape, size and nuclear-envelope assembly. *Journal of Cell Science*, *122*(10), 1477–1486.

Westerhof, N., & O'Rourke, M. F. (1995). Haemodynamic basis for the development of left ventricular failure in systolic hypertension and for its logical therapy. *Journal of Hypertension*, *13*(9), 943–952.

Wickenden, A. (1998). The role of action potential prolongation and altered intracellular calcium handling in the pathogenesis of heart failure. *Cardiovascular Research*, *37*(2), 312–323.

Wilkins, B. J., Dai, Y. S., Bueno, O. F., Parsons, S. A., Xu, J., Plank, D. M., et al. (2004). Calcineurin/NFAT coupling participates in pathological, but not physiological, cardiac hypertrophy. *Circ Res*, *94*, 110-8.

Wu, A. Z., Xu, D., Yang, N., Lin, S.-F., Chen, P.-S., Cala, S. E., & Chen, Z. (2016). Phospholamban is concentrated in the nuclear envelope of cardiomyocytes and involved in perinuclear/nuclear calcium handling. *Journal of Molecular and Cellular Cardiology*, *100*, 1–8.

Wu, X., Zhang, T., Bossuyt, J., Li, X., McKinsey, T. A., Dedman, J. R., et al. (2006). Local InsP3-dependent perinuclear Ca^{2+} signaling in cardiac myocyte excitation-transcription coupling. *Journal of Clinical Investigation*, *116*(3), 675–682.

Xu, M., Zhou, P., Xu, S.-M., Liu, Y., Feng, X., Bai, S.-H., et al. (2007). Intermolecular Failure of L-type Ca2+ Channel and Ryanodine Receptor Signaling in Hypertrophy. *PLoS Biology*, *5*(2), e21.

Zhang, T., Brown, J. H. (2004). Role of Ca^{2+}/calmodulin-dependent protein kinase II in cardiac hypertrophy and heart failure. *Cardiovascular Research*, *63*(3), 476–486.

Zwadlo, C., & Borlak, J. (2005). Disease-associated changes in the expression of ion channels, ion receptors, ion exchangers and Ca2+-handling proteins in heart hypertrophy. *Toxicology and Applied Pharmacology*, *207*(3), 244–256.

8. List of abbreviations

$[Ca^{2+}]$	Calcium concentration
$[Ca^{2+}]_{rest}$	Resting calcium concentration
$[Na^{+}]$	Sodium concentration
AC	Adenylyl-cyclase
ACE	Angiotensin-converting enzyme
AM	acetoxymethyl group
ANOVA	Analysis of variance
ANP	Atrial natriuretic peptide
AP	Action potential
APS	Ammoniumpersulfate
AT	Angiotensin
ATP	Adenosine triphosphate
BAPTA	1, 2-bis (o-aminophenoxy) ethane- N, N, N, N′-tetraacetic acid
BCA	Bicinchoninic acid
BDM	2,3-Butanedione 2-Monoxime
BNP	Brain natriuretic peptide
Br-Ph Blue	Bromophenol blue sodium salt
BSA	Bovine serum albumin
C, cyto	Cytoplasmic region
Caff	Caffeine
CaM	Calmodulin
CaMKII	Ca^{2+}/calmodulin-dependent protein kinase II
cAMP	Cyclic adenosine monophosphate
CaN	Calcineurin
CaT	Calcium concentration transient
CICR	Ca^{2+}-induced Ca^{2+} release
CN	Central nuclear region
CnA	Calcineurin A subunit

CnB	Calcineurin B subunit
CPA	Cyclopiazonic acid
CSQ	Calsequestrin
Ctrl	Control
DADs	Delayed afterdepolarizations
DAG	Diacylglycerol
DAPI	4', 6-diamidino-2-phenylindole
ddH2O	Double distilled water
dF	Fluorescence amplitude
DMSO	Dimethyl sulfoxide
DNA	Deoxyribonucleic acid
DTT	Dithiothreitol
E	Epinephrine
E-C	Excitation-contraction
E-T	Excitation-transcription
EADs	Early afterdepolarizations
ECM	Extracellular matrix
EDTA	Ethylenediaminetetraacetic acid
EF	Ejection fraction
EGTA	Ethylene glycol tetraacetic acid
E_m	Emission or membrane potential
ET	Endothelin
ETR	Endothelin receptor
E_x	Excitation
F	Fluorescence at systolic free calcium concentration
FACS	Fluorescence-activated cell sorting
FGF	Fibroblast growth factor
F_{max}	Fluorescence at saturating free calcium concentration
F_{min}	Fluorescence at zero free calcium concentration
F_o	Fluorescence at diastolic free calcium concentration
F_{rest}	Fluorescence at resting free calcium concentration
GAPDH	Glyceraldehyde 3-phosphate dehydrogenase

GPCR	G-protein coupled receptor
G_{α}	Guanosine triphosphate -binding protein α subunit
$G_{\beta\gamma}$	Guanosine triphosphate -binding protein βγ subunit
H3	Histone 3
HAT	Histone acetyltransferase
HCl	Hydrochloric acid
HDAC	Histone-deacetylase
HEPES	4-(2-hydroxyethyl)-1-piperazineethanesulfonic acid
HF	Heart failure
HHD	Hypertensive heart disease
HHpEF	Heart failure with preserved ejection fraction
HHrEF	Heart failure with reduced ejection fraction
HRP	Horseradish peroxidase
$I_{Ca,\ L}$	L-type calcium channel mediated Ca^{2+} current
IGF	Insulin-like growth factor
IgG	Immunoglobulin G
$I_{Na/Ca}$	Sodium/calcium exchange current
IP3	Inositol 1,4,5-trisphosphate
IP3R	Inositol 1,4,5-trisphosphate receptor
I_{to}	Transient outward potassium current
K_d	Calcium dissociation constant of the indicator
$K_{d,app}$	Apparent calcium dissociation constant of the indicator
kDa	Kilo Dalton
LA	Left atria
LSCM	Laser scanning confocal microscopy
LTCC	L-type calcium channel
LV	Left ventricle
LW	Lung weight
MACS	Magnetic-activated cell sorting
MAP	Mean arterial pressure
MEF	Myocyte enhancer factor
MeOH	Methanol

MgAc	Magnesium acetate
MHC	Myosin heavy chain
MMPs	Matrix metalloproteinases
MPTP	Mitochondrial permeability transition pore
N, nuc	Nucleoplasmic region
NA	Nuclear area or numerical aperture
Na^+/K^+ ATPase	Sodium-potassium ATPase
NADH	Nicotineamide adenine dinucletide
NCX	Sodium-calcium exchanger
NE	Nuclear envelope or norepinephrine
NF	Non-failing stage
NFAT	Nuclear factor of activated T cells
NLS	Nuclear localization sequence
NP-40	Tergitol-type NP-40
NPC	Nuclear pore complexe
NT	Nuclear tubule
Nup	Nucleoporin
PA	Plasminogen activator
PAA/BIS	Polyacrylamide/N,N'-methylene-bisacrylamide
PAGE	Polyacrylamide gel electrophoresis
PBS	Phosphate buffered saline
pCaMKII-T286	CaMKII phosphorylated at threonine 286
PCM	Pericentriolar material
PIP2	Phosphatidylinositol 4,5-bisphosphate
PKA	Protein kinase A
PKC	Protein kinase C
PKD	Protein kinase D
PLB	Phospholamban
PLC	Phospholipase C
PMSF	Phenylmethylsulfonyl fluoride
PN	Perinuclear region
Ponceau S	Ponceau S, Acid Red 112

pPLB-S16	Phospholamban phosphorylated at serine 16
pPLB-T17	Phospholamban phosphorylated at threonine 17
pRyR-S2808	Ryanodine receptor phosphorylated at serine 2808
pRyR-S2814	Ryanodine receptor phosphorylated at serine 2814
r	Correlation coefficient
R	Fluorescence signal normalized to F_{rest}
RA	Right atria
RAAS	Renin-angiotensin-aldosterone system
R_f	Dynamic range
RNA	Ribonucleic acid
rpm	Revolutions per minute
RT	Room temperature
RV	Right ventricle
RyR	Ryanodine receptor
SDS	Sodium dodecyl sulfate
SEM	Standard error of the mean
SERCA	Sarcoplasmic reticulum calcium-ATPase
SHR	Spontaneously hypertensive rats
SL	Sarcolemma
SN	Subnucleolemmal region
SNS	Sympathetic nervous system
SR	Sarcoplasmic reticulum
T	Tissue lysate
TBS	Tris buffered saline
TBST	Tris-buffered saline and Tween 20 buffer
TEMED	Tetramethylethylenediamine
TGF	Transforming growth factor
TIMPs	Tissue inhibitor of matrix metalloproteinases
TKR	Tyrosine kinase receptor
TL	Tibia length
TnC	Troponin C
TnI	Troponin I

Tris	Tris(hydroxymethyl)aminomethane
Tween 20	Polysorbate 20
UV	Ultraviolet
vs.	Versus
WKY	Wistar Kyoto rats

9. List of figures

Introduction.....6

Figure 3-1. The risk for cardiac events in hypertension. 8
Figure 3-2. Multiple determinants for left ventricular hypertrophy. 9
Figure 3-3. The vicious cycle of HF. 15
Figure 3-4. Excitation-contraction coupling. 18
Figure 3-5. Ca^{2+} mishandling in HF. 24
Figure 3-6. Role of histone acetylation and deacetylation. 26
Figure 3-7. Ca^{2+}-dependent transcriptional activation in cardiac myocytes. 28
Figure 3-8. Mechanisms of nucleoplasmic [Ca^{2+}] regulation. 31
Figure 3-9. Development of hypertension and HHD throughout the lifespan of SHR. 33
Figure 3-10. Nuclear [Ca^{2+}] regulation during the onset of hypertrophy and HF. 35

Materials and methods.....37

Figure 4-1. Langendorff system. 42
Figure 4-2. Principles of Ca^{2+} measuring using non-ratiometric and ratiometric methods. 44
Figure 4-3. Structure of Fluo-X-dyes (A) and major properties of Fluo-4 (B). 46
Figure 4-4. Fluo-4-AM loading into the cells. 47
Figure 4-5. Principles of LSCM. 50
Figure 4-6. Laser scanning confocal microscope setup. 51
Figure 4-7. Analyses of CaTs. 52
Figure 4-8. Mag-Fluo-4/AM structure (A) and spectral properties (B). 57

Results 72

Figure 5-1. Cytoplasmic and nucleoplasmic CaT characteristics of field stimulated ventricular myocytes from 12-14 weeks old WKY and SHR. 75

Figure 5-2. In situ calibration of Fluo-4 fluorescence in 12-14 weeks old WKY and SHR ventricular myocytes. 77

Figure 5-3. Cytoplasmic and nucleoplasmic Ca^{2+} handling in ventricular myocytes from WKY and SHR at 6 weeks of age. 79

Figure 5-4. SR and perinuclear Ca^{2+} load and fractional release in ventricular myocytes from WKY and SHR at 12-14 weeks of age. 81

Figure 5-5. NE Ca^{2+} load estimated by caffeine-evoked decrease of Mag-Fluo-4 fluorescence. 82

Figure 5-6. Structural characteristics of ventricular myocytes and nuclei from 12-14 weeks old WKY and SHR. 84

Figure 5-7. Ca^{2+} propagation into and inside of the nucleus. 86

Figure 5-8. Isolation of cardiomyocyte nuclei from left ventricular tissue samples. 87

Figure 5-9. Staining of nuclei of ventricular myocytes loaded with Fluo-4 with fluorescent nucleic acid dye Syto-16. 89

Figure 5-10. Expression of major SR/NE Ca^{2+} release proteins in tissue lysates versus isolated cardiomyocyte nuclei. 91

Figure 5-11. Expression of major SR/NE Ca^{2+} reuptake proteins in tissue lysates versus isolated cardiomyocyte nuclei. 92

Figure 5-12. Expression of CaMKIIδ, HDAC5 and acetyl-H3 in tissue lysates versus isolated cardiomyocyte nuclei. 93

Figure 5-14. Grouping of 15-25 months old SHR into SHR with (HF) and without (NF) heart failure based on the presence or absence of pulmonary edema. 97

Figure 5-15. Fluo-4 fluorescence analyses of cytoplasmic and nucleoplasmic CaTs in electrically stimulated ventricular myocytes from 15-25 months old WKY and SHR. 99

Figure 5-16. Calibrated [Ca^{2+}] data of cytoplasmic and nucleoplasmic CaTs of electrically stimulated ventricular myocytes from 15-25 months old WKY and SHR. 101

Figure 5-17. Correlation between the tau of decay and the rise time of cytoplasmic and nucleoplasmic CaTs in WKY, SHR-NF and SHR-HF left ventricular cells.103
Figure 5-18. SR and perinuclear Ca^{2+} load and fractional Ca^{2+} release in ventricular myocytes from 15-25 months old WKY, SHR-NF and SHR-HF.....105
Figure 5-19. Morphology of ventricular myocytes and nuclei from 15-25 months old WKY, SHR-NF and SHR-HF.....107
Figure 5-20. Correlation of kinetic parameters of nucleoplasmic CaTs with the density of nuclear tubules in 15-25 months WKY and SHR.....109
Figure 5-21. Ca^{2+} propagation into and inside of the nucleus in left ventricular myocytes from 15-25 months old WKY, SHR-NF and SHR-HF.....111
Figure 5-22. Expression of major sarcolemmal Ca^{2+} handling proteins in left ventricular tissue lysates from 15-25 months old WKY and SHR-HF. 112
Figure 5-23. Expression of major SR Ca^{2+} release proteins in LV tissue lysates from WKY vs SHR-HF.....114
Figure 5-24. Expression of major SR Ca^{2+} reuptake proteins in LV tissue lysates from WKY vs SHR-HF.....116
Figure 5-25. Protein levels of total CaMKII and the autophosphorylated form of CaMKII (pCaMKII-T286) in LV tissue lysates from WKY vs SHR HF. 117
Figure 5-26. Expression and CaMKII phosphorylation of major Ca^{2+} handling proteins, tPLB/SERCA2a and IP3R2 expression in LV tissue from SHR as a function of lung weight (LW) (normalized to tibia length, TL). 118

Discussion.....120

Figure 6-1. Alterations of Ca^{2+} signaling and gene transcription in LV myocytes from SHR in early HHD. 127
Figure 6-2. Alterations of Ca^{2+} signaling in LV myocytes from SHR in advanced HHD. 136

10. List of tables

Table 4-1. Basic isolation Tyrode's solution (1 l, pH 7.4) 39
Table 4-2. Solutions made from basic isolation Tyrode's solution 40
Table 4-3. Tyrode's solution used for loading and recording (1 l, pH=7.4) 48
Table 4-4. Two main solutions for preparing calibration solutions (pH 7.4) 54
Table 4-5. Preparation of calibration solutions 54
Table 4-6. Adding inhibitors to calibration solutions 55
Table 4-7. Homogenization (lysis) buffer 61
Table 4-8. 4x Lämmli buffer (sample loading buffer), pH 6.8 63
Table 4-9. Preparation of 1 M Tris-HCl, pH 6.8 63
Table 4-10. Composition of 16% Tris-tricine running gel 64
Table 4-11. Composition of 6% stacking gel for Tris-tricine-SDS-PAGE 64
Table 4-12. Preparation of 3 M Tris HCl/SDS (3x), pH 8.45 64
Table 4-13. Running buffer for 4-20% gradient gels (Tris-glycine-SDS-PAGE), pH 8.3 65
Table 4-14. Running buffers for Tris-tricine-SDS-PAGE 65
Table 4-15. Transfer buffer containing 20% methanol 66
Table 4-16. Tris-buffered saline (TBS) buffer, pH 7.5 68
Table 4-17. Primary antibodies 68
Table 4-18. Secondary antibodies 70

11. Publications

11.1. Original manuscripts

Plačkić, J., Preissl, S., Nikonova, Y., Pluteanu, F., Hein, L., & Kockskämper, J. (2016). Enhanced nucleoplasmic Ca^{2+} signaling in ventricular myocytes from young hypertensive rats. *Journal of Molecular and Cellular Cardiology*, *101*, 58–68.

Mederle, K., Gess, B., Pluteanu, F., **Plačkić, J.**, Tiefenbach, K.-J., Grill, A., et al. (2016). The angiotensin receptor-associated protein Atrap is a stimulator of the cardiac Ca^{2+}-ATPase SERCA2a. *Cardiovascular Research*, *110*(3), 359–370.

Pluteanu, F., Hess, J., **Plačkić, J.**, Nikonova, Y., Preisenberger, J., Bukowska, A., et al. (2015). Early subcellular Ca2+ remodelling and increased propensity for Ca2+ alternans in left atrial myocytes from hypertensive rats. *Cardiovascular Research*, *106*(1), 87–97.

Plačkić, J. (2010). The mechanism of HPV - induced cervical carcinogenesis. *Hemijski pregled (Journal of Serbian Chemical Society)*, 51(4), 84-89.

11.2. Abstracts and poster presentations

2016

Kiess T., **Plačkić J.**, Kockskämper J. Modulation of the nuclear calcium handling in ventricular myocytes by stimulation of β-adrenergic receptors. Herbsttagung der Deutschen Gesellschaft für Kardiologie – Herz- und Kreislaufforschung e.V. (DGK), Berlin, Germany, 06.10.16-08.10.16

2015

Nikonova Y., Pluteanu F., **Plačkić J.**, Herzog B., Kockskämper J. Left atrial hypertrophy and reduced contractility and intracellular sodium concentration in atrial myocytes from hypertensive rats during the development of heart failure. Herbsttagung der Deutschen Gesellschaft für Kardiologie − Herz- und Kreislaufforschung e.V. (DGK), Berlin, Germany, 08.10.15-10.10.15

Kiess T., Pluteanu F., **Plačkić J.**, Kockskämper J. Cytoplasmic calcium transients are a major determinant of nucleoplasmic calcium transients in ventricular myocytes. Herbstagung der Deutschen Gesellschaft für Kardiologie – Herz- und Kreislaufforschung e.V., Berlin, Germany, 08.10.15-10.10.15

Pluteanu F., Nikonova Y., **Plačkić J.**, Preisenberger J., Rinne A., Kienitz M. C., Kockskämper J. Impaired sarcolemmal and sarcoplasmic reticulum calcium handling in atrial myocytes during early hypertension and left ventricular hypertrophy in rats. 81. Jahrestagung der Deutschen Gesellschaft für Kardiologie – Herz- und Kreislaufforschung e.V., Mannheim, Germany, 08.04.15-11.04.15

Pluteanu F., Holzapfel A., Nikonova Y., Ivanova T., Preisenberger J., Herzog B., **Plačkić J.**, Kockskämper J. Alterations in calcium handling in atrial myocytes from old hypertensive rats during transition from compensated left ventricular hypertrophy to heart failure, 81. Jahrestagung der Deutschen Gesellschaft für Kardiologie – Herz- und Kreislaufforschung e.V., Mannheim, Germany, 08.04.15-11.04.15

2014

Pluteanu F., Preisenberger J., Heß J., Nikonova Y., **Plačkić J.**, Kockskämper J. Altered Ca^{2+} homeostasis and Ca^{2+} alternans in left atrial myocytes of spontaneously hypertensive rats. 58th Annual Biophysical Society meeting, San-Francisco, California, USA, 15.02.14-18.02.14

Plačkić J., Pluteanu F., Nikonova Y., Preisenberger J., Kockskämper J. Subcellular calcium handling during transition from hypertrophy to heart failure in ventricular myocytes of spontaneously hypertensive rats. 80. Jahrestagung der Deutschen Gesellschaft für experimentelle und klinische Pharmakologie und Toxikologie, Hannover, Germany, 01.04.14-03.04.14.

2013

Plačkić J., Pluteanu F., Kockskämper J. Increased nuclear Ca^{2+} signaling in ventricular myocytes from 12 weeks old spontaneously hypertensive rats. 92nd Annual Meeting of the German Physiological Society, Heidelberg, Germany, 02.03.13-05.03.13

Preisenberger J., Pluteanu F., **Plačkić J.**, Kockskämper J. Subcellular Ca homeostasis in ventricular myocytes from Zucker Diabetic Fatty rats. 79. Jahrestagung der Deutschen Gesellschaft für Experimentelle und Klinische Pharmakologie und Toxikologie e. V., Halle, Germany, 05.03.13-07.03.13

Preisenberger J., Pluteanu F., **Plačkić J.**, Kockskämper J. Zytoplasmatische und nukleoplasmatische Ca-Homöostase in Ventrikelmyozyten diabetischer Ratten, 79. Jahrestagung der Deutschen Gesellschaft für Kardiologie – Herz- und Kreislaufforschung e.V., Mannheim, Germany, 03.04.13-06.04.13

2012

Pluteanu F., Kiess T., Sack C., Nikonova Y., **Plačkić J.**, Roderick H. L., Kockskämper J. Endothelin-1 alters calcium transients in atrial myocytes from spontaneously hypertensive rats. 91st Annual meeting of German Physiological Society, Dresden, Germany, 22.03.12-25.03.12

Plačkić J., Pluteanu F., Kockskämper J. Nuclear calcium signalling during the development of hypertension-induced hypertrophy in rat ventricular myocytes. 91st Annual Meeting of the German Physiological Society, Dresden, Germany, 22.03.12-25.03.12

Plačkić J., Pluteanu F., Kockskämper J. Early hypertension-induced alterations of nuclear Ca^{2+} signalling in ventricular myocytes. Annual Congress of the Heart Failure Association of the European Society of Cardiology, Belgrade, Serbia, 19.05.12-22.05.12

2011

Plutenau F., Heß J., Nikonova Y., **Plačkić J.**, Kockskämper J. Atrial calcium handling in spontaneously hypertensive rats. Herbst- und Jahrestagung der Deutschen Kardiologischen Gesellschaft, Düsseldorf, Germany, 06.10.11-08.10.11

Curriculum vitae

This page containes personal information. It is therefore excluded from online publication.
Diese Seite enthält persönliche Daten. Sie ist daher nicht Bestandteil der Online-Veröffentlichung.

Acknowledgements

First I would like to express special thanks to my supervisor Prof. Dr. Jens Kockskämper. With his positive attitude he managed to encourage and inspire me during the difficult moments of my research projects. Also, I am very grateful to him for being such a good friend to me and helped me a lot at the beginning when I arrived in Marburg. I was lucky to have someone like him around, with a great expertise and a very warm personality.

I would like in particular to thank Prof. Dr. L. Hein and Dr. Sebastian Preissl for performing the isolation and purification of cardiac nuclei.

I would also like to thank Dr. H. L. Roderick for kindly providing the IP3R antibody.

I would like to thank Prof. Dr. Moritz Bünemann, Prof. Dr. Carsten Culmsee and Prof. Dr. Cornelius Krasel on their suggestions and knowledge that they shared with me to help me progress in my work.

Many thanks to Dr. Florentina-Cornelia Pluteanu for all the knowledge regarding the methods and lab organization she provided me with.

I would also like to thank all my colleagues from the Institute of pharmacology and clinical pharmacy. I am extremely grateful to Tobias, Judit, Simon, Eleni, Jonny, Hauke, Bertram, Katharina, Sophia, Birgit, Gaya and Debia for being great and supportive colleagues. Special thank to Tobias Kiess, who helped me with translating the summary of my work to german and was always a good friend, to Emma Esser for her great help with all the formalities and to Ulrich Korell for technical help.

I want to acknowledge the great colleague and friend I made during the phD, Yulia Nikonova. I am thankful for all unforgettable moments with her. Nothing would be the same without her. I feel lucky and grateful that I made a friend for life.

I also want to acknowledge my best friends, Marko, Sanja and Natasa for believing in me!

I am deeply grateful to my mum, dad and my brother for all their love and support.

In the end I want to express the greatest thank to my husband, the love of my life, Dragan Nenad, who always looked after me and reminded me to go further and never forget my potentials and goals. Without him, I would not even dare to move to Marburg. He was my greatest support.

ERKLÄRUNG

Ich versichere, dass ich meine Dissertation

„Alterations of nuclear Ca2+ regulation in ventricular myocytes during development and progression of hypertensive heart disease''

selbständig ohne unerlaubte Hilfe angefertigt und mich dabei keiner anderen als der von mir ausdrücklich bezeichneten Quellen bedient habe. Alle vollständig oder sinngemäß übernommenen sind Zitate als solche gekennzeichnet.

Die Dissertation wurde in der jetzigen oder einer ähnlichen Form noch bei keiner anderen Hochschule eingereicht und hat noch keinen sonstigen Prüfungszwecken gedient.

Marburg, den 10.02.2017

.....
(Jelena Plačkić)